STUDIES ON QUASINORMAL MODES AND LATE -TIME TAILS IN BLACK HOLE SPACETIMES

Thesis submitted to

Cochin University of Science and Technology

in partial fulfillment of the requirements
for the award of the degree of

DOCTOR OF PHILOSOPHY

by

Nijo Varghese
Theory Division
Department of Physics
Cochin University of Science and Technology
Kochi - 682022

October 2012

Studies on Quasinormal Modes and Late-time Tails in Black Hole Spacetimes
PhD thesis in the field of Black Hole Physics

Author
Nijo Varghese
Department of Physics
Cochin University of Science and Technology
Kochi - 22
nijovarghesen@gmail.com

Research Supervisor
Prof V. C. Kuriakose(Rtd.)
Department of Physics
Cochin University of Science and Technology
Kochi - 22
vck@cusat.ac.in

Front cover : Illustration of the scattered waveform from the curvature potential of the black hole.

Back cover : Spacetime curvature around a black hole.

to my family & friends

CERTIFICATE

Certified that the work presented in this thesis is a bonafide research work done by Mr. Nijo Varghese under my guidance in the Department of Physics, Cochin University of Science and Technology, Kochi, India - 682022, and has not been included in any other thesis submitted previously for the award of any degree.

Kochi-22
October, 2012

Prof. V. C. Kuriakose
(Supervising Guide)

DECLARATION

I hereby declare that the work presented in this thesis is based on the original research work done by me under the guidance of Prof. V. C. Kuriakose (Rtd.), Department of Physics, Cochin University of Science and Technology, Kochi, India - 682022, and has not been included in any other thesis submitted previously for the award of any degree.

Kochi-22
October, 2012

Nijo Varghese

Contents

Preface

Black hole's response to external perturbations will carry significant information about these exotic objects. Its response, shortly after the initial 'kick', is known to be ruled by the damped oscillation of the perturbating field, called *quasinormal modes*(QNMs), followed by the *tails* of decay and is the characteristic of the background black hole spacetime.

In the last three decades, several shortcomings came out in the Einstein's General Theory of Relativity(GTR). Such issues come, especially, from observational cosmology and quantum field theory. In the first case, for example, the observed accelerated expansion of the universe and the hypothesized mysterious dark energy still lack a satisfactory explanation. Secondly, GTR is a classical theory which does not work as a fundamental theory, when one wants to achieve a full quantum description of gravity. Due to these facts modification to GTR or alternative theories for gravity have been considered. Two potential approaches towards these problems are the *quintessence* model for dark energy and *Hořava-Lifshitz*(HL) gravity. Quintessence is a dynamical model of dark energy which is often realized by scalar field mechanism. HL gravity is the recently proposed theory of gravity, which is renormalizable in power counting arguments. The two models are considered as a potential candidate in explaining these issues.

In this thesis, the signature of these new theories are probed on the evolution of field perturbations on the black hole spacetimes in the theory.

Chapter 1 gives a general introduction to black holes and its perturbation formalism. Various concepts in the area covered by the thesis are also elucidated in this chapter.

Chapter 2 describes the evolution of massive, charged scalar field perturbations around a Reissner-Nördstrom black hole surrounded by a static and spherically symmetric quintessence. The complex frequencies of the normal modes associated with the evolution are evaluated using third order WKB approximation approach. The influences of quintessence on the QNMs are studied. The dependence of QNMs on the charge of the black bole, mass and charge of perturbing scalar field and the quintessential parameters are also clarified.

Chapter 3 comprises the evolution of massless scalar, electromagnetic and gravitational fields around spherically symmetric black hole whose asymptotes are defined by the quintessence, with special interest on the late-time behavior. The complete evolution profile is obtained through numerical methods for different values of quintessence state parameter and compare the results with case in the absence of quintessence. We examine how the different multipoles of perturbation for different spin fields evolve with time. Possible reasons for the different behavior of late-time tails are discussed.

Chapter 4 examines the evolution of Dirac field around a Schwarzschild black hole surrounded by quintessence. Detailed numerical simulations are done to analyze the nature of field on different surfaces of constant radius.

Chapter 5 is dedicated to the study of the evolution of massless fields around the black hole geometry in the HL gravity. From a knowledge of the evolution of scalar, electromagnetic and Dirac perturbations around black holes, we try to distinguish the the nature of the HL theory from that of GTR. QNM and tail phases are studied using the numerical integration and the WKB approximation method.

Chapter 6 concerns the study of the evolution of massive scalar field in the spacetime geometry of black hole in HL gravity by numer-

ical analysis. Different regimes of the late-time evolution are studied in detail.

Chapter 7 summarizes the substantial findings of the works presented in the thesis and suggests future scopes of the works that can be undertaken.

Notations and conventions

Throughout the thesis we have chosen the natural unit systems with $c = 1 = G$. Signature of spacetime metric: $(-,+,+,+)$. Semicolon after a vector or tensor stand for its covariant derivative. Prime over any quantity denotes derivative of that quantity w.r.t the radial coordinate and dot represents the time derivative. Indices μ, ν, a and b generally run over $0, 1, 2, 3$. The letter c is used in this thesis for the normalization factor of quintessence.

Publications related to the work presented in the thesis:

In refereed journals

1. "Quasinormal modes of Reissner-Nördstrom black hole surrounded by quintessence", **Nijo Varghese** and V. C. Kuriakose, *Gen. Relativ. Gravit.*, **41** 1249 (2009).

2. "Evolution of electromagnetic and Dirac perturbations around a black hole in Hořava gravity", **Nijo Varghese** and V. C. Kuriakose, *Mod. Phys. Lett. A*, **26**, 1645 (2011).

3. "Evolution of massive fields around a black hole in Hořava gravity", **Nijo Varghese** and V. C. Kuriakose, *Gen. Relativ. Gravit.*, **43**, 2755 (2011).

4. "Late-time tails of fields around a Schwarzschild black hole surrounded by quintessence", **Nijo Varghese** and V. C. Kuriakose. *Gen. Relativ. Gravit.*, DOI: 10.1007/s10714-012-1463-z.

5. "Decay of Dirac field around Schwarzschild black hole surrounded by quintessence", **Nijo Varghese** and V. C. Kuriakose. (to be submitted for publication)

In conferences/seminars

1. "Evolution of electromagnetic perturbation around black hole in Hořava gravity", **Nijo Varghese** and V. C. Kuriakose, *26^{th} meeting of the Indian Association for General Relativity and Gravitation* (IAGRG-26), Allahabad, India (2011).

2. "Evolution of massive fields around black hole in Hořava gravity", **Nijo Varghese** and V. C. Kuriakose, *VII^{th} International Conference on Gravitation and Cosmology*(ICGC), Goa, India(2011).

3. "Late-time evolution of massive fields around black hole surrounded by quintessence", **Nijo Varghese** and V. C. Kuriakose, *International Conference on Modern Perspectives of Cosmology and Gravitation*(COSGRAV), Kolkatta, India (2012).

Other publications to which author has contributed:

1. "Absorption cross-section of Reissner-Nördstrom and Schwarzschild-de Sitter extremal black hole", Sini R., **Nijo Varghese** and V. C. Kuriakose, *Int. J. Mod. Phys. A,* **23**, 4011 (2008).

2. "Effect of cosmic string in spherically symmetric Black Hole on the Dirac perturbation", Sini R., **Nijo Varghese** and V. C. Kuriakose, *Mod. Phys. Lett. A.* **25**, 111 (2010).

Acknowledgements

In the past few years, I have been hovering around precarious black holes and many people supported me to be on the right track without falling into it. It is a great pleasure to thank all those people who influenced my life during the past few years and contributed, in different ways, to this thesis.

Foremost, I would like to express my deepest sense of gratitude to my supervisor Prof. V. C. Kuriakose, who offered his continuous advice and encouragement throughout my time as his student. I have been extremely lucky to have a supervisor who cared so much about his students, give enough freedom to work and spend much of his time for guiding us. His patience, motivation, enthusiasm and elderly advices helped me in all the time of my research. It was a wonderful experience with him, to be a part of various science popularization programs, especially with the IRC telescope.

I extend my sincere thanks to the present Head, Department of Physics, Prof. B. Pradeep and former Heads, for providing me the necessary facilities for my research. I would like to express my sincere gratitude to Prof. Ramesh Babu T, my Doctoral Committee member for the helps and inspiration that I have received. I am thankful to all my teachers of the Department of Physics, for their support and encouragement right from my post graduation days. I am also thankful to all the office and library staff of the Department of Physics for all the help and cooperation.

I am grateful to Dr. Alexander Zhidenko, Universidade Federal do ABC, Brazil, for the helping me in developing the numerical code. I would like to thank IUCAA Resource Center, Kochi, were I have done much of the numerical simulations for this thesis.

I am much indebted to my colleagues in the theory group for all

the wonderful time I shared with them. I wish to thank my seniors, Chitra, Jisha, Sini, Nima chechies and Radhakrishnan chettan, for all the support and help that I got during the early stages of my research. I am very much thankful to Vivek for his advice and helps. I am grateful to Vinayaraj, Arun V and Vineeth for the friendship they offered me in my early days. Many thanks to Tharanath, my roommate and colleague. Shaju sir was always an inspiration for me since my B.Sc. days. I also thank Saneesh, Lini, Prasobh, Prasia, Anoop, Navaneeth, Praseetha, Rijeesh, Naseef for their nice company.

A good support system is important for surviving and staying sane in the research field. I was lucky to be in the middle of good caring friends in a fun filled environment. Priyesh and Sanal were always a constant source of support, care and encouragement for me. Arun was there to loose the tension with his jolly talks. I have greatly enjoyed the company of Rajeshmon and Subin. All friends in OED lab, though I am not naming, have offered me a good company. Thanks to all. I am also thankful to Rajesh CS and Bhavya for their friendship. It was a nice memorable experience with our car and its 'tightly packed' trips for movies. The wonderful evenings in the badminton court at the department was a great refreshment for me. I thank all friends in the department for the nice time I had with them.

I gratefully acknowledge the financial assistance given by University Grants Commission(UGC), India in the form of RFSMS Fellowship and Cochin University of Science and Technology through UJRF.

Lastly, and most importantly, I express my profound gratitude from my deep heart to my parents and sister for all the love, patience and support they gave me throughout these years.

Nijo Varghese

1
Introduction

One of the greatest creations of speculative science is the Einstein's General Theory of Relativity. Its first solution-a black hole- is happened to be more strange and mysterious. The words of John Wheeler, the coiner and popularizer of the name 'black hole', expresses this enchantment.

"Of all the entities I have encountered in my life in physics, none approaches the black hole in fascination. And none, I think, is a more important constituent of this universe we call home. The black hole epitomizes the revolution wrought by general relativity. It pushes to the extreme-and therefore tests to the limit-the features of general relativity (the dynamics of curved spacetime) that set it apart from special relativity (the physics of static, "flat"spacetime) and the earlier mechanics of Newton. Spacetime curvature. Geometry as part of physics. Gravitational radiation. All of these things become, with black holes, not tiny corrections to older physics, but the essence of newer physics."

–John Archibald Wheeler

Let me introduce black holes through the words of Kip Thorne[1],

"...black hole: a hole in space with a definite edge into which anything can fall and out of which nothing can escape, a hole with a gravitational force so strong that even light is caught and held in its

grip, a hole that curves space and warps time..... well-tested laws of physics predict firmly that black holes exist. In our galaxy alone there may be millions, but their darkness hides them from view. Astronomers have great difficulty finding them."

–Kip S. Thorne

It is this weird nature made the black hole deeply entrenched in human imagination and one of the most studied objects in science.

1.1 From "dark stars" to "black holes"

The first scientific ideas on regions of gravity so strong that light cannot escape, were kicked to the late 1780s. Combining Newtons theory of gravitation with his corpuscular theory of light, John Mitchell, a British natural philosopher, presented the idea of '*dark stars*'at the Royal Society, London. He argued that if a star is compact enough, the escape velocity on its surface may be greater than the velocity of light corpuscles, and the star becomes invisible. Later in 1797, mathematician Laplace promoted the same idea and he wrote on his book,

"It is therefore possible that the greatest luminous bodies in the Universe are on this very account invisible."

–Pierre-Simon Laplace

But the general acceptance of wave theory of light in the begining of 19^{th} century forced him to drop out the notion of dark stars.

The modern understanding of black holes begins when Karl Schwarzschild derived an exact solution for Einstein's field equation in 1916, almost immediately after Einstein formulated his relativistic theory of gravity.

His solution showed that if the mass of the compact object confined with in a critical circumference, the space will be strongly curved and the flow of time at the star's surface will be infinitely dilated. A star as small as a critical circumference, called Schwarzschild radius, must appear completely dark. This did not seem at all reasonable to physicists and astrophysicists of 1920s or even as late as the 1960s. Even Eddington, a relativity expert of his time and Einstein himself opposed the 'Schwarzschild singularity'theory.

But several discoveries in the 1930s made them recognized as realistic objects. Among them three major developments were,

- Chandrasekhar's 1931 proof that there is an upper limit on the mass of white dwarfs ($M \leq 1.4 M_{\odot}$)
- Chadwick's 1932 discovery of the neutron and the subsequent idea – due to Baade and Zwicky – that entire stars made up of these particles may exist. Such neutron stars would be limited to a mass less than something like $3M_{\odot}$.
- the seminal work on gravitational collapse by Oppenheimer and Snyder from 1939, that provided the first demonstration of how the implosion of a star forms a black hole[2].

Eventhough these findings confirmed that the black holes are theoretically possible, it had to wait until 1970, for the first observation evidence for the actual existence of black holes in the Universe. It came from the detection of Cygnus X-1, one of the strongest X-ray sources we can detect from Earth. It is widely believed that the Cygnus X-1 is a binary black hole system with a companion smaller than Earth but with a mass greater than that of a neutron star.

Presently we have many black hole candidates, with stronger evidences due to the advanced optical, X-ray and radio telescopes. It is

now strongly suspect that almost all galaxies contain gigantic black holes in their centers, millions or even billions of times more massive than the Sun. Our own galaxy, Milky Way is expected to harbor a supermassive black hole, known as Sagittarius A*, at the center[3]. Several gravitational wave operators are now actively searching for the signal coming from black holes and may make it possible to directly observe them in the near future.

1.2 Characteristics of black hole

Eventhough black holes possess a complex mysterious nature, they have a perfect mathematical description. The mathematically defined black hole is the picture of simplicity as Chandrasekher wrote in his monograph[4],

"The black holes of nature are the most perfect macroscopic objects there are in the Universe: the only elements in their construction are our concepts of space and time. And since the general theory of relativity provides only a single unique family of solutions for their descriptions, they are the simplest objects as well."

–S. Chandrasekher

As we mentioned already, the Schwarzschild solution is the first solution of Einstein's field equation, represents spacetime outside a spherically symmetric massive object. The line element, which describes such a geometry is given as,

$$ds^2 = -\left(1 - \frac{2M}{r}\right) dt^2 + \left(1 - \frac{2M}{r}\right)^{-1} dr^2 + r^2(d\theta^2 + \sin^2\theta d\phi^2). \tag{1.1}$$

An important property of this solution is that it is independent of the temporal, t coordinate and depends only on r and that it is determined by only a single parameter, M, its mass. Far from the center of gravity($r \to \infty$) the spacetime dissolve to the flat Minkowski spacetime,

$$ds^2 = \eta_{\mu\nu} dx^\mu dx^\nu = -dt^2 + dr^2 + r^2(d\theta^2 + \sin^2\theta d\phi^2). \tag{1.2}$$

One can notice from Eq.(1.1) that the gravity of the massive object not only curves the space around it but warp the time near its premises. One can visualize the Schwarzschild spacetime in the embedded diagram shown in Figure 1.1 and observe the following points.

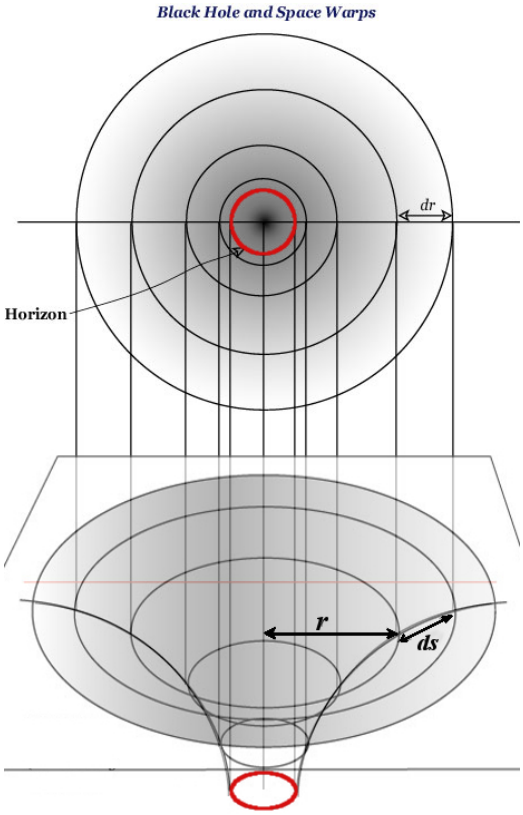

Figure 1.1: Embedded diagram of Schwarzschild black hole.

The solution is singular at two values of the radial coordinate, $r = r_e = 2M$ and $r = 0$. The first one is a coordinate singularity that can be transformed away by choosing suitable coordinates systems. The second one is the actual gravitational singularity marked by an infinite curvature. The radial distance, r_e is called the Schwarzschild radius and it marks a boundary called the event horizon of the black hole, which is a causality barrier through which anything can go inside but nothing can come out.

Schwarzschild black hole is the simplest case, with only one parameter determines its geometry, its mass. A theorem known as *'no-hair theorem'*[5] limits the other properties of a black hole reaching to an external observer. According to this theorem a black hole formed by the gravitational collapse of a charged rotating star, will rapidly relax to the stationary state, characterized by only three quantities, its mass, charge and angular momentum(MQJ). Any other *hair*, will disappear after the collapsing body settles down to its stationary configuration(Section 1.4.2). Consequently there are four varieties of black holes in GTR,

Black hole	Signatures
Schwarzschild	M
Reissner-Nördstrom(RN)	M and Q
Kerr	M and J
Kerr-Newmann	M, Q and J

I summarizes this section with the words of Wheeler,

"[The black hole] teaches us that space can be crumpled like a piece of paper into an infinitesimal dot, that time can be extinguished like a blown-out flame, and that the laws of physics that we regard as 'sacred', as immutable, are anything but."

–John Archibald Wheeler

1.3 Linear perturbations of black hole

The concept and formulation of black hole perturbation theory dates back to 50's and was first introduced by Regge and Wheeler in their seminal paper [6]. Their intention was to study the stability of the equilibrium configuration of black hole represented by the Schwarzschild spacetime. The relevance of the stability problem was of two kind. Firstly the notion of black holes were not widely accepted at that time. Unless these objects formed by the gravitational collapse are proved to survive the perturbations, that can be expected in the collapse, one cannot treat them as the final state of the massive stars. Secondly, being solutions of Einstein's equation does not ensure the stability of the black holes.

Since Einstein's equations is highly nonlinear in metric tensor, it is very difficult to analyze the generic perturbation around black hole spacetime. So Regge and Wheeler confined their study in to a linearized level. They investigated the question of stability up to terms of the first order in the departure from sphericity. This approximation leads to linear equations and it is possible to decompose the given disturbances in to normal modes using tensor spherical harmonics. Now if the complex frequiencies of these modes have negative imaginary parts, then one can conclude that the black hole is stable and unstable if the imaginary parts are positive. We briefly explain the the Regge-Wheeler equation describing the black hole perturbation.

1.3.1 Gravitational perturbations

The spherically symmetric uncharged stationary background spacetime is described by,

$$\begin{aligned} ds^2 &= \bar{g}_{\mu\nu} dx^\mu dx^\nu \qquad (1.3) \\ &= -\left(1 - \frac{2M}{r}\right) dt^2 + \left(1 - \frac{2M}{r}\right)^{-1} dr^2 + r^2(d\theta^2 + \sin^2\theta d\phi^2). \end{aligned}$$

Consider small perturbations, $h_{\mu\nu}$ in background spacetime, $\bar{g}_{\mu\nu}$ with $|h_{\mu\nu}|/|\bar{g}_{\mu\nu}| \ll 1$, such that the total metric can be taken as the sum of unperturbed background metric and the perturbation,

$$g_{\mu\nu} = \bar{g}_{\mu\nu} + h_{\mu\nu}. \qquad (1.4)$$

Now we want to construct the Einstein equation for this perturbed system up to the linearized level. So in the calculation we only keep quantities up to first order in $h_{\mu\nu}$, at each step. Rising and lowering of indices are done using the background metric. For example,

$$h^{\mu\nu} = \bar{g}^{\mu\alpha}\bar{g}^{\beta\nu} h_{\alpha\beta}. \qquad (1.5)$$

Variation of Ricci tensor can be found from the expression[80]

$$\delta R_{\mu\nu} = -\delta\Gamma^{\beta}_{\mu\nu;\beta} + \delta\Gamma^{\beta}_{\mu\beta;\nu}, \qquad (1.6)$$

where the variation of affine connections is,

$$\delta\Gamma^{\alpha}_{\beta\gamma} = \frac{1}{2} g^{\alpha\nu}(h_{\beta\nu;\gamma} + h_{\gamma\nu;\beta} - h_{\beta\gamma;\nu}), \qquad (1.7)$$

Einstein field equation for the perturbated system is,

$$\delta G_{\mu\nu}(g) = -8\pi\delta T_{\mu\nu}, \qquad (1.8)$$

where $G_{\mu\nu}(g)$ is the Einstein tensor computed from the total metric $g_{\mu\nu}+h_{\mu\nu}$. Since we are considering perturbations in the Schwarzschild exterior, which is empty, the field equation reduced to,

$$R_{\mu\nu}(g) = 0, \tag{1.9}$$

where $R_{\mu\nu}(g)$ is the Ricci tensor computed from the total metric $g_{\mu\nu} + h_{\mu\nu}$. Since we assume that the perturbation is small, taking terms up to linear in $h_{\mu\nu}$, above equation can be expanded as,

$$R_{\mu\nu}(\bar{g}) + \delta R_{\mu\nu}(h) = 0, \tag{1.10}$$

where $R_{\mu\nu}(\bar{g})$ is the Ricci tensor computed from the unperturbed metric $\bar{g}_{\mu\nu}$ which we know will vanish and the equation becomes,

$$\delta R_{\mu\nu}(h) = 0. \tag{1.11}$$

With the expressions Eqs.(1.6) and (1.7) in hand one can compute the perturbation equation, Eq.(1.11). Making use of the spherical symmetry of the background, we can decouple the angular part of the perturbation equation and obtain an equation depending on the radial and time variables. Any arbitrary perturbations can be decomposed in to normal modes and for any given value of the angular momentum ℓ, associated with these modes, there are two classes of perturbations. Even $(-1)^{\ell}$ and odd $(-1)^{\ell+1}$ parity perturbations. Here we proceed considering the axial perturbation case since the two were shown to have a similar QNM spectra. The canonical form of odd wave perturbations in Regge-Wheeler gauge[6] is,

$$h_{\mu\nu} = \begin{vmatrix} 0 & 0 & 0 & h_0(r) \\ 0 & 0 & 0 & h_1(r) \\ 0 & 0 & 0 & 0 \\ h_0(r) & h_1(r) & 0 & 0 \end{vmatrix} sin\theta \frac{\partial}{\partial\theta} P_\ell(cos\theta) e^{-i\omega t}. \tag{1.12}$$

Substituting Eq.(1.12) in Eq.(1.11) we can separate the angular and radial parts of the equation and we get the following radial equations by equating $\delta R_{\theta\phi}$, $\delta R_{r\phi}$ and $\delta R_{t\phi}$ to zero, respectively as[7],

$$\frac{i\omega h_0}{\left(1-\frac{2M}{r}\right)} + \frac{d}{dr}\left[\left(1-\frac{2M}{r}\right)h_1\right] = 0, \tag{1.13}$$

$$\frac{i\omega}{\left(1-\frac{2M}{r}\right)}\left(\frac{dh_0}{dr} - \frac{2h_0}{r}\right) + h_1\left[\frac{\ell(\ell+1)}{r^2} - \frac{\omega^2}{\left(1-\frac{2M}{r}\right)} - \frac{2}{r^2}\right] = 0, \tag{1.14}$$

$$\left(1-\frac{2M}{r}\right)\left[\frac{1}{2}\frac{d^2h_0}{dr^2} + i\omega\left(\frac{1}{2}\frac{dh_1}{dr} + \frac{h_1}{r}\right)\right] + h_0\left[\frac{2M}{r^3} - \frac{\ell(\ell+1)}{2r^2}\right] = 0. \tag{1.15}$$

Defining $\psi(t,r) = \left(1-\frac{2M}{r}\right)\frac{h_1}{r}$ the above equations can be combined to get a second order equation, after eliminating $h_0(r)$.

$$\frac{d^2\psi_\ell}{dr_*^2} + \left(\omega^2 - V_{eff}\right)\psi_\ell = 0 \tag{1.16}$$

were we have employed the radial tortoise coordinate, defines as $r_* = r + 2Mln\left(\frac{r}{2M} - 1\right)$, such that it pushes the event horizon, $2M$ all the way to $-\infty$. As,

$$\begin{aligned} r &\longrightarrow +\infty, \quad r_* \longrightarrow +\infty, \\ r &\longrightarrow 2M, \quad r_* \longrightarrow -\infty. \end{aligned} \tag{1.17}$$

The effective potential, V_{eff} appearing in Eq.(1.16), usually called the Regge-Wheeler potential, is given by,

$$V_{eff} = \left(1 - \frac{2M}{r}\right)\left(\frac{\ell(\ell+1)}{r^2} - \frac{6M}{r^3}\right). \tag{1.18}$$

The effective potential plotted in Figure 1.2. The potential is positive real everywhere and has a maximum just outside the event horizon at $r \simeq 3.3M$. The asymptotic structure of the potential shows an inverse-square fall off as $r_* \to +\infty$ and vanishes exponentially as $r_* \to -\infty$. Modes with larger multipoles will experience a higher potential barrier.

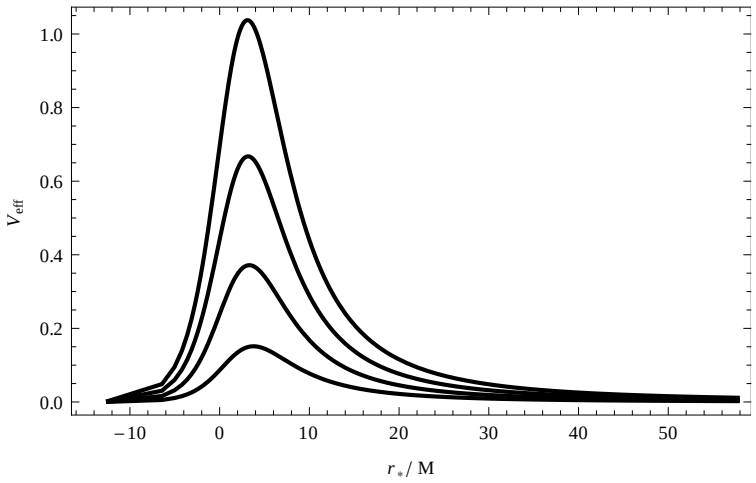

Figure 1.2: The Regge-Wheeler potential for different multipoles of perturbation. Curves from bottom to top are for $l = 2, 3, 4$ and 5.

Perturbations with even parity, can also be reduced to obtain a second order equation of the form, Eq.(1.16), but with a more complicated form for the potential, called the Zerilli potential[8]. But it looks very similar to the Regge-Wheeler potential, shown in Figure 1.2 and has nearly identical properties[4].

Now the study of stability is reduced to finding the solutions of the differential equation, Eq.(1.16). With the time dependence of perturbation as $e^{-i\omega t}$, if the perturbation equation allows solutions having positive imaginary part for frequency, then the perturbations will grow exponentially in time and leads to an unstable configuration. If the frequiencies have positive imaginary parts, then the perturbations will decay in time and finally settle to the equilibrium configuration. A satisfactory explanation to this problem was first provided by Vishveshwara[9]. By examining the asymptotic behavior of the solutions in Kruskal coordinates, he proved that the perturbations with imaginary frequency are physically unacceptable and hence that the Schwarzschild metric is stable. A rigorous proof was given later by Kay and Wald[10].

1.3.2 Perturbations by classical wave fields

When a nearly spherical star collapses through its gravitational radius, non spherical perturbations can be expected in its electromagnetic and various other spin fields coupled to sources in the stars, along with the gravitational disturbances. One can also study the perturbation of these fields in curved spacetime, using the field theory.

If the fields are assumed to be week, the slight deformation in the background black hole spacetime, caused by the energy-momentum tensor of the field, can be neglected. The general approach to solving these problems is as follows. The field is expanded in spherical harmonics, scalar harmonics for scalar field($s = 0$), vector harmonics for electromagnetic field($s = 1$) and tensor harmonics for gravitational field($s = 2$). Each spherical harmonics represented by the multipole number, ℓ can evolve separately satisfying an equation of the form

Eq.(1.16), with an effective potential characteristic of the field under consideration. For massless integer spin fields, in the Schwarzschild background spacetime, we can write[11](A detailed derivation for various field perturbations are presented in the coming chapters),

$$V = \left(1 - \frac{2M}{r}\right)\left(\frac{\ell(\ell+1)}{r^2} + \sigma\frac{2M}{r^3}\right) \tag{1.19}$$

where σ depends on the spin, s of the perturbing field as, $\sigma = 1-s^2$ and is given by,

$$\sigma = \begin{cases} +1 & \text{scalar field} \\ 0 & \text{electromagnetic field} \\ -3 & \text{odd gravitational perturbation.} \end{cases} \tag{1.20}$$

The fermionic field($s = 1/2$) has a different form for potential[12], even though it has similar shape as shown in Figure 1.2.

$$V_{\pm} = \frac{|k|\left(1-\frac{2M}{r}\right)^{1/2}}{r^2}\left[|k|\left(1-\frac{2M}{r}\right)^{1/2} \pm \frac{M}{r} \mp \left(1-\frac{2M}{r}\right)\right]. \tag{1.21}$$

The particular shape of the potential and Eq.(1.16) suggest many similarities with the standard scattering problem in the quantum mechanics. The underlying physical problem is the scattering of waves by one dimensional potential barrier[4]. So, once the potential is obtained, one can use the standard analyzing tools in the quantum theory, with appropriate boundary conditions, associated with the the black hole spacetime.

1.4 Time evolution of perturbation

Even though the initial intention of the formulation perturbation equation was to address the stability problem, later it was widely

used for the study of various dynamical processes involving black hole, from the realization that the perturbation method is adequate to describe various interaction of black hole with its surroundings. All these disturbances can be described by the perturbation equation provided the perturbation is very small and the particular behavior of potential appearing in all these problems suggests the similarity with the one dimensional scattering problem in standard quantum mechanics.

It was Vishveshwara[13] who made the first attempt to apply the principles of the standard quantum theory to the scattering problem of gravitational waves by the black holes. His motivation as he later remembered[14] was *"how do you observe a solitary black hole? To me the answer seemed obvious. It had to be through scattering of radiation, provided the black hole left its fingerprint on the scattered wave."*

The striking feature that he observed, in his classical scattering experiment was, in his own words[14], *"So, I started pelting the black hole with Gaussian wave packets. If the wave packet was spatially wide, the scattered one was affected very little. It was like a big wave washing over a small pebble. But when the Gaussian became sharper, maxima and minima started emerging, finally leveling off to a set pattern when the width of the Gaussian became comparable to or less than the size of the black hole. The final outcome was a very characteristic decaying mode, to be christened later as the quasinormal mode. The whole experiment was extraordinarily exciting.*

The remarkable thing about the discovery of the scattering experiment was that the resulted wave pattern is completely independent of the initial shape of the scattering waveform. This can be shown by numerical integration of the time dependent form of Eq.(1.16),

with out assuming the harmonic time dependence. Figure 1.3 demonstrates this feature, where we have plotted the outcome of scattering of gravitational wave packets by the Schwarzschild spacetime.

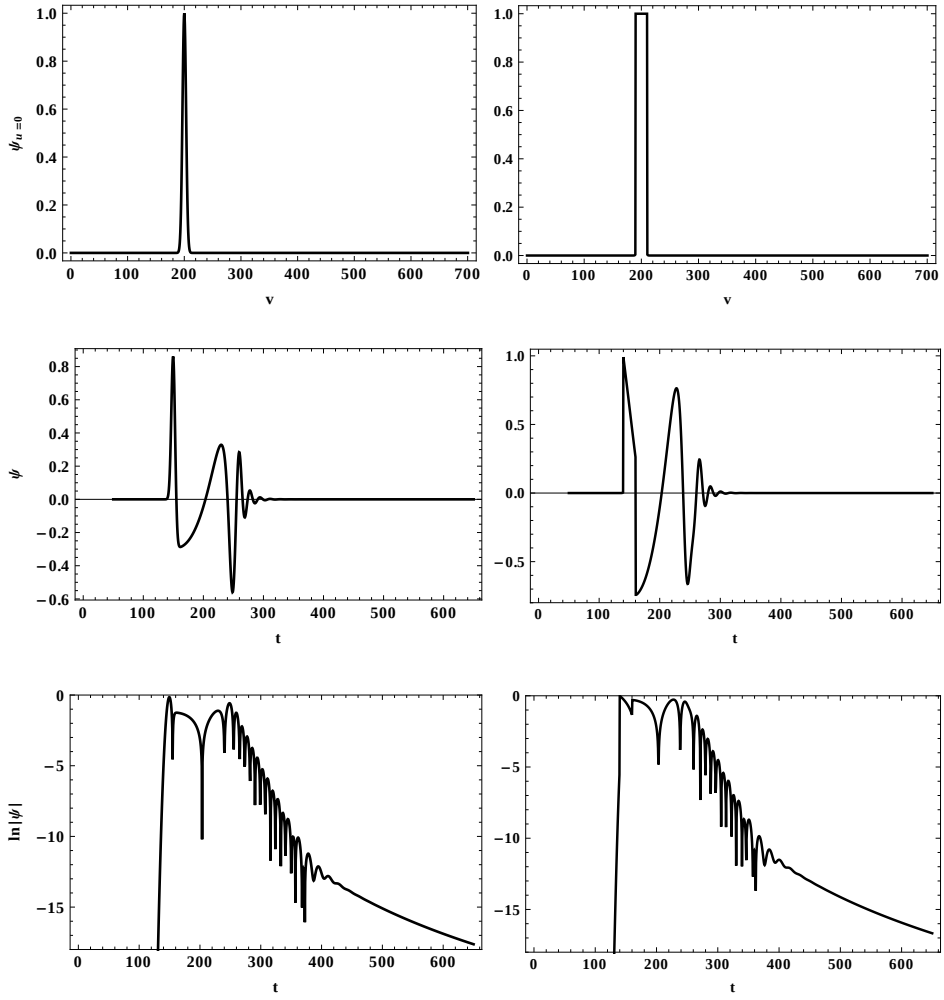

Figure 1.3: Simulations showing the temporal evolution of the $l = 2$ mode of gravitational perturbation around Schwarzschild black hole with different initial shapes for the perturbing wave packet.

In the first set of simulations we sent a Gaussian wave packet

and the scattered waveform is shown in linear scale and the absolute value of the wavefuncion in logarithmic scales, to visualize the weak waveform at late times. In the second set we use a square wave packet and the scattered waveform is analyzed. The remarkable thing that can be read from the simulations is that after a transient phase, where the waveforms show the trails of the particular shape of the perturbing waveform, there comes different phases of evolution for which the waveforms are identical for the both cases.

For any generic perturbation, an observer at a fixed distance outside the black hole can easily distinguish the following stages of the wave evolution:

1. a transient stage formed by direct emission from the source of perturbation,

2. the stage comprised by the damped characteristic oscillations-the quasinormal modes,

3. late-time the so called 'tail'decay stage dominates.

Figure 1.4 shows these phases of evolution. The observer first records the original waveform from the perturbing source, then the exponentially decaying oscillating phase. Finally the QNMs are suppressed by the tails of waves. As we already mentioned, the last two stages are completely independent of the initial shape of the perturbing agent, but depends entirely on the background spacetime under consideration.

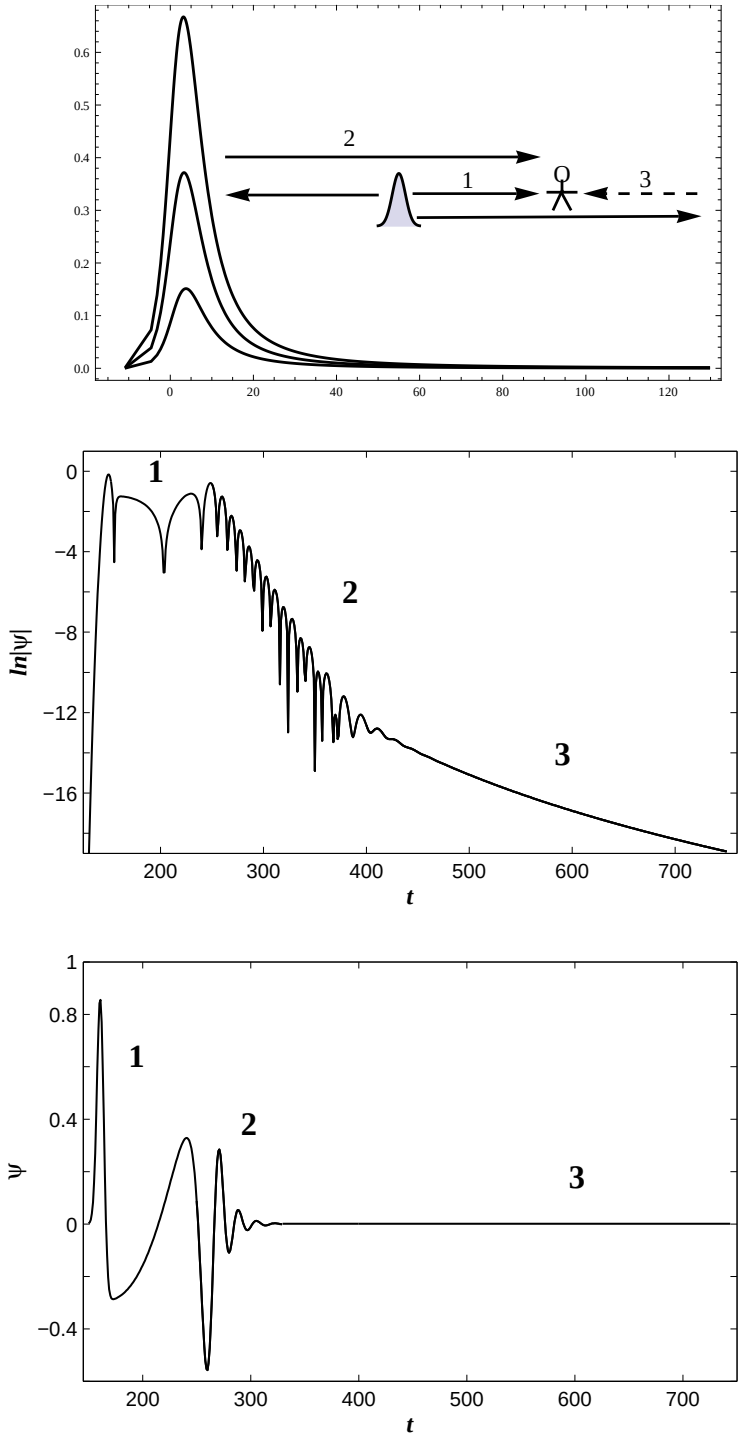

Figure 1.4: Different stages of the time evolution of gravitational perturbation reported by an distant observer.

1.4.1 QNMs of black holes

The asymptotic form of the effective potentials, $V(r_* \to \pm\infty) \to 0$, suggests that the solution behaves as plane waves near the boundaries, $r_* \to \pm\infty$,

$$\psi \sim \begin{cases} A_{in}e^{-i\omega r_*} - A_{out}e^{i\omega r_*} & as \quad r_* \to +\infty, \\ B_{in}e^{-i\omega r_*} & as \quad r_* \to -\infty, \end{cases} \tag{1.22}$$

where we have to impose purely ingoing boundary condition at the black hole event horizon $r_* \to -\infty$, means waves entering in to the black hole and obviously nothing can come out. QNMs are the manifestation of the resonance oscillations of the black hole spacetime itself and it dominates the soon after the initial transient stage. During this stage of evolution we require a purely outgoing boundary condition at $r_* \to +\infty$. This means the incoming waves already passed and there is no other waves coming from ∞ to disturb the system and we set $A_{in} = 0$ in Eq.(1.22). While applying this boundary condition in to Eq.(1.16), one can obtain a discrete set of solutions, the QNMs having the time dependence, $e^{-i\omega_q t}$ with complex frequencies called the quasinormal(QN) frequencies.

$$\omega_q = \omega_R + i\omega_I \tag{1.23}$$

The real part of the QN frequency, ω_R corresponds to the actual oscillation frequency and the absolute value of the imaginary part, $|\omega_I|$ represents the rate at which each mode damps or grows. If the black hole is stable against the perturbations, it should have negative imaginary part for the QN frequencies, so that the perturbations will damp exponentially and the black hole can come to its equilibrium configuration. In this case part of the energy of the perturbations is carried away to infinity in the form gravitational radiations and

another part goes in to the black hole through the event horizon. In this sense these modes are not normal but 'quasinormal'.

It was Chandrasekhar and Detweiler who first computed the quasinormal frequencies of the Schwarzschild black hole and explored their properties[15].

Why QNMs are important?

QNMs emerged in the quest of understanding the stability of black holes. Even though one can not judge the stability completely, the existence of QNMs with $\omega_I < 0$ can at least ensures that the perturbations will decay with time and the BH is stable for that multipole order of perturbation. This is because the QNMs do not form a complete set and consequently, a general perturbation cannot be written as a combination of these modes[16].

The present interests in studying the QNMs can broadly classified in to two, astrophysical and theoretical.

(i) Astrophysical interests

The QNMs dominate the radiation from most dynamical process that involve a black hole. This ranges from the formation of black hole in a gravitational collapse to the collision of black holes: no matter how we kick a black hole, its response will be dominated by QNMs at intermediate time. If the new generation gravitational wave detectors manage to detect a gravitational wave signal from a black hole, the dominated contribution to such a signal will be the fundamental QNMs. The fundamental QN frequency for the quadrupole mode($\ell = 2$) in Schwarzschild spacetime is given by,

$$M\omega = 0.37367 - 0.08896i. \tag{1.24}$$

Converting to physical units, the frequency and damping time are

given by,

$$\begin{aligned} \nu &= 2\pi 5142(M\omega_R)\frac{M_\odot}{M}Hz \approx 12\frac{M_\odot}{M}kHz, \\ \tau &= \frac{1}{2\pi 5142(M\omega_I)}\frac{M}{M_\odot}s \approx 0.347\frac{M}{M_\odot}ms. \end{aligned} \tag{1.25}$$

The band width of ground based gravitational interferometer like Virgo and LIGO comes in the range about $10 - 40Hz$, up to few kHz. If the signal are sufficiently strong these detectors can detect the signals emitted by an oscillating black hole with mass in the range,

$$10M_\odot \lesssim M \lesssim 10^3 M_\odot. \tag{1.26}$$

The expected band width of the space based interferometer, LISA is $10^{-4}Hz$ to $10^{-1}Hz$, and this can detect the signal from black holes with mass range,

$$10^5 M_\odot \lesssim M \lesssim 10^8 M_\odot. \tag{1.27}$$

It is worthwhile to mention that the predicted black hole at the center of our galaxy, Sagittarius A^* have a mass $M \simeq 4.31\times 10^6 M_\odot$[3].

Although these studies refer to very idealized situations, they have been very useful because they showed that quasi-normal modes can be excited, and because they provided a first understanding of the mechanisms underlying the mode excitation. However, astrophysical phenomena are much more complicated, and only recently major advances in numerical techniques allowed the modeling of more realistic processes involving black holes. Black hole coalescence is probably the most violent process occurring in the Universe (after the big bang), and it is expected to be the most powerful source of gravitational waves to be detected by interferometric detectors Virgo and LIGO. Once we succeeded in recording these signals, one can easily deduce the parameters of the black hole in the precess, from

the fact that these signals in QNM stage depend only on the black hole parameters[17].

(ii) Theoretical interests

The extreme gravity of the black holes makes them the popular testing ground for the ideas of quantum gravity as the Hydrogen atom for the quantum mechanics. Consequently interpretations of their oscillations are also have a major role in understanding various puzzles in fundamental physics.

There are attempts to interpret the black area spectrum using the highly damped quasinormal modes. In 1974 Bekenstein proposed a heuristic argument to quantize black hole that the horizon area of a black hole is an adiabatic invariant, and therefore he conjectured that the black hole should have a discrete eigenvalue spectrum[18]. Later Hod concluded that the quantization condition of the black hole surface area should be of the form[19],

$$A_n = n\gamma l_p^2; \qquad n = 1, 2, ... \tag{1.28}$$

where l_p^2 is the Plank's length and γ is an undefined dimensionless constant. He further made use of the results of Nollert[20] that the highly damped QNMs of Schwarzschild black hole is independent of the multipole index and spin of field and is the characteristics of the black hole itself,

$$M\omega = 0.0437123 - \frac{i}{4}(n + \frac{1}{2}) + O[(n + 1)^{-1/2}], \tag{1.29}$$

and made the crucial observation that the real part of the this QNM exactly agrees with the expression $ln3/8\pi$. Identifying ω_R as the "transition frequency", he calculated the change ΔA in the area corresponds to a change, ΔM in mass,

$$\Delta M = \hbar\omega_R = \frac{\hbar l n 3}{8\pi M} \tag{1.30}$$

Since the area, A of Schwarzschild black hole, $A = 16\pi M^2$, Hod concluded that the $\Delta A = 4ln3l_p^2$ and identified the factor appearing in Eq.(1.28) as $\gamma = 4ln3$[19]. Statistical physics arguments also suggests that $\gamma = 4lnk$, k being a constant. These findings trigger a wealth of research on the QNM spectrum of various black holes. But the attempts to interpret the QNMs of Kerr black hole is still not succeeded.

Apart from their role in the quantization of black hole area, study of QNMs find significance in the correspondence between the anti-de Sitter(black hole solution with negative cosmological constant) spacetime and the Conformal Field Theory(CFT)[21]. The interpretation is that the decay of QNMs of black hole in AdS corresponds to relaxing of thermal state in CFT, to its equilibrium. Exact QNMs of AdS black holes[153] are usful for these studies.

For these reasons QNMs of black hole were extensively investigated in the past, for great variety of black hole spacetimes and for different types of field perturbations. Two excellent reviews on the topic are wrote in 90's[22, 23]. Recent reviews on the topic are available in [24–26].

1.4.2 Late-time tails

As we have already seen, the QNM stage in the evolution of perturbation around black holes lasts only for a limited period of time and is not the asymptotic behavior. At late times, the perturbations do not cut off sharply but decays as the 'tails' of perturbation. This observation was first made by Price[11], while studying the dynamics of nonspherical gravitational collapse. His original motivation was to see how does an imploding star with tiny mountains on its surface results in a perfectly spherical black hole. The answer he found

was, as now known as Price's theorem: "*Whatever can be radiated is radiated.*" It means the protrusions or any perturbations on the surface of the collapsing star will be converted in to ripples in the spacetime(gravitational radiation) once the horizon is formed, will get radiated away and makes the hole with a perfectly spherical shape[1].

Price showed that at late times of the formation a black hole described by the Schwarzschild spacetime, any multipoles with $\ell \geq s$, called the radiative multipole, of a field perturbation with spin, s, die out with a power-law tails,

$$\psi \sim t^{-(2\ell+p+1)}, \tag{1.31}$$

where $p = 1$, if a static ℓ-pole field is present outside the star, prior to the onset of collapse and if there is no field initially outside the star, but an ℓ-pole perturbation develops during the collapse process, then $p = 2$. Figure 1.5 demonstrates the numerical simulation of this feature for the later case.

Modes with $\ell < s$ do not evolve with time. These represent the conserved quantities and they are nonradiative. For gravitational perturbation, $s = 2$, a perturbation with $l = 0$ describes the change in the black hole mass and $\ell = 1$ describes an increment of small angular momentum. In the case of electromagnetic perturbation($s = 1$), the $\ell = 0$ mode represents the radially pointing electric field lines.

Later, in[27] a detailed analytical analysis supported by numerical results of massless fields around Schwarzschild and RN black hole showed that power-law tails are also present on null infinity where they decay as $u^{-(\ell+p)}$ and on future event horizon as $v^{-(2\ell+p+1)}$. Studies on the rotating black holes also suggest that the power-law tails holds for non-spherical black holes also[28–30]. Numerical analysis of fully non-linear dynamics of the fields, also indicates the same power-law decay pattern[31, 32].

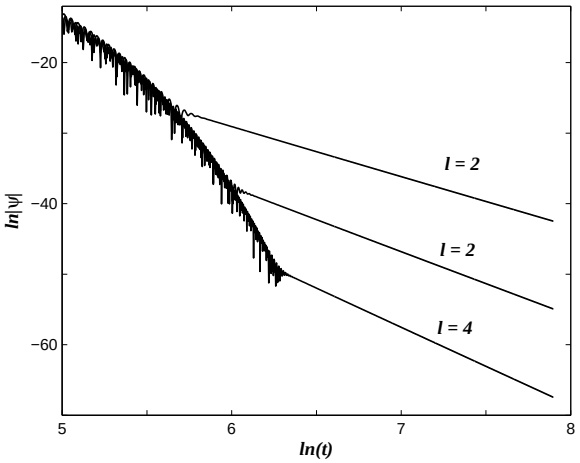

Figure 1.5: Late-time decay of gravitational perturbations around Schwarzschild spacetimes. Absolute value of wave amplitude, $|\psi|$ is plotted against time in logarithmic scales. A straight line in log-log plot corresponds to a power-law decay in time. At late times the perturbations decay as, $\psi \sim t^{-7}$, t^{-9} and t^{-11}, for $\ell = 2, 3$ and 4 multipoles of perturbations.

The late-time tails are due to the backscattering of the primary wave from the effective potential at great distances(asymptotic curvature). By a systematic study of various potentials Ching *et al.*[33] and later by Hod[34] had shown that the Schwarzschild case with a power-law tail is exceptional among the class of the potentials having a logarithmic spatial dependence and the the inverse power-law decay is a property of asymptotically flat spacetimes.

Why late-time tails are significant?

Price's theorem explains the mechanism of the working of '*no-hair theorem*' which predicts that any "hair"other than mass, charge and angular momentum, will disappear after a collapsing body settles

down to its stationary state. The physical mechanism responsible for the vanishing of these hairs is the radiative tails. For this reason the study of late-time tails are intriguing on its own.

Ching's[33] study revealed that depending on the spatial asymptotic, the late-time decay is not necessarily a power law in time. and that different behaviors should be expected in black-hole spacetimes that have different asymptotic properties. This is indeed the case. The existence of an exponentially decaying tails contrasting the power-law tails in asymptotically flat situation, was reported for spacetime with a non vanishing cosmological constant[35, 36].

The study of late-time tails has crucial relevance to the exploration of the internal structure of black holes. For black holes with more than one horizon, for example a charged black hole(which have a inner Cauchy horizon), the radiation that goes through the event horizon will eventually be blue shifted by an arbitrary large amount at the inner horizon[37]. The mass function of the black hole diverges at the Cauchy horizon called mass inflation and this effect is expected to preserve the causality. One of the key ingredient which determines the strength of the mass-inflation singularity at the Cauchy horizon inside charged and rotating black holes is radiative decay along outer horizon[38]. The knowledge of radiative tails on the event horizon provides the input for the internal wave evolution of such problem.

1.5 An overview to the thesis

1.5.1 Motivations

Black holes are the testing ground for many of our understandings about gravity, since they are the centers of extreme gravity. Since we can't expect any electromagnetic signals coming from a black hole, the

of the response of black holes to the external perturbations outside its event horizon is the best way to get information from these objects. As we have explained in the previous sections, these responses are dominated by the QNMs and late-time tails of the perturbations. Besides some relation to the perturbative field, the relaxation process reflects a characteristic of the background geometry.

On the other hand several shortcomings of Einstein's GTR were pointed in the past and there are several modifications to the GTR have been proposed motivated from observational evidences and other fundamental issues in the theory. Black hole perturbation in two such modified theories is the subject of study of this thesis.

The first one is the quintessence model put forward to explain the observed accelerated expansion of our Universe[49–51]. Second modification is a proposed model theory of renormalizable gravity called Hořava-Lifshitz gravity[52–54]. The evolution of field and the spectra of QNMs may be different in these theories of gravity and would help us to distinguish these theories.

1.5.2 Methods used

One can study the time evolution of perturbation once the solution of Eq.(1.16) is obtained. But the complex nature of effective potential precludes the exact solution in most cases. Several methods were introduced to tackle the evolution equation. These ranges from the direct numerical integration of the time-independent perturbation equation to various analytical approximations like Pöschl-Teller potential approximation, WKB techniques. The method of continued fractions and Horowitz-Hubeny method give accurate values of QNMs.

We use two effective methods for our studies, the WKB technique

and characteristic integration method.

- WKB method is a semi-analytic method originally developed by Schutz and Will[55], modifying the standard WKB technique to get QNMs for the lowest order. They made use of the barrier shape of the effective potential. The two WKB solutions were matched across both turning points simultaneously and obtain a formula for QNMs. Later Iyer and Will[56] carried this approach to third WKB order and Konoplya[57] to sixth order to get more and more accurate results and is found to be accurate for low lying modes. Comparing with other numerical methods, WKB method gives result with a relative error 0.5%, for lower frequency modes[58] and can be used to explore the QNM behavior of black holes efficiently, without going to the complicated numerical methods. This method is explained in Chapter 2.

- The most direct approach to study the evolution of perturbation is the numerical integration of the time-dependent perturbation equation and obtain directly the wave form. An effective method was developed in[27], after recasting the wave equation, in the null coordinates and using the finite difference scheme. This approach gives the complete evolution profile with prominent frequencies of the QNM stage and the late-time behavior. This method is described in Chapter 3.

We take the mass of the hole, M equal to unity for the numerical calculations unless otherwise mentioned and measure other quantities like charge of the black hole and mass and charge of fields etc., in terms of black hole mass.

1.5.3 Outline

The evolution of field perturbations in black hole spacetimes in the modified theories of gravity is the subject of study of the present thesis. The signature of new theories on the evolution of fields on the black hole spacetimes is probed. The entire work presented in the thesis is divided in to five chapters and a final concluding chapter.

In the following three chapters we describes the investigations on the black holes in a quintessence filled Universe. **Chapter 2** comprise the evolution of massive charged scalar field perturbations around a Reissner-Nördstrom black hole surrounded quintessence. The QNMs are evaluated and its behavior is analyzed for various parameters involved in the problem. **Chapter 3** contains the study of the late-time evolution of massless integer spin fields around Schwarzschild black hole surrounded by quintessence. The complete evolution profile is obtained through numerical method and the late-time decay is studied in detail. **Chapter 4** examines the late-time behavior of Dirac field around Schwarzschild black hole encircled by quintessence.

Next two chapters describes our attempts to distinguish the Hořava-Lifshitz gravity from standard GTR, from the knowledge of the evolution of field around spherically symmetric black hole in these theories. This part is split up in to two chapters. **Chapter 5** is dedicated to the study of the evolution of massless field perturbations in the spacetime geometry black hole in the HL gravity. The QNM and late-time phase of evolution is obtained and compared with the results in GTR. **Chapter 6** concerns the study of the evolution of massive scalar field in the spacetime geometry of black hole in HL gravity by numerical analysis.

Chapter 7 presents the overall conclusion of the works described in the thesis and in the light of this, future scops are discussed.

2

Massive, charged scalar field around a charged black hole surrounded by quintessence

2.1 Introduction

2.1.1 The expanding Universe

During 1920s, Alexander Friedmann showed that the Einstein's equation admits a solution with an expanding Universe. Initially Albert Einstein declined this notion because, like most of the 20th century physicists, he believed in the concept of a static Universe and five years earlier he had published a static model of the Universe. Later, Einstein admitted his mistake and conceded that his field equations do allow the possibility of an expanding universe.

In 1929, Edwin Hubble, who was analyzing the spectra of light coming from distant galaxies, made the remarkable discovery which completely revolutionized astronomy. He noticed that the spectra coming from most of the galaxies are shifted towards the red region indicating that they are moving away from us. By cataloging the distances to these galaxies Hubble formed what we now know as "Hubble's Law": the residing velocity of the distant galaxy is proportional to its distance from us and thus he concluded that the universe is

expanding. These discoveries made the building block of the modern Big Bang theory.

Later in 1980, the cosmic inflation model of the universe was proposed by Alan Guth to overcome some of the enigma of the Big Bang cosmologies. The model predicts a flat Universe and the total energy density of the Universe is equal to the critical density, the energy density required for the universe to be spatially flat. Observations point towards a spatially flat Universe and the prediction of inflation theory is consistent with current measurements of CMB anisotropy by the WMAP spacecraft. But current calculations suggest the total matter density of the Universe only amounts to about one third of the required critical density indicating the presence of a missing component.

In 1998, two groups of scientists, the High-z Team headed by Schmidt and Riess[59] and the Supernova Cosmology Project by Perlmutter[60] independently made another path breaking discovery in modern cosmology. Analyzing the type Ia supernovae (SNe Ia) at high redshifts, they reached the conclusion that the expansion of the universe is now accelerating rather than holding steady or decelerating. The discovery of cosmic acceleration opens a deep mystery because the two known constituents of the universe, ordinary matter and radiation will gravitationally attract each other and therefore should lead to a slowing down of the expansion. Since the expansion is speeding up we are forced to believe that there is some mysterious form of energy density called dark energy permeating all around the universe which pushes the galaxies each other against their gravitational attraction, thus causing the expansion of the Universe to speed up. At present we hardly know what exactly this dark energy is, how it originates or how it works.

The field equation describing the dynamics of the Universe can take the form of an equation for the second time derivative of the expansion factor,

$$\frac{\ddot{a}}{a} = -\frac{4\pi}{3}\sum_i(\rho_i + 3p_i). \tag{2.1}$$

Both the energy and the pressure govern the dynamics of the Universe and the algebraic combination, $\sum_i(\rho_i + 3p_i)$ contributed by the gravitational effect of various components determines the expansion rate. It is customary to define the parameter representing each component of the mass-energy, by the ratio of their pressure to density, known as equation of state(EOS), $\epsilon_i = p_i/\rho_i$. For ordinary gas, ϵ_i is positive, ordinary matter $\epsilon_i = 0$ and for radiation $\epsilon_i = 1/3$. Each component contributes an amount $-4\pi\rho_i(1 + 3\epsilon_i)$ to the expansion factor $\ddot{a}/a$. Since the energy density, ρ_i is a positive quantity, it requires a component with sufficient negative pressure(ϵ_i drops below -1/3) for a positive value of $\ddot{a}/a$. Thus ark energy requires a negative pressure to drive the acceleration of the Universe. We can take this to be the defining property of dark energy.

2.1.2 The Cosmological constant

The simplest and oldest candidate for dark energy is the cosmological constant, Λ, which was first introduced by Einstein for the purpose of constructing a static model of the Universe. When he applied GTR to cosmology Einstein could not get a stationary solution to the field equations. So he modified the original field equations by adding a positive constant term to the field equations and adjusted the value of the constant so that the gravitational attraction of matter would exactly counterbalanced by this term. Later, he regretfully dropped this idea knowing the findings of Hubble.

However, observations including the discovery of cosmic acceleration and measurements of the CMBR have brought the cosmological constant back in to the picture. If the cosmological constant had a slightly larger value than Einstein proposed for getting a static solution, its repulsion would exceed the attraction of matter, and induces cosmic acceleration. Cosmological constant has ϵ precisely equal to -1. It has the same value everywhere in space for all time, and is chemically inert. Even though the model with cosmological constant (ΛCDM) provides a reasonably good match to the observations, there are some fundamental issues.

The cosmological constant, Λ was later identified to be mathematically equivalent to the vacuum energy, an energy inherent to empty space itself. The principle of quantum field theory allows the quantum fluctuation in empty space and the resulting zero-point energy for empty space. An estimate of the total vacuum energy produced by all known fields predicts the vacuum energy density $\rho_{\Lambda}^{cal} \approx 10^{76} GeV^4$. But this predicts a huge amount-123 orders of magnitude more than than the present observed value $\rho_{\Lambda}^{obs} \approx 10^{-47} GeV^4$. This is called the cosmological constant problem[61, 62] and a fundamental solution to this problem has not yet been found.

So it requires some cancellation mechanism which zeros out most of the vacuum energy. One proposal is that there may be some secret symmetry in fundamental physics results in a cancellation of large effects. But it is hard to conceive why the mechanism only cancels to 120 decimal places instead of making the cosmological constant exactly zero. To explain the amount of dark energy today, the value of the cosmological constant would have to be fine tuned at the creation of the universe to have the proper value.

2.1.3 Quintessence models

Fortunately, vacuum energy is not the only way to generate cosmic acceleration. Alternatively, dark energy may be a transient phenomenon and the realm of possibilities goes under the rubric of *quintessence*[49–51]. The word quintessence stands for '*fifth element*'in the ancient and in medieval philosophy, earth, air, fire and water being the other four components that constitute the Universe, according to their imagination. It seems adequate to give this name to the contribution to the overall mass-energy content of the Universe, in addition to the previously known baryons, leptons, photons and dark matter.

Unlike Λ, which has the same value everywhere in space for all time, quintessence is dynamical, which can interact with matter, vary with space and evolve in time. For quintessence, ϵ has no fixed value, but it must be $\leq -1/3$, for a repulsive nature. Quintessence generates the required repulsive force from the energy resulting from the potential energy of a dynamical field, a mechanism similar to the inflationary cosmology theory, in which the inflation field drives the expansion in the early Universe. But the repulsive force excreted by quintessence is much weaker than the inflation. Quintessence may take many forms. The simplest model for quintessence is the energy density associated with a scalar field, ϕ slowly rolling down in a potential $V(\phi)$. The energy density for a homogeneous scalar field is a sum of kinetic, and potential energies and pressure is the difference of the two,

$$\rho = \frac{1}{2}\dot{\phi}^2 + V(\phi); \qquad p = \frac{1}{2}\dot{\phi}^2 - V(\phi). \tag{2.2}$$

The kinetic term has positive pressure and the potential term has negative pressure and the total pressure can be negative if the field rolls slowly enough that the kinetic energy density is less than

the potential energy density. To realize the cosmic acceleration the equation of state,

$$\epsilon_\phi \equiv \frac{p}{\rho} = \frac{\frac{1}{2}\dot{\phi}^2 - V(\phi)}{\frac{1}{2}\dot{\phi}^2 + V(\phi)}, \tag{2.3}$$

must be less than $-1/3$. Quintessence is characterized by its equation of state, $-1/3 \geq \epsilon > -1$. The smaller the value of ϵ, the greater its acceleration effect. Quintessence with ϵ near -1 may be the closest reasonable approximation. Since the value of ϵ differs from that of vacuum energy, quintessence produces a different rate of cosmic acceleration. Even though these dynamical dark energy candidates lack a concrete motivation from fundamental physics, quintessence hypothesis is found to be fit with many of the current observations. More precise measurements of supernovae over a longer span of distances and imprint on the CMB anisotropy and mass power spectrum may separate the two cases in future.

2.2 Quintessence and black holes

The exact solution for the Einstein's equations for a static spherically symmetric charged black hole surrounded by the quintessential matter under the condition of additivity and linearity in energy momentum tensor is obtained by Kiselev[63]. The general metric of spherically symmetric static gravitational fields is given by,

$$ds^2 = e^\nu dt^2 - e^\lambda dr^2 - r^2(d\theta^2 + \sin^2\theta d\phi^2). \tag{2.4}$$

Now the Einstein's equation for this spacetime have the form,

$$2T_t^t = -e^{-\lambda}\left(\frac{1}{r^2} - \frac{\lambda'}{r}\right) + \frac{1}{r^2}, \tag{2.5}$$

$$2T_r^r = -e^{-\lambda}\left(\frac{1}{r^2} + \frac{\nu'}{r}\right) + \frac{1}{r^2}, \tag{2.6}$$

$$2T_\theta^\theta = 2T_\phi^\phi = -\frac{1}{2}e^{-\lambda}\left(\nu'' + \frac{\nu'^2}{2} + \frac{\nu' - \lambda'}{r} - \frac{\nu'\lambda'}{2}\right), \tag{2.7}$$

where prime denotes differentiation with respect to r. The principle of linearity and additivity defines as,

$$T_t^t = T_r^r \Rightarrow \lambda + \nu = 0. \tag{2.8}$$

Under this condition, the energy momentum tensor for the quintessence is given by,

$$\begin{aligned} T_t^t &= T_r^r = \rho_q, \\ T_\theta^\theta &= 2T_\phi^\phi = -\frac{1}{2}\rho_q(3\epsilon + 1), \end{aligned} \tag{2.9}$$

where ϵ is the quintessence EOS which is connected to the density as,

$$\rho = \frac{-c}{2}\frac{3\epsilon}{r^{3(1-\epsilon)}}. \tag{2.10}$$

Since the density of energy to be positive for quintessence, $\rho > 0$ and ϵ to be negative, we demand that the normalization factor $c \geq 0$. Defining $\lambda = -ln(1+f)$, we get an equation for f as,

$$(3\epsilon + 1)f + 3(1+\epsilon)rf' + r^2 f'' = 0, \tag{2.11}$$

with the solutions of the form, $f = 1 - \frac{r_g}{r} - \frac{c}{r^{3\epsilon+1}}$, c and r_g being normalization factors. Thus the general form of spherically symmetric charged solutions for Einstein's equation describing black hole with energy momentum tensor satisfies the additivity and linearity condition, so that the metric is given by,

$$ds^2 = -f(r)dt^2 + f(r)^{-1}dr^2 + r^2 d\Omega^2, \tag{2.12}$$

with,

$$f(r) = \left(1 - \frac{2M}{r} + \frac{Q^2}{r^2} - \frac{c}{r^{3\epsilon+1}}\right), \quad d\Omega^2 = (d\theta^2 + \sin^2\theta d\phi^2), \tag{2.13}$$

M and Q can be identified as the mass and the charge of the black hole respectively. In the limit $c = 0$, the metric reduces to the pure RN spacetime.

The studies on QNMs of black holes were started in the presence of quintessence, after the spacetime for a black hole with quintessential matter were derived by Kiselev. Earlier works considered the simplest case, the Schwarzschild black hole surrounded by quintessence [64–68] and obtained the QNMs by WKB method.

But one can expect a charged black hole, formed when the matter which collapses to form a black hole have a net charge and a charged perturbations will develop outside the collapsing star. And if quintessence exists everywhere in the universe, it will surely distort the spacetime around black holes. So it is interesting to see how the perturbations of RN black hole behave in the presence of quintessence. In this work we are addressing this question by considering massive charged scalar field perturbations.

2.3 Scalar field around charged black hole surrounded by quintessence

2.3.1 Evolution of scalar perturbations

Now we consider massive charged scalar filed perturbations around the charged black hole spacetime given by Eq.(2.12). The scalar per-

turbations can be described by the Klein-Gordon(KG) equation[37, 72],

$$\Phi_{;\mu\nu}g^{\mu\nu} - ieA_\mu g^{\mu\nu}(2\Phi_{;\nu} - ieA_\nu\Phi) - ieA_{\mu;\nu}g^{\mu\nu}\Phi = m^2\Phi, \quad (2.14)$$

where A_μ is the electromagnetic potential and e and m are the charge and mass of the scalar field. In a spherically symmetric space-time specified by Eq.(2.12), the KG equation can be simplified to,

$$\begin{aligned}\frac{1}{f(r)}\partial_t^2\Phi - \frac{1}{r^2}\left(r^2 f(r)\partial_r^2 + 2rf(r)\partial_r + r^2\partial_r f(r)\partial_r\right)\Phi + \\ \left(-\frac{1}{r^2 sin\theta}\left(sin\theta\partial_\theta^2 + cos\theta\partial_\theta\right) - \frac{1}{r^2 sin^2\theta}\partial_\phi^2\right)\Phi - \\ \left(2ieA_t g^{tt}\partial_t - e^2A_t^2 g^{tt}\right)\Phi = \ 0. \quad (2.15)\end{aligned}$$

Expanding the charged scalar field in scalar spherical harmonics,

$$\Phi = \frac{1}{r}\sum_{l,m}\eta_m^l(t,r)Y_l^m(\theta,\phi), \quad (2.16)$$

the wave equation can be reduced to an equation for the scalar function, $\eta_m^l(t,r)$ for each multipole moment:

$$\frac{\partial_t^2\eta}{rf(r)} + \frac{\ell(\ell+1)}{r^3} - \frac{2ieA_t\partial_t\eta}{rf(r)} - \frac{e^2A_t^2}{f(r)} - \frac{\partial_r f(r)}{r^2} - f(r)r\partial_r^2\eta = 0, \quad (2.17)$$

where the centrifugal term comes from the action of the angular momentum operator on the spherical harmonics,

$$\begin{aligned}-\left(\partial_\theta^2 + cot\theta\partial_\theta + 1/sin^2\theta\partial_\phi^2\right)Y_l^m(\theta,\phi) &= \vec{L}^2Y_l^m(\theta,\phi) \quad (2.18)\\ &= \ell(\ell+1)Y_l^m(\theta,\phi).\end{aligned}$$

Now using the coordinate transformation defined by,

$$dr_* = \frac{dr}{f(r)}, \tag{2.19}$$

we can rewrite the perturbation equation as,

$$\partial_t^2\eta - 2ieA_t\partial_t\eta - \partial_{r_*}^2\eta + f(r)\left[\frac{l(l+1)}{r^2} + \frac{\partial_r f(r)}{r} + m^2\right]\eta - e^2A_t^2\eta = 0. \tag{2.20}$$

The time component of the electromagnetic potential, $A_t = C - \frac{Q}{r}$, with C being a constant and to avoid this physically unimportant quantity, we define,

$$\eta = e^{ieCt}\psi, \tag{2.21}$$

The auxiliary field, ψ assumes to have a harmonic time dependence $e^{-i\omega t}$. Now the radial perturbation equation can be written as,

$$\frac{\partial^2\psi}{\partial r_*^2} + \Theta\psi = 0, \tag{2.22}$$

where $\Theta = \omega^2 - V^2$, V being the effective scattering potential, arises from the curvature of the spacetime, is given by,

$$V = f(r)\left(\frac{l(l+1)}{r^2} + \frac{2M}{r^3} - \frac{2Q^2}{r^4} + \frac{c(3\epsilon+1)}{r^{3\epsilon+3}} + m^2\right) + \frac{2eQ\omega}{r} - e^2\frac{Q^2}{r^2}. \tag{2.23}$$

It can be noticed that the effective potential depends not only on the parameters, M, Q, ℓ and e but also on the frequency of perturbation, ω. This will make it difficult to evaluate the quasinormal mode frequencies using the WKB approximation. Figure2.1 shows the general behavior of the potential. It can be observed that the height of the potential barrier decreases if quintessence is present and the asymptotic value, $V(r \to \infty)$ increases with mass of the field.

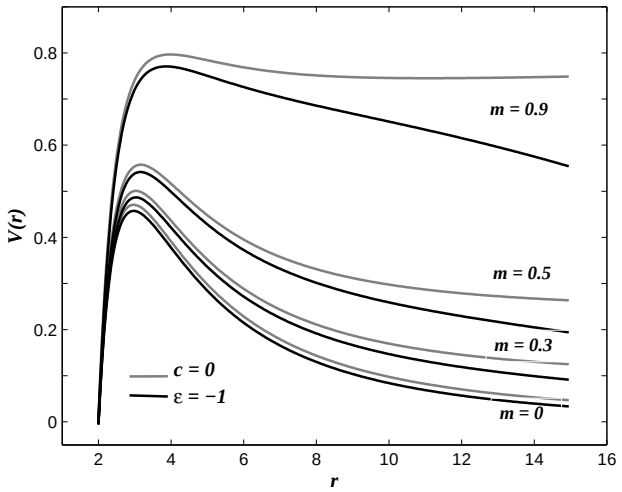

Figure 2.1: Effective potential for different field masses for $l = 3, Q = 0.1, e = 0, \epsilon = -1$ and $c = 0.01$ along with the the Schwarzschild case($c = 0$).

2.3.2 Quasinormal modes of perturbations

The third order WKB approximation method can be used to determine the complex normal mode frequencies of black hole. This method gives a simple condition which can be used to get the discrete, complex frequencies of the normal modes,

$$\frac{i\Theta_0}{\sqrt{2\Theta_0''}} - \Lambda(n) - \Omega(n) = n + \frac{1}{2}, \tag{2.24}$$

where n is the mode number, Λ and Ω are second and third order WKB correction terms,

$$\Lambda = \frac{1}{(-2\Theta_0'')^{1/2}} \left[\frac{1}{8} \left(\frac{\Theta_0^{(4)}}{\Theta_0''} \right) \left(\frac{1}{4} + \alpha^2 \right) - \left(\frac{\Theta_0'''}{\Theta_0''} \right)^2 \frac{\left(7 + 60\alpha^2\right)}{288} \right], \tag{2.25}$$

$$\Omega = \frac{1}{(-2\Theta_0'')}\left\{\frac{5}{6912}\left(\frac{\Theta_0'''}{\Theta_0''}\right)^4\left(77+188\alpha^2\right)-\frac{1}{384}\left(\frac{\Theta_0'''^2\Theta_0^{(4)}}{\Theta_0''^3}\right)\left(51+100\alpha^2\right)+\frac{1}{2304}\left(\frac{\Theta_0^{(4)}}{\Theta_0''}\right)^2\left(67+68\alpha^2\right)+\frac{1}{288}\left(\frac{\Theta_0'''\Theta_0^{(5)}}{\Theta_0''^2}\right)\left(19+28\alpha^2\right)+\frac{1}{288}\left(\frac{\Theta_0^{(6)}}{\Theta_0''}\right)\left(5+4\alpha^2\right)\right\}, \tag{2.26}$$

$$\alpha = n+\frac{1}{2}, \quad n=\begin{cases} 0,1,2,.....Re(E)>0 \\ -1,-2,-3,.....Re(E)<0 \end{cases} \tag{2.27}$$

where,

$$\Theta_0^{(n)} = \left.\frac{d^n\Theta}{dr_*^n}\right|_{r_*=r_*(r_0)}, \tag{2.28}$$

denotes the nth derivatives of Θ evaluated at r_0, the value of r at which V attains maximum. Here a complexity arises from the fact that the potential V is a function of frequency ω. This makes difficult to calculate the numerical value of r_0. We make use of the procedure suggested by Konoplya[73] to find r_0 by fixing all the parameters other than ω, on which V depends and then find the value of r at which V attains maximum as a numerical function of ω. Substituting this value of r_0, we have found the values of real and imaginary parts of ω which satisfies the condition (2.24) by numerical methods.

It is a general experience that the quasinormal frequencies with lower mode number will decay slowly and are relevant to the description of fields around the black hole. So we consider frequencies of low lying modes for our study. For a charged black hole the relative error of third order WKB method is of the order of 10^{-2} for $l=3$, $n=0$ mode[74]. We put the normalization factor, $c=0.01$, so that

the deviation of frequencies from the pure RN case can be clearly understood and is much larger than the relative WKB error. In what follows we examine the behavior of QNMs.

First, we analyze the dependence of QNMs on the charge of the black hole, Q, in the presence of quintessence. Figures2.2 and 2.3 shows the real and imaginary parts of ω as a function of Q for fixed $l = 3, n = 0, e = 0.1, m = 0.1$ and for different values of ϵ. The case with absence of quintessence is also plotted. The plot shows that the quasinormal frequencies for scalar field in a charged black hole is influenced by quintessence. The magnitudes of real and imaginary parts of ω is lower in the presence of quintessential field. This implies that due to the presence of quintessence, the quasinormal mode frequencies for scalar field in RN black hole damps more slowly. In the presence of quintessence, $Re(\omega)$ increases monotonically with the increase in Q while the magnitude of $Im(\omega)$ first decreases, falling to

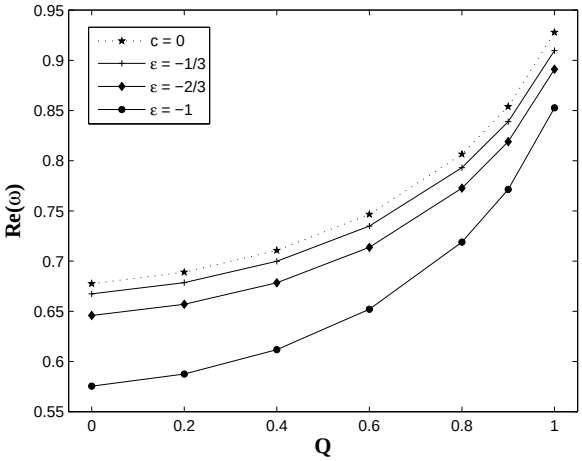

Figure 2.2: $Re(\omega)$ as a function of Q for $l = 3, n = 0, e = 0.1, m = 0.1$ and for different values of ϵ with $c = 0.01$. The dotted line represents the no quintessence case(c=0).

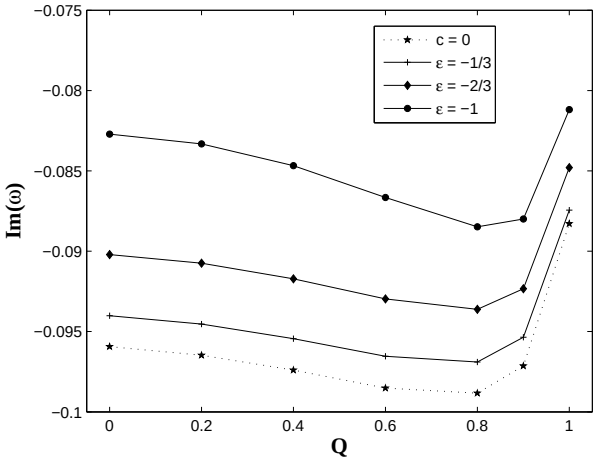

Figure 2.3: $Im(\omega)$ as a function of Q for $l = 3, n = 0, e = 0.1, m = 0.1$ and for different values of ϵ with $c = 0.01$. The dotted line represents the no quintessence case(c=0).

a minimum around $Q = 0.8$ and thereafter increases sharply. If we discard quintessence ($c = 0$) the results coincide with those obtained in [75, 76].

Figure2.4 shows the explicit dependence of $Re(\omega)$ and $Im(\omega)$ with quintessential parameters c and ϵ for fixed $l = 3, n = 0, e = 0, Q = 0.5$ and $m = 0.1$. For a fixed c, as the value of ϵ increases, $Re(\omega)$ increases while the magnitude of $Im(\omega)$ increases meaning damping is less for lower values of ϵ. As the normalization factor c increases, $Re(\omega)$ decreases and magnitude of $Im(\omega)$ decreases. In Figure2.5 $Re(\omega)$ and $Im(\omega)$ are plotted as functions of e with $l = 3, n = 0, m = 0.1$ for $Q = 0.1, 0.3$ and different values of ϵ. Dotted line represents absence of quintessence(c=0). The variation is almost linear. In the presence of quintessence, the magnitudes of $Re(\omega)$ and $Im(\omega)$ increase with e, as in the no quintessence case ($c = 0$), but with lower values of $Re(\omega)$ and $|Im(\omega)|$. A neutral field decays slower than a charged field.

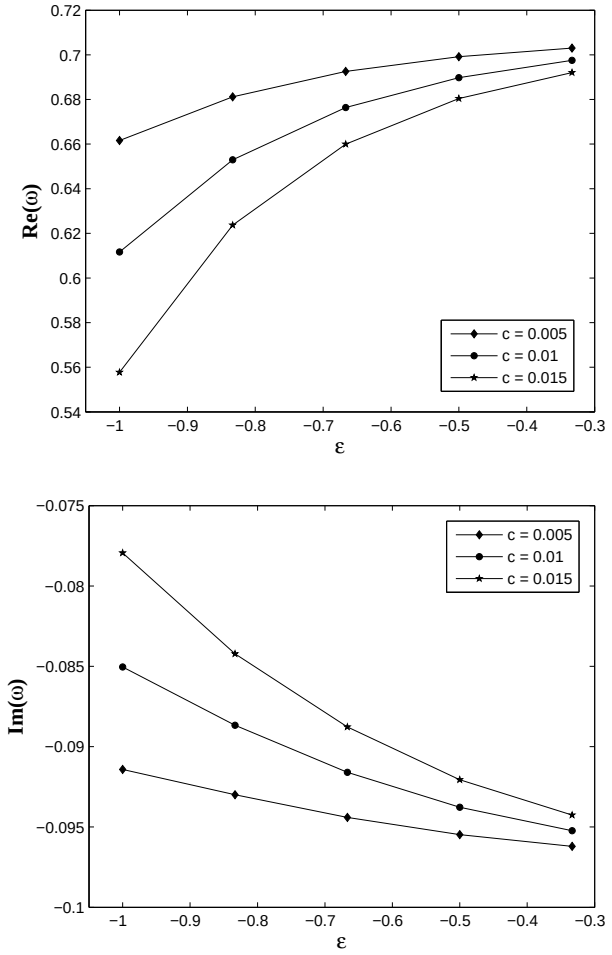

Figure 2.4: Variation of $Re(\omega)$ and $Im(\omega)$ with quintessence parameters ϵ and c, for $l = 3, n = 0, e = 0, Q = 0.5$ and $m = 0.1$

Finally, we study the role of mass of scalar field on quasinormal frequencies. For low-lying QNMs, to occur tunneling, ω^2 must be smaller than the peak value of the potential $V(r = r_{max})$ and the energies of the field are always larger than m^2[12]. This means that there is a maximum value for mass, m_{max} beyond which quasinormal modes will not exist. The value of m_{max} can be calculated from the

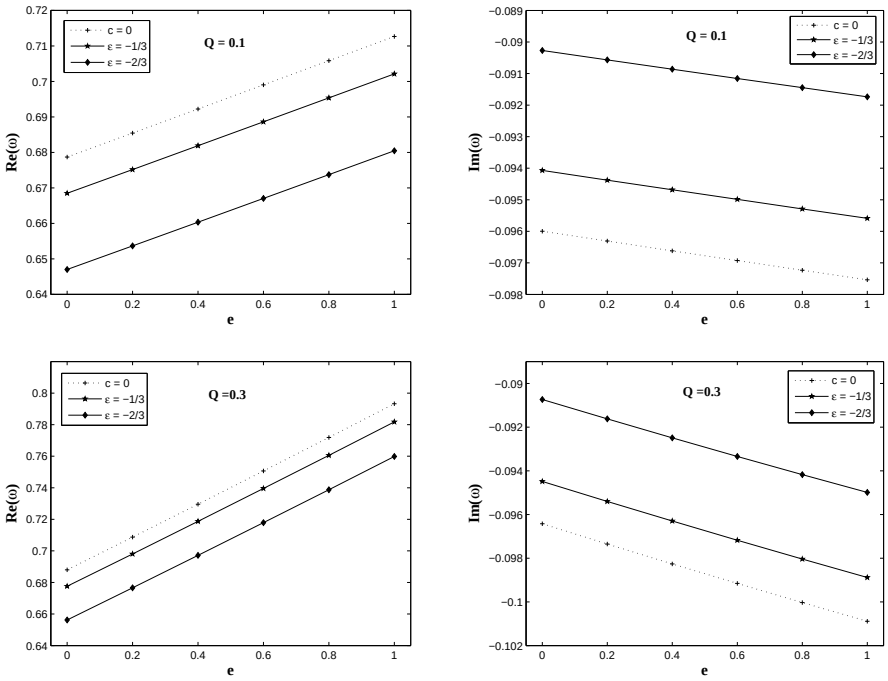

Figure 2.5: Variation of $Re(\omega)$ and $Im(\omega)$ with e, for $l = 3, n = 0, m = 0.1$, $Q = 0.1, 0.3$ and different values of ϵ. Dotted curve is for $c = 0$.

condition for the existence of quasinormal modes,

$$V(r_{\max,}\omega = m_{\max}) = (m_{\max})^2 \tag{2.29}$$

These values of m_{max} obtained for different values of ϵ are tabulated in Table2.1. In the presence of quintessence, m_{max} decreases because quintessence lowers the height of the potential barrier as we have seen in Figure2.1 and when $\epsilon = -1$, it has the lowest value.

WKB approximation gives less accurate results as the mass of the field increases but we can use this method to obtain the qualitative dependence of QNMs on field mass. The dependence of QNMs on mass of scalar field is plotted in Figures2.6 and 2.7. $Re(\omega)$ increases

c	ϵ	m_{max}
0	–	0.88516
0.01	-1/3	0.86762
0.01	-2/3	0.81848
0.01	-1	0.67582

Table 2.1: The limit of mass of scalar field, m_{max} for the existence of quasinormal frequencies with $l = 3, e = 0, Q = 0.1$

with increase in mass, while $|Im(\omega)|$ decreases, which indicates that QNMs of massive fields damp slowly. This behavior is in agrement with numerical results obtained in [75].

But QNMs behave abnormally near m_{max}. This is due to the fact that for larger values of field mass, the potential looses its barrier shape by broadening the potential peak as shown in Figure2.1 and WKB method gives less accurate results. Lower modes show less abnormality showing that WKB method is more accurate for fundamental modes. An interesting feature, we noticed is that this abnormal behavior is lower in the presence of quintessence and when the quintessential parameter $\epsilon = -1$, we can get a satisfactory curve because of the peak of effective potential broadens much less in the presence of quintessence comparing with the normal case(c=0) as understood from Figure2.1 and quintessence helps to retain barrier shape and give more accurate results at larger mass range.

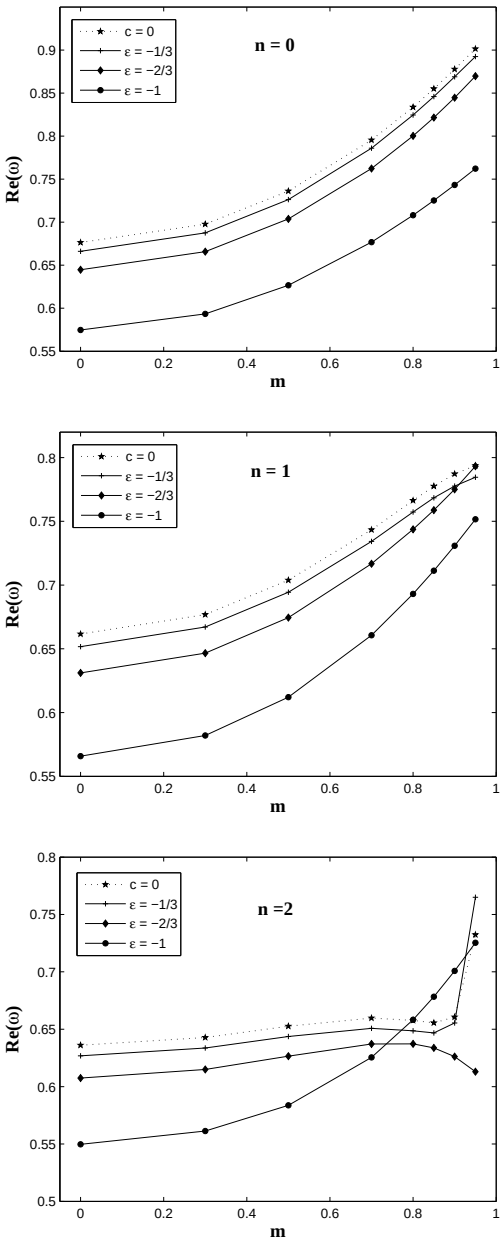

Figure 2.6: Variation of $Re(\omega)$ with m, for $l = 3, e = 0, Q = 0.1, n = 0, 1, 2$ and different values of ϵ. Dotted curve represents the Schwarzschild case.

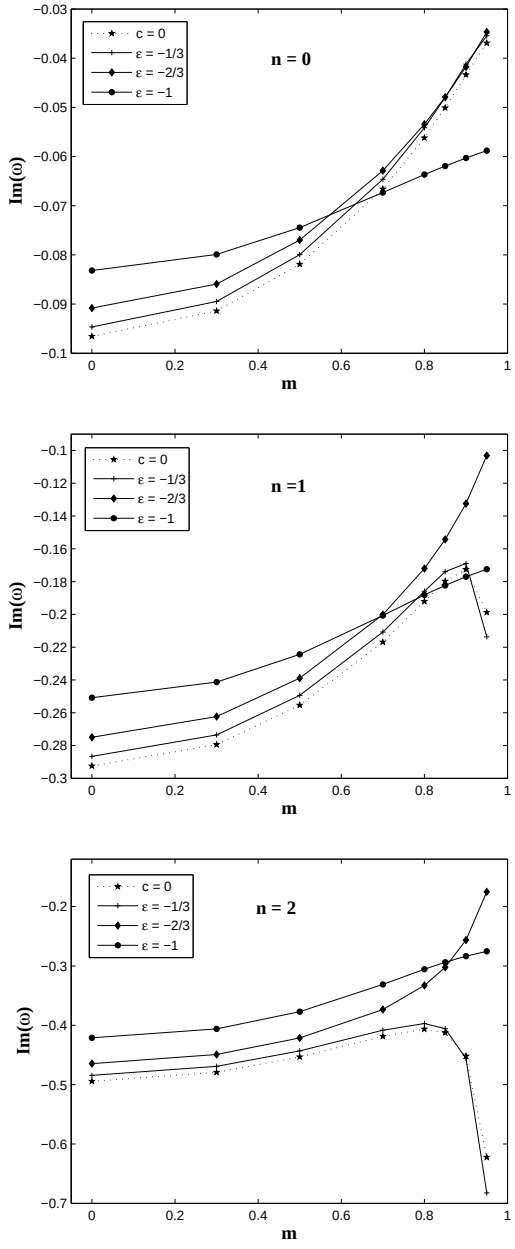

Figure 2.7: Variation of $Im(\omega)$ with m, for $l = 3, e = 0, Q = 0.1, n = 0, 1, 2$ and different values of ϵ. Dotted curve is for the Schwarzschild case.

2.4 Conclusion

The studies on the perturbations of black holes in accelerated expanding Universe with quintessence model for dark energy are presented in this chapter. Massive charged scalar field perturbations are considered around the charged black hole immersed in quintessence and WKB approximation method are used to evaluate the associated QNMs. The results show that quintessence influences the QNMs of charged black hole. It shows a decrease in the oscillation frequency and slowing up in the damping of QNMs in the quintessence present case than the asymptotically flat spacetime case. The behavior of QNMs vary as the equation of state for the quintessence changes. The damping are less for lower values of ϵ. The dependence of QNMs on other parameters such as charge of black hole Q, charge and mass of scalar field is similar to that obtained in quintessence less case, but with lower oscillation frequency and higher damping time. The effect of quintessence is to retain the barrier shape of effective potential for larger field masses and thus to reduce the abnormal behavior of QNMs evaluated using WKB method at these mass ranges.

3

Late-time tails of Schwarzschild black hole surrounded by quintessence

3.1 Introduction

PRESENTLY we have a clear picture about the late-time behavior of the radiating fields around black holes with asymptotically flat spacetime, during the process of gravitational collapse. All the radiative multipole ($\ell \geq s$) of any field with spin s, will completely radiated away during the late stage of collapse with a power-law fall off of the field $t^{-(2\ell+p+1)}$ at late times[11]. The non-radiatable multipoles ($\ell < s$) of the collapsing star are happened to be the only three non vanishing hairs of the subsequently formed black hole and the mechanism responsible for the relaxing to this final asymptotic state is the late-time decay. The study of the radiative tails of perturbations at late times plays a crucial role in the exploration of the internal structure of black holes[77]. The knowledge of late-time radiative tails serve as initial data for studies of the interior of the black hole and plays a major role in the analysis of the stability of inner Cauchy horizon.

The late-time tails in black hole spacetimes are understood as a

result of particular form of the effective potential far away from the black hole. The tails are generated by the scattering of the waves off by the effective potential at great distances. By a systematic study of various potentials Ching *et al.*[33] and later by Hod[34] had shown that the inverse power-law decay is a property of asymptotically flat spacetimes and that different behaviors should be expected in black-hole spacetimes that have different asymptotic properties.

The evolution of fields propagating on spacetime with a non vanishing cosmological constant was addressed in[35] and suggested that an exponential decay of the tails replaces the power-law behavior observed in asymptotically flat spacetimes. The first detailed numerical investigation in to the late-time behavior of fields propagating in black hole in de Sitter spacetimes were performed by Brady et al.[36, 78]. They have studied, in some detail, the behavior of a massless, minimally coupled scalar field propagating on spherically symmetric spacetimes with a positive cosmological constant and demonstrated the existence of exponentially decaying tails at late times. The evolution of electromagnetic and gravitational perturbations propagating on black holes with de Sitter backgrounds were studied in[81].

Spherically symmetric black hole solutions[63] were obtained in quintessence model of dark energy and many authors[64–71] considered the evolution of various fields around black holes surrounded by quintessence. All these studies are based on the calculation of the QNMs using the third order WKB approximation method while the late-time behavior remained unexplored till now. In fact the late-time decay is determined by the asymptotic curvature of the spactime, so it is interesting to see how the fields evolve in a spacetime in which the asymptotic structure is modified by the quintessence field.

3.2 Fields around black hole surrounded by Quintessence

To explore the late-time behavior of field perturbations in a black hole spacetime in the presence of quintessence, we here consider the static, spherically symmetric, uncharged black hole surrounded by the quintessential matter. The relevant metric is obtained in[63],

$$ds^2 = -f(r)dt^2 + f(r)^{-1}dr^2 + r^2(d\theta^2 + \sin^2\theta d\phi^2), \tag{3.1}$$

where,

$$f(r) = \left(1 - \frac{2M}{r} - \frac{c}{r^{3\epsilon+1}}\right), \tag{3.2}$$

and ϵ is the quintessential state parameter and c, the normalization factor. It is difficult to analyze the evolution of perturbations around the above metric for arbitrary values of the parameter ϵ. For our study we take three special cases of the quintessence parameter, $\epsilon = -1/3, -2/3, -1$ and the Schwarzschild case($c = 0$), so that the calculations become viable.

Case1 $\epsilon = -1/3$ **:** the black hole event horizon is located at $r_{e1} = 2M/(1-c)$, corresponding to zero of the function, $f(r)$ and the tortoise coordinate can be defined as,

$$r_* = r + r_{e1} ln(r - r_{e1}). \tag{3.3}$$

Case2 $\epsilon = -2/3$ **:** here, in addition to the black hole event horizon at $r = r_{e2}$ the spacetime possesses a cosmological horizon at $r = r_{c2}$, with $r_{e2} < r_{c2}$. In terms of these horizons we can write $f(r)$ as,

$$f(r) = \frac{c}{r}(r - r_{e2})(r_{c2} - r). \tag{3.4}$$

The surface gravity associated with the horizons at $r = r_i$, is defined by

$$\kappa_i = \frac{1}{2}|df/dr|_{r=r_i}, \tag{3.5}$$

and we get,

$$\kappa_{e2} = \frac{c(r_{c2} - r_{e2})}{2r_{e2}}, \qquad \kappa_{c2} = \frac{c(r_{e2} - r_{c2})}{2r_{c2}}. \tag{3.6}$$

These quantities allow us to write,

$$\frac{1}{f} = \frac{1}{2\kappa_{e2}(r - r_{e2})} + \frac{1}{2\kappa_{c2}(r - r_{c2})}. \tag{3.7}$$

Now we can get an expression for the tortoise coordinate, $r_* = \int f^{-1}dr$ as,

$$r_* = \frac{1}{2\kappa_{e2}} ln \left| \frac{r}{r_{e2}} - 1 \right| + \frac{1}{2\kappa_{c2}} ln \left| 1 - \frac{r}{r_{e2}} \right|. \tag{3.8}$$

Case3 $\epsilon = -1$**:** this is the extreme case of quintessence, the Schwarzschild-de Sitter(SdS) spacetime. The roots of the polynomial equation, $f(r) = 0$ corresponding to the the event horizon at $r = r_{e3}$, the cosmological horizon at $r = r_{c3}$ and a negative root at $r = r_0 = -(r_{e3} + r_{c3})$, with $r_0 < r_{e3} < r_{c3}$.

We can recast the function $f(r)$ as,

$$f(r) = \frac{c}{r}(r - r_{e3})(r_{c3} - r)(r - r_0). \tag{3.9}$$

The surface gravity associated with the horizons are given by,

$$\begin{aligned} \kappa_{e3} &= \frac{c(r_{c3} - r_{e3})(r_{e3} - r_0)}{2r_{e3}}, \\ \kappa_{c3} &= \frac{c(r_{c3} - r_{e3})(r_{c3} - r_0)}{2r_{c3}}, \\ \kappa_0 &= \frac{c(r_{e3} - r_0)(r_{c3} - r_0)}{2(-r_0)}. \end{aligned} \tag{3.10}$$

Writing $f(r)^{-1}$ as,

$$\frac{1}{f} = \frac{1}{2\kappa_{e3}(r - r_{e3})} + \frac{1}{2\kappa_{c3}(r_{c3} - r)} + \frac{1}{2\kappa_0(r - r_0)}, \tag{3.11}$$

we can define the tortoise relation in terms of the horizons and the corresponding surface gravity as[78],

$$r_* = \frac{1}{2\kappa_{e3}} ln \left| \frac{r}{r_{e3}} - 1 \right| - \frac{1}{2\kappa_{c3}} ln \left| 1 - \frac{r}{r_{c3}} \right| + \frac{1}{2\kappa_0} ln \left| \frac{r}{r_0} - 1 \right|. \tag{3.12}$$

3.3 Evolution of fields

3.3.1 Scalar perturbations

The evolution of massless scalar field Φ is governed by the Klein-Gordon equation (Eq.2.14 with $m = e = 0$),

$$\Box\Phi = \frac{1}{\sqrt{-g}} \partial_\mu (\sqrt{-g} g^{\mu\nu} \partial_\nu) \Phi = 0, \tag{3.13}$$

Using the scalar spherical harmonics(Eq.2.16), the radial part of the perturbation equations (Eq.3.13) can be decoupled from their angular parts and reduced to the form,

$$\left(-\frac{\partial^2}{\partial t^2} + \frac{\partial^2}{\partial r_*^2} \right) \psi_\ell(t, r) = -V_\ell(r) \psi_\ell(t, r), \tag{3.14}$$

with the effective potential,

$$V_{SC} = f(r) \left(\frac{\ell(\ell + 1)}{r^2} + \frac{2M}{r^3} + \frac{c(3\epsilon + 1)}{r^{3\epsilon+3}} \right). \tag{3.15}$$

3.3.2 Electromagnetic perturbations

The evolution of the electromagnetic(EM) field is described by the Maxwell's equation,

$$F^{\mu\nu}_{;\nu} = 0, \qquad with \quad F_{\mu\nu} = A_{\nu,\mu} - A_{\mu,\nu}, \tag{3.16}$$

where A_μ is the electromagnetic vector potential. Since the background is spherically symmetric, the vector potential A_μ can be represented as 4-dimensional vector spherical harmonics[79],

$$A_\mu(t,r,\theta,\phi) = \sum_{\ell,m} \left(\begin{bmatrix} 0 \\ 0 \\ \frac{a^{\ell m}(t,r)}{\sin\theta}\partial_\phi Y_{\ell m} \\ -a^{\ell m}(t,r)\sin\theta\partial_\theta Y_{\ell m} \end{bmatrix} + \begin{bmatrix} f^{\ell m}(t,r)Y_{\ell m} \\ h^{\ell m}(t,r)Y_{\ell m} \\ k^{\ell m}(t,r)\partial_\theta Y_{\ell m} \\ k^{\ell m}(t,r)\partial_\theta Y_{\ell m} \end{bmatrix} \right). \tag{3.17}$$

The parity of first term in the vector harmonics is $(-1)^{\ell+1}$ (magnetic) and that of the second term is $(-1)^\ell$ (electric). For odd parity, the components of electromagnetic tensor $F^{\theta\nu}$ are obtained as,

$$F^{\theta t} = \frac{cosec\theta}{r^2 f}\frac{\partial a}{\partial t}\frac{\partial Y_{\ell m}}{\partial \phi}, \tag{3.18}$$

$$F^{\theta r} = \frac{-cosec\theta f}{r^2}\frac{\partial a}{\partial r}\frac{\partial Y_{\ell m}}{\partial \phi}, \qquad F^{\theta\theta} = 0, \tag{3.19}$$

$$\begin{aligned} F^{\theta\phi} &= \frac{-cosec\theta}{r^4}\left(\frac{1}{sin^2\theta}\frac{\partial^2 Y_{\ell m}}{\partial\phi^2} + \frac{1}{sin\theta}\frac{\partial}{\partial\theta}\left(sin\theta\frac{\partial Y_{\ell m}}{\partial\theta}\right)\right)a \\ &= \frac{cosec\theta}{r^4}\ell(\ell+1)Y_{\ell m}a. \end{aligned} \tag{3.20}$$

The covariant derivative of electromagnetic tensor, $F^{\theta\nu}_{;\nu}$ are obtained as,

$$F^{\theta t}_{;t} = \frac{-cosec\theta}{2r^2 f}\left(ff'\frac{\partial a}{\partial r} - 2\frac{\partial^2 a}{\partial t^2}\right)\frac{\partial Y_{\ell m}}{\partial\phi}, \tag{3.21}$$

$$F^{\theta r}_{;r} = \frac{-cosec\theta}{2r^3}\left(rf'\frac{\partial a}{\partial r} - 2f\left(\frac{\partial a}{\partial r} - r\frac{\partial^2 a}{\partial r^2}\right)\right)\frac{\partial Y_{\ell m}}{\partial \phi}, \tag{3.22}$$

$$F^{\theta\theta}_{;\theta} = 0, \qquad F^{\theta\phi}_{;\phi} = \frac{cosec\theta}{r^4}\left(\ell(\ell+1)a - rf\frac{\partial a}{\partial r}\right)\frac{\partial Y_{\ell m}}{\partial \phi}. \tag{3.23}$$

Now the Maxwell's equation becomes,

$$F^{\theta\nu}_{;\nu} = 0 \Rightarrow \left[\ell(\ell+1)f - r^2\left(\frac{\partial}{\partial r}f^2\frac{\partial}{\partial r} - \frac{\partial^2}{\partial t^2}\right)\right]a^{\ell m}(t,r) = 0 \tag{3.24}$$

Other equations obtained from Eq.(3.16) are equivalent to the above equation. Using the tortoise coordinate defined by $dr_* = \frac{1}{f}dr$ the above equation can be reduced in to Eq.(3.14), with,

$$V_{EM} = f(r)\left(\frac{\ell(\ell+1)}{r^2}\right), \tag{3.25}$$

where the wave function, $\psi_\ell = a^{\ell m}$. The even parity wave also satisfy the above equation with the wave function having the functional dependence, $\psi_\ell = \frac{r^2}{\ell(\ell+1)}\left(h^{\ell m}_{,t} - f^{\ell m}_{,r}\right)$.

3.3.3 Gravitational perturbations

Equation governing the gravitational perturbation(GR) is,

$$R_{\mu\nu}(g+h) = 0, \tag{3.26}$$

where $R_{\mu\nu}(g+h)$ is the Ricci tensor computed from the total metric $g_{\mu\nu} + h_{\mu\nu}$. Here the variation on right hand side of Einstein's equation, Eq.(1.8) is taken to be zero since we are considering three special cases of quintessence state parameter and assuming it to be

fixed, at least for the interval of time that we have considered here for the evolution of perturbation.

Any arbitrary perturbations can be decomposed into normal modes, since the background we are considering is spherically symmetric. For any given value of the angular momentum ℓ, associated with these modes, there are two classes of perturbations. Even, $(-1)^{\ell}$ and odd, $(-1)^{\ell+1}$ parity perturbations. Here we are considering only the axial perturbation for our study. The two were shown to have a similar QNM spectra and late-time behavior in de Sitter spacetime[81]. The canonical form of odd wave perturbations in Regge-Wheeler gauge[6], keeping the time dependence, can be written as,

$$h_{\mu\nu} = \begin{vmatrix} 0 & 0 & 0 & h_0(r) \\ 0 & 0 & 0 & h_1(r) \\ 0 & 0 & 0 & 0 \\ h_0(r) & h_1(r) & 0 & 0 \end{vmatrix} sin\theta \frac{\partial}{\partial\theta} P_\ell(cos\theta) Q(t). \quad (3.27)$$

Following the calculations described in Section 1.3.1, we get the radial equations,

$$\frac{h_0}{f}\frac{dQ}{dt} - \frac{d\,(f h_1)}{dr} Q = 0, \quad (3.28)$$

$$\frac{1}{f}\frac{dQ}{dt}\left(\frac{2h_0}{r} - \frac{dh_0}{dr}\right) + h_1\left\{\frac{\ell(\ell+1)}{r^r} + \frac{1}{f}\frac{d^2Q}{dr^2} - \frac{2}{r^2} - \frac{6c\epsilon}{r^{3\epsilon+3}}\right\}Q = 0. \quad (3.29)$$

Eqs.(3.28) and (3.29) comes from $\delta R_{\theta\phi} = 0$ and $\delta R_{r\phi} = 0$, respectively.

Defining $\psi(t,r) = \frac{f h_1(r)}{r} Q(t)$ and employing the tortoise coordinate, the above two equations can be combined to get a second order equation, Eq.(3.14) after eliminating $h_0(r)$. The effective potential of the system is,

$$V_{GR} = f(r)\left(\frac{\ell(\ell+1)}{r^2} - \frac{6M}{r^3} - \frac{c(3\epsilon+3)}{r^{3\epsilon+3}}\right). \tag{3.30}$$

Now we analyze the nature of the effective potentials. Figures 3.1 and 3.2 show the potentials experienced by the scalar, EM and GR fields. To clearly see the behavior of the potential between the horizons, we choose the value of the parameter $c = 10^{-5}$ for $\epsilon = -1$ case and a larger value of $c = 10^{-2}/2$ for $\epsilon = -2/3$ case, so that we can bring down the separation between the horizons.

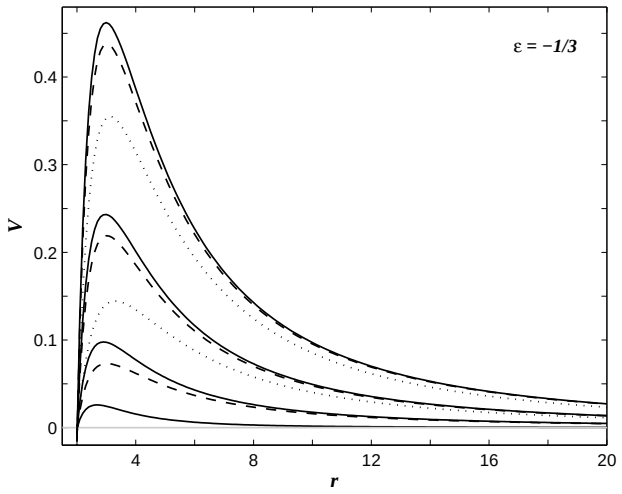

Figure 3.1: Plot of effective potentials for $\epsilon = -1/3$ with $c = 10^{-2}/2$. Set of curves form *bottom* to *top* is for $\ell = 0, 1, 2$ and 3 modes. The scalar(*solid curves*), EM(*dashed*) and GR(*dotted*) fields are drawn.

For $\epsilon = -1/3$(Figure 3.1), the effective potential of scalar field is positive definite for $r_* \in [-\infty, +\infty]$ and have a potential barrier near the event horizon but vanish asymptotically as $r_* \to \pm\infty$. But for smaller values of the quintessence parameter, $\epsilon = -2/3$ and -1(Figure 3.2), after a barrier nature near the event horizon, the potentials with

$\ell = 0$ mode of scalar field, vanish at some $r_* = r_*^0$ and there after form a negative well in the range $r_*^0 < r_* < +\infty$.

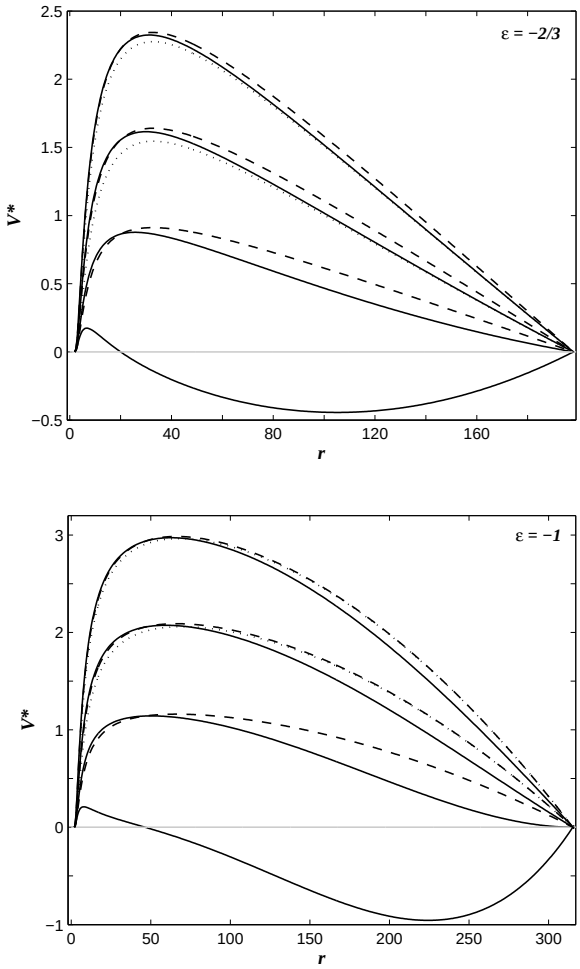

Figure 3.2: Plot of effective potentials for $\epsilon = -2/3$ with $c = 10^{-2}/2$ and $\epsilon = -1$ with $c = 10^{-5}$. In each plot set of curves from *bottom* to *top* is for $\ell = 0, 1, 2$ and 3 modes. The scalar(*solid curves*), EM(*dashed*) and GR(*dotted*) fields are drawn. At large distances, GR potential is merged with the scalar case for $\epsilon = -2/3$ and with EM case for $\epsilon = -1$. The potential is scaled as $V^* = V(r_e - r)^2(\ell + 1/2)$, to enhance the nature at large r.

3.4 Numerical integration and results

The complex nature of the potentials makes it difficult to obtain the exact solutions of Eq.(3.14) and we have to tackle the problem by numerical methods. An efficient method to study the evolution of field were developed in[27], after recasting the wave equation, Eq.(3.14), in the null coordinates, $u = t - r_*$ and $v = t + r_*$ as,

$$-4\frac{\partial^2}{\partial u \partial v}\psi(u,v) = V(u,v)\psi(u,v). \tag{3.31}$$

To discretize the wave equation we replace the derivatives with the finite differences,

$$\begin{aligned}\frac{\partial \psi}{\partial u}(u_i, v_j) &\to \frac{\psi(u_i + \triangle u, v_j) - \psi(u_i, v_j)}{\triangle u}, \\ \frac{\partial \psi}{\partial v}(u_i, v_j) &\to \frac{\psi(u_i, v_j + \triangle v) - \psi(u_i, v_j)}{\triangle v}.\end{aligned} \tag{3.32}$$

Denoting the wavefunction on the uniformly spaced grid points of the null rectangle(Figure 3.3), as ψ_N, ψ_W, ψ_E and ψ_S with an overall grid scale factor of $\triangle u = \triangle v = h$, we use the following finite difference scheme for Eq.3.31,

$$\psi_N = \psi_W + \psi_E - \psi_S - \frac{h^2}{8}V(P)(\psi_W + \psi_E) + O(h^4), \tag{3.33}$$

where the potential is evaluated on the centroid P, $((u_S + u_W)/2$, $(u_S + u_E)/2)$.

To perform the numerical integration on an uniformly spaced grid, we have to specify the initial conditions. Since the late-time behavior of the wave function is found to be insensitive to the initial data, we set null data on u axis and a Gaussian profile on v axis,

$$\psi(u, v = 0) = 0, \qquad \psi(u = 0, v) = Ae^{-\frac{(v-v_0)^2}{2\sigma^2}}. \tag{3.34}$$

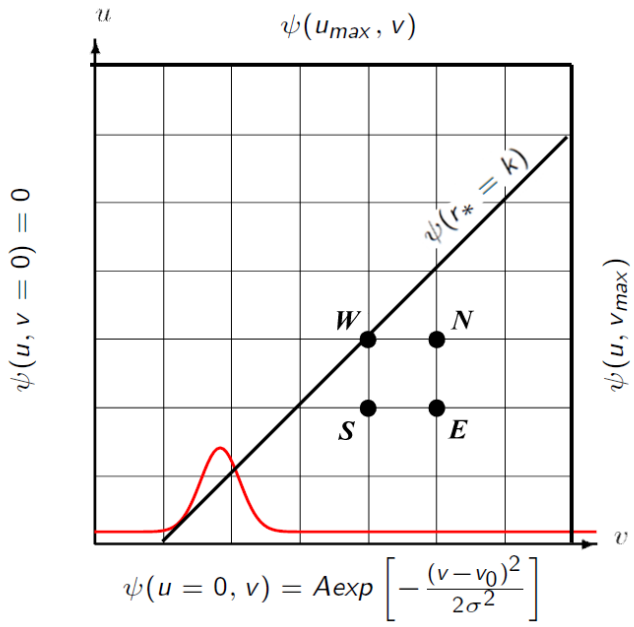

Figure 3.3: The null grid for the numerical integration.

In all our calculations in this chapter, we set the initial Gaussian distribution with width, $\sigma = 3$ centered at $v_0 = 10$. Due to the linearity of the equation one has the freedom to choose the amplitude of the initial wave $A = 1$. To proceed the integration on the above numerical scheme one has to find the value of the potential at $r(r_*) = r((v-u)/2)$ at each step. Employing the Newton-Raphson method one can invert Eqs.(3.3), (3.8) and (3.12) and get $r(r_*)$ for the characteristic integration.

Figure 3.4 shows typical evolution profile of scalar field in a black hole surrounded by quintessence, in comparison with that in the pure Schwarzschild spacetime. We observe that the evolution shows deviations from the Schwarzschild case, after initial transient phase. The damped single frequency oscillation(QNM) phase and the late-

time tail of decay in the final phase shows the characteristics of the quintessence. We analyze each phase in detail.

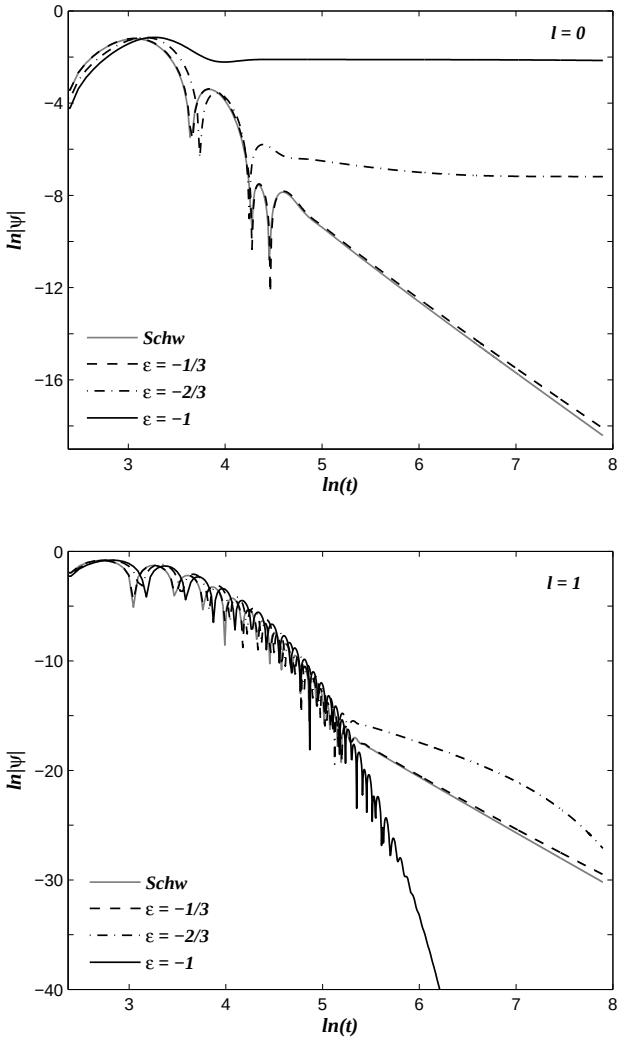

Figure 3.4: Log-log graph of the evolution of scalar field in a quintessence filled black hole spacetime with quintessence parameters $\epsilon = -1/3, -2/3, -1$ and $c = 10^{-2}/2$, in comparison with that in the pure Schwarzschild($Schw$) spacetime. The case of $\ell = 0$ mode is shown in the *top* panel and $\ell = 1$ on the *bottom* panel.

3.4.1 Quasinormal modes

QNMs of various field perturbations around black hole surrounded by quintessence were evaluated in [64–71] using third order WKB method. The typical nature of QNM phase can be seen in Figure 3.5, where we have shown the evolution profiles of the different fields in a quintessence surrounded black hole for $\ell = 2$, in comparison with the corresponding mode in the pure Schwarzschild black hole. On the *left* panel the decay of scalar field is shown for $\epsilon = -2/3$ and -1 along with the Schwarzschild case.

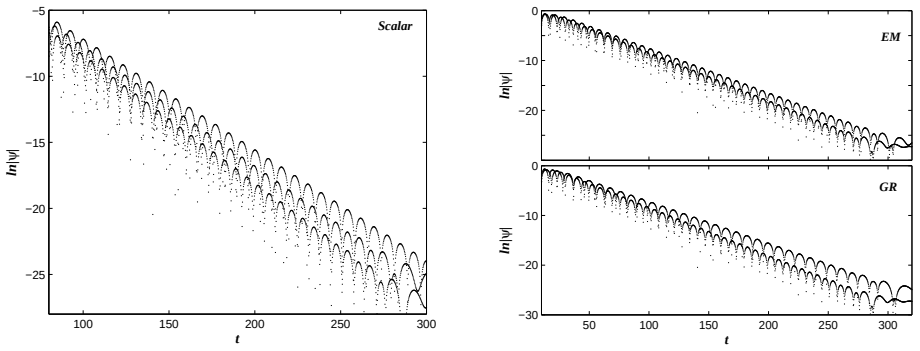

Figure 3.5: Semi-log graph of the QNM phase of evolution for the $\ell = 2$ modes of various fields. The plot on the *left* is for scalar field where the curves from *bottom* to *top* is for the Schwarzschild, $\epsilon = -2/3$ and -1 cases, respectively. On the *right*, EM and GR fields are shown where *bottom* curve in each sub plot represents the Schwarzschild case and the other ones are for $\epsilon = -2/3$. We take $c = 10^2/2$ for these plots. All the three fields damp more slowly in the presence of quintessence.

It can be seen that the decay of the fields in the QNM phase is slower in the presence of quintessence than in the pure Schwarzschild cases. Also the damping is lower for smaller values of ϵ. This result is not in agreement with the results presented in [64], where

they obtained that a massless scalar field damps more rapidly due to quintessence. Electromagnetic and gravitational field perturbations also show similar behavior as that of scalar field, in the QNM phase. So we have shown the $\epsilon = -2/3$ case only in the plots. These results are in agreement with the observations made in [65–67], using the WKB method.

3.4.2 Late-time tails

The QNM phase is followed by the regime of late-time tails of field decay. We find that the nature of late-time tails are sensitive to the parameters of quintessence, the angular momentum index and also the type of field perturbations under consideration. Below we discuss the different cases in detail.

$\ell = 0$ mode

Scalar field perturbations can have the $\ell = 0$ mode, while EM and GR fields can only have modes with $\ell \geq 1$ and $\ell \geq 2$ respectively. From Figure 3.4, which is a log-log plot, it can be seen that for the $\ell = 0$ mode, scalar field with $\epsilon = -1/3$ case of quintessence has the form of a power-law tail, with slightly slower decay rate than the corresponding Schwarzschild tail.

The peculiar shape of potentials for $\epsilon = -2/3$ and -1(Figure 3.2) reflects in the late-time tails, that the fields settle to a residual constant value, rather than decaying to zero. We have evaluated the field, $\phi = \psi/r$ on the surface of constant r(at $r_* = 10$), the cosmological horizon(approximated by the null surface $v = v_{max}$) and the black hole event horizon(approximated by the null surface $u = u_{max}$). In the asymptotic late times, field settles to the same constant value ϕ_0, on all these surfaces, as shown in Figure 3.6. It was first observed

in[36], for scalar field in the SdS spacetime and they have shown that at late times,

$$\phi \mid_{\ell=0} \simeq \phi_0 + \phi_1(r)e^{-2k_{c3}t}. \tag{3.35}$$

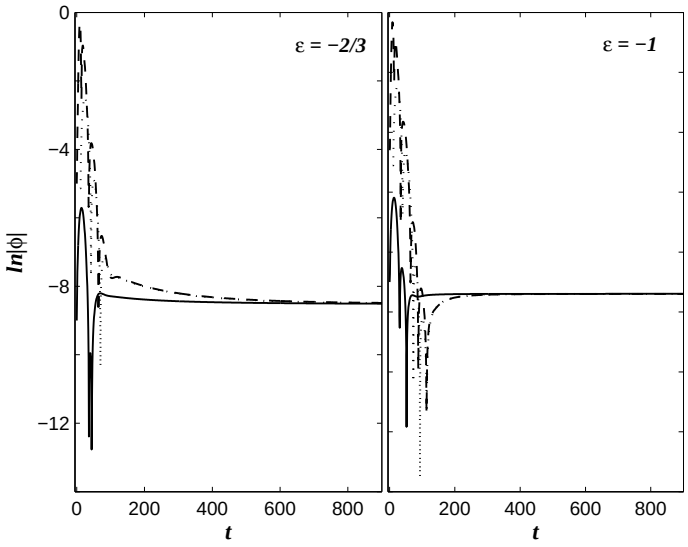

Figure 3.6: The decay of $\ell = 0$ mode of scalar field with quintessence parameters $\epsilon = -2/3$ with $c = 10^{-2}/2$, and $\epsilon = -1$ with 10^{-5}. The fields are evaluated on the constant surface $r_* = 10$(*dotted curves*), black hole event horizon(*dashed curves*) and cosmological horizon(*solid curves*).

Figure 3.7 demonstrates the $\ell = 0$ mode of scalar field for different values of c. The smaller the value of c, the later the field descends to the constant value, ϕ_0. The dependence of ϕ_0, on the parameter c is shown in Figure 3.8. We observe that the asymptotic value of field scales as $\psi_0 \sim c^{0.995}$, when $\epsilon = -1$ as found in[36] and as $\psi_0 \sim c^{1.873}$, when $\epsilon = -2/3$.

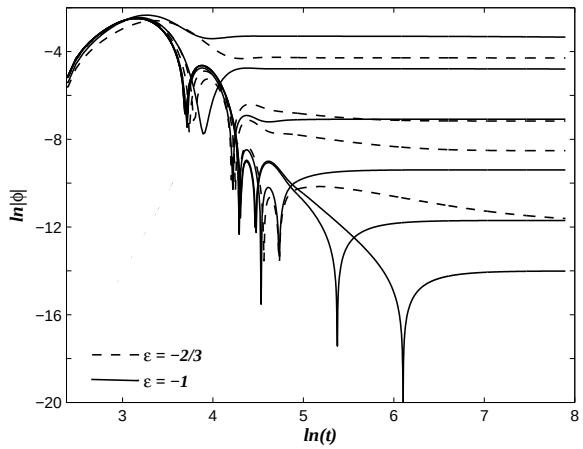

Figure 3.7: The decay of $\ell = 0$ mode of scalar field with quintessence parameters $\epsilon = -2/3$ with $c = 10^{-1}/2, 10^{-2}, 10^{-2}/2$ and 10^{-3}, and $\epsilon = -1$ with $c = 10^{-2}/2, 10^{-3}, 10^{-4}, 10^{-5}, 10^{-6}$ and 10^{-7}.

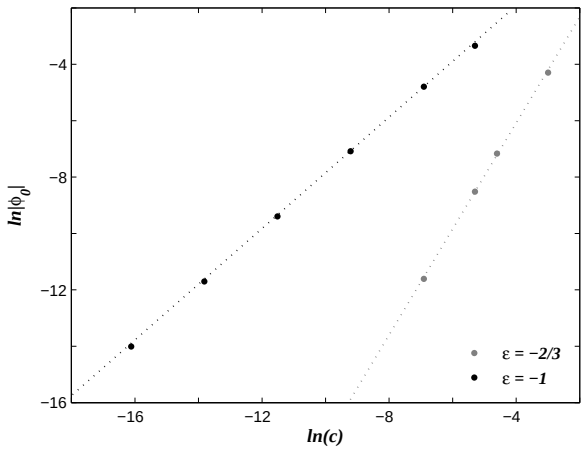

Figure 3.8: The asymptotic value of scalar field, ϕ_0 versus c, in logarithmic scale. A linear fit(*dotted lines*) gives the slopes 1.873, for $\epsilon = -2/3$ and 0.995, for $\epsilon = -1$.

$\ell > 0$ modes

Now we report the results obtained for the decay of $\ell > 0$ modes of field perturbations. Figure 3.9 demonstrates the evolution of scalar, EM and GR fields around a black hole surrounded by quintessence with $\epsilon = -1/3$, along with pure Schwarzschild case. The fields, ψ are evaluated on the surface $r_* = 10$. A straight line in such a plot shows a power-law tail. The late-time tails follow the power-law decay for $\epsilon = -1/3$, but with a smaller decay rate, than the Schwarzschild case of, $\psi \sim t^{-(2\ell+3)}$. For the quintessence case with $c = 10^{-2}/2$, we get $\psi \sim t^{-(2\ell+2.7)}$.

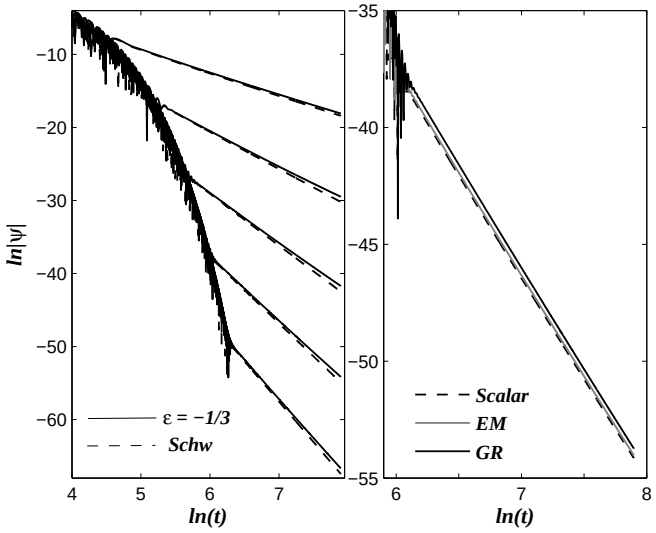

Figure 3.9: Log-log plot of the evolution of fields for $\epsilon = -1/3$, with $c = 10^{-2}/2$. On the *left*, the decay of scalar field is shown in comparison with the Schwarzschild case. Curves from *top* to *bottom* is for $\ell = 0, 1, 2, 3$ and 4. The decay has a lower power-law constant, $t^{-(2\ell+2.7)}$ for quintessence case. The $\ell = 3$ mode of different fields is shown on the *right*. All the field has an identical tail of decay for $\epsilon = -1/3$.

As the value of the quintessence parameter decreases to $\epsilon = -2/3$ and to -1, though in the intermediate time the fields follow the power-law decay, in the asymptotic late-time it deviates from the power-law form. Figure 3.10 is a semi-log plot of the decay of scalar, EM and GR perturbations for the $\epsilon = -2/3$ case with $c = 10^{-2}/2$. A straight line in such a plot corresponds to an exponential decay. We can see from the plot that for $\ell > 0$, the intermediate time power-law form of decay is replaced by an exponential decay of field, in the asymptotic late-time. In particular, in the asymptotic late times, the decay can be fitted in the forms,

$$\begin{aligned} \psi &\sim e^{-pk_{c2}\ell t}, \qquad for \quad Scalar \quad and \quad GR, \\ \psi &\sim e^{-k_{c2}(\ell+1)t}, \qquad for \quad EM, \end{aligned} \tag{3.36}$$

where p is some constant, for the plots shown in Figure 3.10 with $c = 10^{-2}/2$ we get $p = 1.089$. The evolution of field for the $\epsilon = -1$ case is plotted in Figure 3.11, in semi-log scale, where we have chosen $c = 10^{-5}$, in order to see the decay for large ℓ. All the $\ell > 0$ modes at late-time relax as an exponential tail, according to the form,

$$\begin{aligned} \psi &\sim e^{-k_{c3}\ell t}, \qquad for \quad Scalar, \\ \psi &\sim e^{-k_{c3}(\ell+1)t}, \qquad for \quad EM \quad and \quad GR. \end{aligned} \tag{3.37}$$

The late-time tails are generated by the scattering of the waves by the potential at great distances. By a systematic study of various potentials Ching *et al.*[33] and later by Hod[34] had given the following heuristic picture. The late-time tails reported by an observer at r_* are caused by the waves that are scattered by the potential, $V(r'_*)$ at the point $r'_* \gg r_*$ and at late times, $\psi \propto V(r'_*) \simeq V(t/2)$.

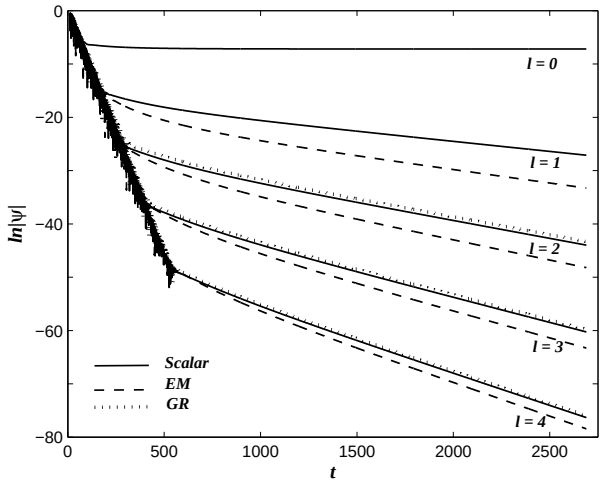

Figure 3.10: Semi-log plot of the decay of scalar, EM and GR perturbations for $\epsilon = -2/3$ with $c = 10^{-2}/2$. GR has an identical decay pattern as that of scalar field.

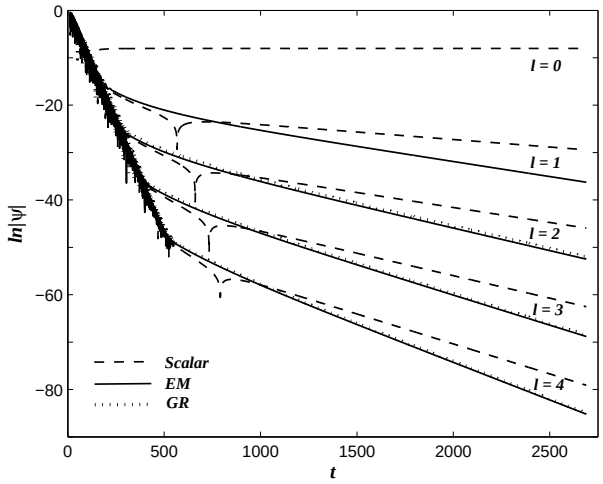

Figure 3.11: Semi-log plot of the decay of scalar, EM and GR perturbations for $\epsilon = -1$ with $c = 10^{-5}$. The gravitational perturbations are merged with the EM profiles

Their studies showed that the inverse power-law decay is a property of asymptotically flat spacetimes, and that different behaviors should be expected in black-hole spacetimes that have different asymptotic properties. The results that we obtained can be explained as follows. For $\epsilon = -1/3$, all the fields have inverse power nature of the effective potentials as that in asymptotically flat spacetime and lead to inverse power-law decay of fields at late times. When $\epsilon = -2/3$ and -1 the potentials exponentially drop off in the asymptotic region, $V(r_*) \sim e^{-k_c r_*}$ and one can expect an exponential tail of the forms Eq.(3.36) and (3.37) at late times.

3.5 Conclusion

This chapter investigates the late-time behavior of various field perturbations in the geometry of black hole residing in an universe expanding with acceleration, adopting the quintessence model of dark energy. Massless scalar, EM and GR perturbations are considered around a spherically symmetric uncharged black hole with the asymptotes determined by the quintessence.

The evolution picture obtained confirms that in the QNM stage, all the fields decay slowly due to the presence of quintessence. At late times, QNMs are suppressed by the tail form of field decay. As the value of the quintessential parameter ϵ, decreases, the late-time decay of $\ell = 0$ mode of scalar field gives up the power-law form of decay, relaxing to a constant residual field. This asymptotic values of the field is determined by the value of the parameter ϵ and c. For the behavior of $\ell = 0$ mode when $\epsilon = -2/3$ and -1, there is no analogue case in black holes with flat space. This can be understood as a consequence of cosmological no-hair theorem[35]. Comparing

the situation in SdS spacetime with the scattering inside the charged black hole it was argued that a constant mode can be transmitted to both black hole and cosmological horizons. However the constant solution carries no stress-energy.

For large values of ϵ, the $\ell > s$ modes of scalar, EM and GR perturbations, still show a power-law decay, having a slower decay rate than the corresponding Schwarzschild case. As the value of ϵ decreases, the power-law decay gives way to an exponential decay. The results for the SdS black hole spacetime, the extreme case of quintessence, are consistent with the previous studies[36, 78, 81].

4

Dirac field around Schwarzschild black hole surrounded by quintessence

4.1 Introduction

ACCORDING to the black hole "*no-hair theorem*" a black hole formed by the gravitational collapse of a charged rotating star, will rapidly relax to a stationary state, characterized by three quantities, its mass, charge and angular momentum. Any other *hair*, will disappear after the collapsing body settles down to its stationary configuration. Later counterexamples of this theorem were presented obtaining solutions for black holes with various *hairs*. Among them are black holes dressed with Yang-Mills, Proca-type Yang-Mills, and Skyrme fields in various combinations with Higgs fields[90–92]. Some, but not all, of these black holes are unstable. The manner and rate with which the *hair* of the black hole decays is thus an important question. All known black-hole *no-hair* theorems were extended to spacetimes endowed with a positive cosmological constant[89]. Specifically, they proved that static spherical black holes with positive cosmological constant cannot support scalar fields in convex potentials and Proca-massive vector fields in the region between the black hole and the

cosmic horizon.

Most of the studies on the late-time decay are devoted to integer spin fields. There are only few studies on the fermionic tails. The problem of the late-time behavior of massive Dirac fields in black hole with asymptotically flat spacetime was studied in [84–86]. The intermediate and late-time behavior of massive Dirac field in the static spherically general black hole spacetime is studied in [87]. The late-time behavior of a massive Dirac field in the background of dilaton black hole solutions is investigated in [88]. It is revealed that for black hole in flat spacetimes, the long-lived oscillatory tail of Dirac field, observed at timelike infinity decays as $t^{-5/6}$.

The evolution of fields propagating in de Sitter spacetime were addressed in[35, 36, 78, 81] and they have demonstrated the existence of exponentially decaying tails at late times contrasting the power-law tails in asymptotically flat situation. QNMs of SdS black holes have been calculated for fields of different spin, including the Dirac field, using the sixth-order WKB and Pöschl-Teller approximation[93]. Since the spherically symmetric black hole solutions[63] were obtained in quintessence model of dark energy, there are studies [68, 70] on evolution of Dirac field around black holes surrounded by quintessence. These attempts are based on the calculation of the QNMs using the third order WKB approximation method while the late-time behavior of Dirac perturbations remained unknown. In fact, the late-time decay is determined by the asymptotic curvature of the spactime, so it is interesting to see how Dirac field evolves in a spacetime in which the asymptotic structure is determined by the quintessence field and our study fills this gap.

The rest of the chapter is organized as follows. In Section 4.2 the master wave equation for Dirac field perturbations around black hole

surrounded by quintessence is derived. The results are discussed in Section 4.3. The major conclusion is given in Section 4.4.

4.2 Perturbations of Dirac field

The Dirac equation for a massless field in spacetime $g_{\mu\nu}$, specified by Eq.(3.1) can be written as[94]

$$i\gamma^a e_a^\mu(\partial_\mu + \Gamma_\mu)\Psi = 0, \tag{4.1}$$

where γ^a are the Dirac matrices,

$$\gamma^0 = \begin{pmatrix} 1 & 0 \\ 0 & -1 \end{pmatrix}, \qquad \gamma^i = \begin{pmatrix} 0 & \sigma_i \\ -\sigma_i & 0 \end{pmatrix}, \qquad i = 1, 2, 3, \tag{4.2}$$

σ_i being Pauli matrices. e_a^μ is the tetrad defined by the metric $g_{\mu\upsilon}$,

$$g_{\mu\upsilon} = \eta_{ab} e_\mu^a e_\upsilon^b. \tag{4.3}$$

with $\eta_{ab} = diag(-1, 1, 1, 1)$ being the Minkowski metric. Γ_μ is the spin connections defined by,

$$\Gamma_\mu = \frac{1}{8}\left[\gamma^a, \gamma^b\right] e_a^\upsilon e_{b\upsilon;\mu}. \tag{4.4}$$

Choosing the tetrad to be,

$$e_a^\mu = \begin{pmatrix} f^{-1/2} & 0 & 0 & 0 \\ 0 & f^{1/2}\sin\theta\cos\phi & \frac{\cos\theta\cos\phi}{r} & \frac{\csc\theta\sin\phi}{r} \\ 0 & f^{1/2}\sin\theta\sin\phi & \frac{\cos\theta\sin\phi}{r} & \frac{\csc\theta\cos\phi}{r} \\ 0 & f^{1/2}\cos\theta & \frac{\sin\theta}{r} & 0 \end{pmatrix}, \tag{4.5}$$

The spin connections defined by Eq.(4.4) are,

$$\Gamma_t = \frac{1}{4}\partial_r\left(rf\right)\gamma^0\tilde{\gamma}; \quad \tilde{\gamma} = (\sin\theta\cos\phi\gamma_1 + \sin\theta\sin\phi\gamma_2 + \cos\theta\gamma_3), \tag{4.6}$$

$$\Gamma_r = 0, \quad \Gamma_\theta = \frac{1}{2}\left(1 - f^{1/2}\right)\left(\gamma^3\gamma^1\cos\phi + \gamma^3\gamma^2\sin\phi\right), \tag{4.7}$$

$$\Gamma_\varphi = \frac{1}{2}\left(f^{1/2} - 1\right)\left(\gamma^1\gamma^2\sin\theta + \gamma^1\gamma^3\cos\theta\sin\phi - \gamma^2\gamma^3\cos\theta\cos\phi\right)\sin\theta. \tag{4.8}$$

Now the second term in Eq.(4.1) can be reduced to get,

$$\gamma^a e_a^\mu \Gamma_\mu = \tilde{\gamma}\left(\frac{(r^2 f)'}{4r^2 f^{1/2}} + \frac{f^{1/2}}{2r} - \frac{1}{r}\right) \tag{4.9}$$

Substituting these in Eq.(4.1) results in the following form for the Dirac equation,

$$\frac{i\gamma^0}{f^{1/2}}\frac{\partial\Psi}{\partial t} + \frac{i\tilde{\gamma}f^{1/4}}{r}\frac{\partial}{\partial r}\left(rf^{1/4}\Psi\right) - \frac{i\tilde{\gamma}}{r}\left(\vec{\Sigma}.\vec{L} + 1\right)\Psi = 0, \tag{4.10}$$

where $\vec{L}$ is the standard angular momentum operator with components,

$$\begin{aligned} L_1 &= i\sin\phi\partial_\theta + i\cot\theta\cos\phi\partial_\phi, \\ L_2 &= -i\cos\phi\partial_\theta + i\cot\theta\sin\phi\partial_\phi, \\ L_3 &= -i\partial_\phi, \end{aligned} \tag{4.11}$$

and in the Dirac representation,

$$\vec{\Sigma} = \begin{pmatrix} \vec{\sigma} & 0 \\ 0 & \vec{\sigma} \end{pmatrix}. \tag{4.12}$$

For the separation of variables, we write the wave function as,

$$\Psi = \frac{1}{rf^{1/4}}\Phi, \tag{4.13}$$

where,

$$\Phi(t,r,\theta,\phi) = \begin{pmatrix} iG^{(\pm)}(t,r)\varphi_{jm}^{(\pm)}(\theta,\phi) \\ F^{(\pm)}(t,r)\varphi_{jm}^{(\mp)}(\theta,\phi) \end{pmatrix}, \tag{4.14}$$

with the angular parts of the wave function given by,

$$\varphi_{jm}^{(\pm)} = \begin{pmatrix} \sqrt{\frac{l+1/2\pm m}{2l+1}}Y_l^{m-1/2} \\ -\sqrt{\frac{l+1/2-m}{2l+1}}Y_l^{m+1/2} \end{pmatrix}, \tag{4.15}$$

for $j = l \pm \frac{1}{2}$, and we define,

$$k(\pm) = \begin{cases} -\left(j+\frac{1}{2}\right), & j = l+\frac{1}{2}, \\ \left(j+\frac{1}{2}\right), & j = l-\frac{1}{2}. \end{cases}, \tag{4.16}$$

where $k(-)$ and $k(+)$ are negative and positive integers respectively. The angular functions $\varphi_{jm}^{(\pm)}$ satisfy the eigen equations

$$\mathbf{k}\varphi_{jm}^{(\pm)} = \pm\left(j+\frac{1}{2}\right)\varphi_{jm}^{(\pm)} \quad \text{and} \quad \tilde{\sigma}\varphi_{jm}^{(\pm)} = \varphi_{jm}^{(\mp)}, \tag{4.17}$$

where $\mathbf{k} = \vec{\Sigma}.\vec{L} + 1$ and $\tilde{\sigma} = \sin\theta\cos\phi^1 + \sin\theta\sin\phi\gamma^2 + \cos\theta\gamma^3$. Then the coupled radial equations can be simplified to,

$$f\frac{\partial}{\partial r}\begin{pmatrix} F^{(\pm)} \\ G^{(\pm)} \end{pmatrix} - \frac{(j+1/2)f^{1/2}}{r}\begin{pmatrix} F^{(\pm)} \\ -G^{(\pm)} \end{pmatrix} = -\frac{\partial}{\partial t}\begin{pmatrix} -G^{(\pm)} \\ F^{(\pm)} \end{pmatrix}, \tag{4.18}$$

and moving to the tortoise coordinate, r_* we can write,

$$\frac{\partial}{\partial r_*}\begin{pmatrix} F^{(\pm)} \\ G^{(\pm)} \end{pmatrix} + W_{(\pm)}\begin{pmatrix} -F^{(\pm)} \\ G^{(\pm)} \end{pmatrix} = -\frac{\partial}{\partial t}\begin{pmatrix} -G^{(\pm)} \\ F^{(\pm)} \end{pmatrix}, \quad (4.19)$$

where,

$$W_{(\pm)} = \frac{f^{1/2}k_{(\pm)}}{r}. \quad (4.20)$$

The equations for $F^{(\pm)}$ and $G^{(\pm)}$ can be decoupled to get,

$$\left(-\frac{\partial^2}{\partial r_*^2} + V_{(\pm)1}\right)F = -\frac{\partial^2 F}{\partial t^2}, \quad (4.21)$$

$$\left(-\frac{\partial^2}{\partial r_*^2} + V_{(\pm)2}\right)G = -\frac{\partial^2 G}{\partial t^2}. \quad (4.22)$$

where

$$V_{(\pm)1,2} = \pm\frac{dW_{(\pm)}}{dr_*} + W_{(\pm)}^2, \quad (4.23)$$

Here the $(+)$ case is for k being a positive integer with, $k = j + \frac{1}{2}$ and $j = \ell + \frac{1}{2}$, and the case with negative integer values for k is represented by $(-)$, with $k = -(j + \frac{1}{2})$ and $j = \ell - \frac{1}{2}$. The Dirac potentials appearing in Eq.(4.21) and (4.23) are shown to yield the same spectrum of quasinormal mode frequencies[95]. So here we consider V_1, denoting with the subscript D, and combining the $(+)$ and $(-)$ cases we can write the explicit form for the potential,

$$V_D = \frac{|k|\sqrt{f}}{r^2}\left[|k|\sqrt{f} + \frac{r}{2}\frac{\partial f}{\partial r} - f\right]. \quad (4.24)$$

For $\epsilon = -1/3$, the effective potential is positive definite with $r_* \in [-\infty, +\infty]$ and have a potential barrier near the event horizon but vanishes asymptotically as $r_* \to \pm\infty$. As the parameter ϵ decreases below -1/3, a cosmological horizon is created by the quintessence. Figure 4.1 shows effective potential of the Dirac fields, with $\epsilon = -1$

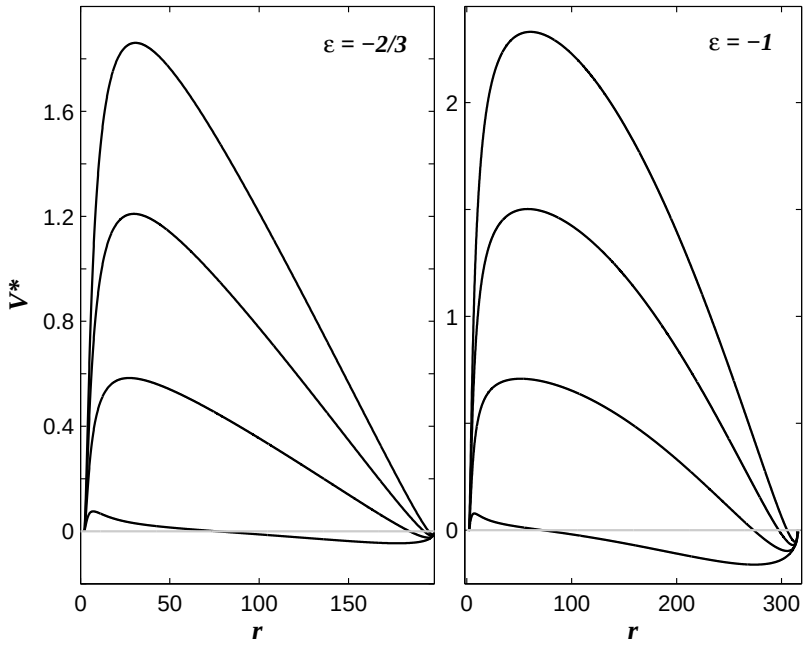

Figure 4.1: Plot of effective potentials experienced by the Dirac field for quintessence parameters $\epsilon = -2/3$ with $c = 10^{-2}/2$ and $\epsilon = -1$ with $c = 10^{-5}$. Curves form *bottom* to *top* is for $\ell = 0, 1, 2$ and 3 modes. The potential is scaled as $V^* = V(r_e - r)^2(\ell + 1/2)$, to enhance the nature at large r. Potentials has a negative dip near CH

and -2/3. In this case, after a barrier nature near the event horizon, the effective potential for all modes, vanishes at some $r_* = r_*^0$ and there after form a negative well in the range $r_*^0 < r_* < +\infty$. This behavior of Dirac field is in contrast with other fields. For scalar field even if the $\ell = 0$ mode shows the negative dip in the potential, all other higher modes have a positive value for the potential between the horizons (Figure 3.2).

4.3 Numerical integration and results

After recasting the wave equations, Eq.(4.21) and (4.22), in the null coordinates, $u = t - r_*$ and $v = t + r_*$ as,

$$-4\frac{\partial^2}{\partial u \partial v}\Psi(u,v) = V(u,v)\Psi(u,v), \tag{4.25}$$

we perform the numerical integration using the method described in Section 3.4. We scale the field as, $\phi = \psi/r$. The evolution of field is monitored on different surfaces viz.,

1. cosmological horizon(CH), approximated by the null surface, $v = v_{max}$,
2. the black hole event horizon(EH), approximated by the null surface, $u = u_{max}$,
3. different surfaces of fixed radius, $r_* = K$, approaching future timelike infinity.

Figure 4.2 shows the evolution profile of the Dirac field around the black hole in a quintessence filled universe along with that in the pure Schwarzschild spacetime. We observe that the evolution of Dirac field shows deviations from the Schwarzschild case, after initial transient phase. The QNM phase and the late-time tail of decay in the final phase show the characteristics of the quintessence and the spin of the field. The fields decay slowly in the QNM phase, if quintessence is present as it was shown in[68, 93], using the WKB method. The QNM phase is followed by the regime of late-time tails of field decay. It is well known that, at late times, the Dirac field perturbations has a power-law decay in the Schwarzschild spacetime and is represented by the straight curves in a log-log plot. We find that the nature of late-time tails of Dirac field is sensitive to the parameters of quintessence.

A. $\epsilon = -1/3$

For quintessence with EOS, $\epsilon \geq -1/3$, there is only one zero for the function, $f(r)$ in Eq.(3.2) and that corresponds to the event horizon of the black hole. It can be observed from Figure 4.2 that for quintessence with EOS, $\epsilon = -1/3$, the decay of Dirac field also shows a power-law tail, but with slightly slower decay rate than the corresponding Schwarzschild tails. For $c = 10^{-2}/2$, we get $\phi \sim t^{-(2\ell+2.7)}$, a slower decay rate than the $\phi \sim t^{-(2\ell+3)}$ of the pure Schwarzschild case. This can be expected since the effective potential for $\epsilon = -1/3$ case has almost the same profile as that of the Schwarzschild spacetime.

B. $\epsilon < -1/3$

As the EOS lowers from -1/3, a cosmological horizon will be created by the quintessence and for Dirac field a negative dip appears in the potential appears. For $\epsilon = -2/3$ and -1, all the ℓ modes of Dirac field relaxes to a constant residual field, at asymptotic late times. This behavior is contrary to other fields, where all the $\ell > 0$ modes are found to be decaying exponentially. Even if the monopole of the scalar field is observed to settle down to a constant asymptotic value, all the higher modes were found to be exponentially decaying. The nature of Dirac field is little surprising and it strengthens the dependence of the unusual dip in the potential and the relaxation of the field to the constant value, although a detailed investigation on this is required. Figure 4.3 shows the evolution profile of the Dirac field for $\epsilon = -2/3$ and -1, and different multiploles. We can fit the decay form as,

$$\phi \mid_{\ell} \simeq \phi_0 \mid_{\ell} + \phi_1(r) e^{-2k_c t}. \tag{4.26}$$

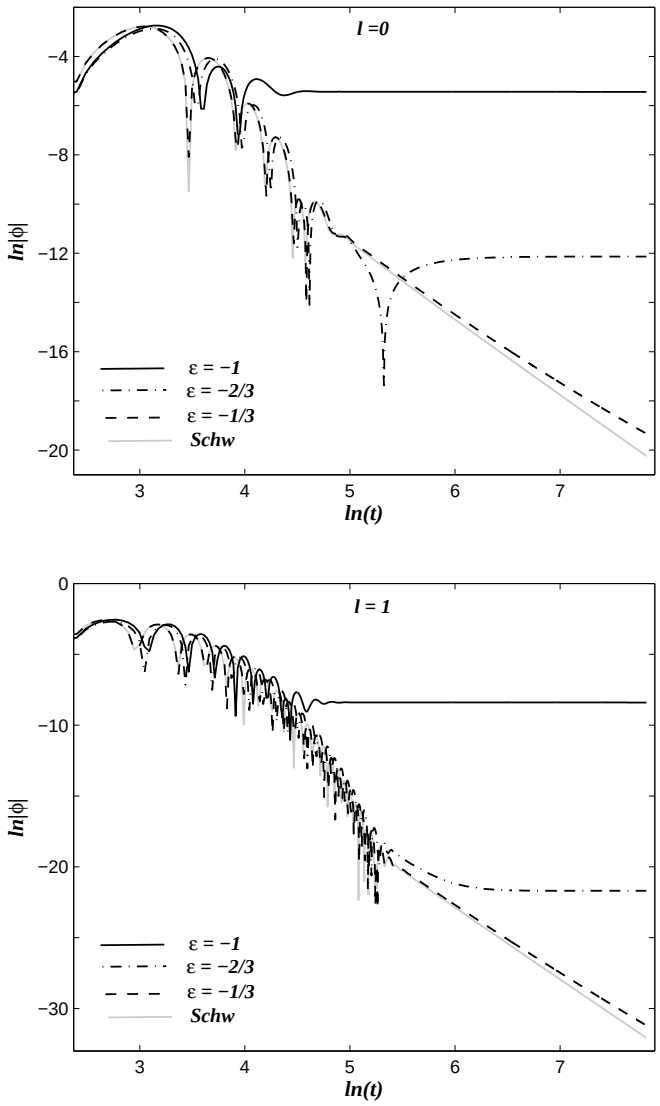

Figure 4.2: Log-log graph of the evolution of Dirac field in a quintessence filled black hole spacetime with $c = 10^{-2}/2$, in comparison with that in the pure Schwarzschild spacetime, evaluated at $r* = 10$. $\ell = 0(top)$ and $\ell = 1(bottom)$ modes for $\epsilon = -1/3, -2/3$ and -1.

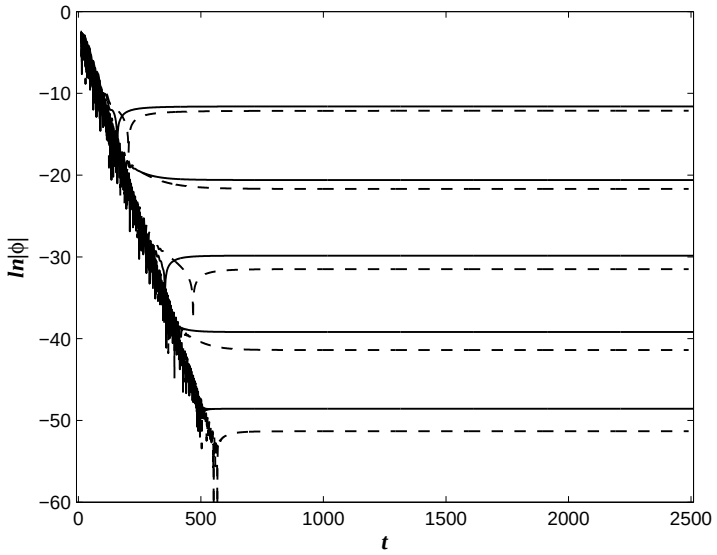

Figure 4.3: Evolution of Dirac field on the surface of fixed radius $r* = 10$. Solid curves are the $\epsilon = -2/3$ case with $c = 10^{-2}/2$ and $\epsilon = -1$ case with $c = 10^{-5}$, is represented by the dashed curves. In each case, curves from *top* to *bottom* is for $\ell = 0, 1, 2, 3$ and 4, respectively

The dependence of the asymptotic residual field, ϕ_0, on the parameter c, is shown in Figure 4.4, on a logarithmic scale. The field is evaluated on the event horizon. For $\epsilon = -1$, a least square fit for $ln|\phi_0| = m1\ ln(c) + c1$, gives the slops, $m1 = 0.973, 1.933, 2.942, 3.915$ and 4.921 for $\ell = 0, 1, 2, 3$ and 4, respectively. For $\epsilon = -2/3$, we get the slops $m1 = 1.768, 3.630, 5.559, 7.330$ and 9.625, for $\ell = 0, 1, 2, 3$ and 4, respectively. These results suggest that,

$$\begin{aligned} \phi_0 &\sim c^{(\ell+1)}, \qquad for \quad \epsilon = -1, \\ \phi_0 &\sim c^{1.782(\ell+1)}, \qquad for \quad \epsilon = -2/3. \end{aligned} \tag{4.27}$$

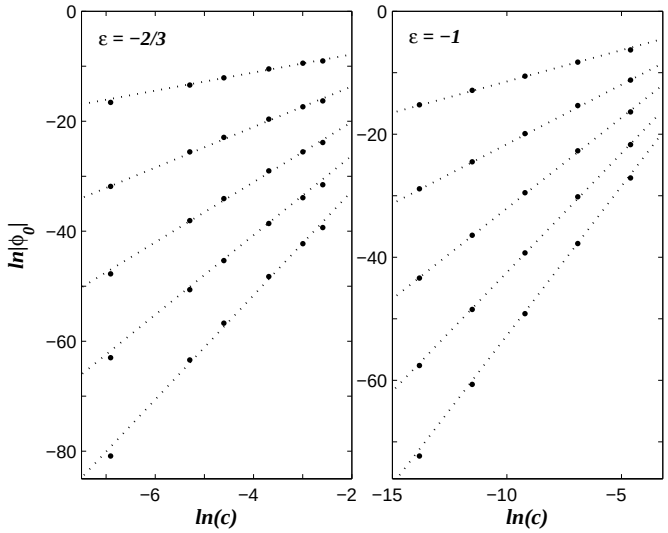

Figure 4.4: The asymptotic value of the Dirac field along EH, ϕ_0, versus c, in logarithmic scale. *Dotted lines* represents a linear fit for each modes. Curves from *top* to *bottom* is for $\ell = 0, 1, 2, 3$ and 4.

To confirm that the behavior of Dirac field is not an artifact of the particular location, we monitor the evolution of the field on different null surfaces of constant radius and on the event and cosmological horizons. Figures 4.5 and 4.6 show the decay of $\ell = 2$ mode of Dirac field on the black hole event horizon, cosmological horizon and three surfaces of fixed radius, $r* = 10, 100$ and 300. The constant asymptotic value of the Dirac field, ϕ_0, varies from the black hole event horizon to the cosmological horizon. The ϕ_0 has a lowest value on the EH, increases as radial position goes farther and farther, and has the highest value on the CH.

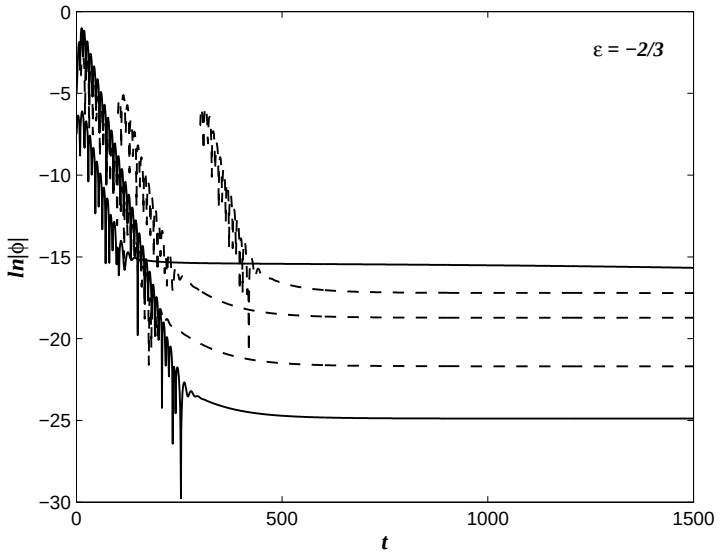

Figure 4.5: The decay of $\ell = 2$ mode of Dirac field with quintessence parameters $\epsilon = -2/3$ with $c = 10^{-2}/2$ on different surfaces. Solid curves represents the field on EH(*bottom*) and CH(*top*). Dotted curves from bottom to top corresponds to the field on surfaces at $r* = 10, 100$ and 300.

Price's original work demonstrates that there can be no static solution to the scalar wave equation that are well behaved at infinity and black hole EH. Even though the $\ell = 0$ mode of the scalar field in the SdS spacetime is observed to settle down to a constant asymptotic value, it relaxes to the *same* constant value on all the surfaces(Figure 3.6). It can be argued that the constant field does not carry any stress energy tensor and it is equivalent to vanishing of the hair. But the behavior of Dirac field is rather intriguing since the all ℓ modes of the field have non zero value at late times and it varies with the position.

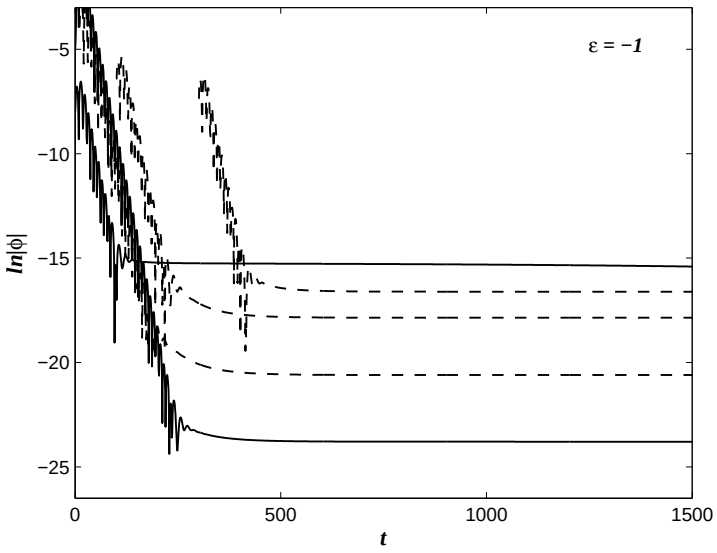

Figure 4.6: The decay of $\ell = 2$ mode of Dirac field with quintessence parameters $\epsilon = -1$ with $c = 10^{-5}$ on different surfaces. Solid curves represents the field on EH(*bottom*) and CH(*top*). Dotted curves from bottom to top corresponds to the field on surfaces at $r* = 10, 100$ and 300.

4.4 Conclusion

The evolution of Dirac field perturbation in the spacetime of a black hole immersed in a quintessence filed, is investigated in this chapter. The quintessence EOS, ϵ plays a dramatic role in the late-time decay of the Dirac field. For $\epsilon = -1/3$ the late-time decay follows a power-law form, but with a lower decay rate than the corresponding Schwarzschild case. As the value of the quintessential parameter ϵ, decreases, the CH forms and a negative dip appears in the effective potential near the CH. For $\epsilon = -2/3$ and -1, the Dirac field do not decay to zero, but relaxes to a constant residual field, at late times. These asymptotic values of the field is determined by the values of

the parameter ϵ and c. This behavior of Dirac field seems to be odd comparing with the scalar, EM and GR perturbations, where the all the $\ell > 0$ modes of the field decay exponentially. The asymptotic value of the Dirac field varies on different surfaces. It has the lowest value on the black hole EH and increase as the radial distance increase and maximizes on the CH. This behavior may indicate the presence of a fermionic hair even though a detailed numerical and analytical studies are required to confirm this result.

5

Massless field perturbations around a black hole in Hořava-Lifshitz gravity

5.1 Gravity and quantization

Gravity, one among all the known four fundamental interactions, is well described by Einstein's General Theory of Relativity at the classical level. The predictions of GTR were tested with high degree of accuracy and successfully passed various classical tests in the weak gravitational field limit.

Most of the everyday physics can work well with GTR, with out a detailed understanding of quantum gravity. But it becomes annoying when one fails to combine the two fundamental theories in physics- Quantum mechanics and GTR- at extream situations like the one at the time of the Big-bang, black hole singularities etc., where both theories come in to play. The classical spacetime continuum concept breaks down at these regimes.

GTR is a classical theory based on the concept of geometry of spacetime. For all other theories the spacetime is an arena where the events can take place but in GTR spacetime itself is a physical entity of the theory. On the other hand electromagnetism, weak and

strong nuclear interactions are well described by standard model of quantum field theory. The consistent implementation of the gravitational interaction into the quantum framework is considered to be an outstanding problem in fundamental physics.

5.1.1 General Relativity and renormalizability

One of the major open challenges facing theoretical physics today is to accommodate general relativity in the framework of quantum field theory. The main problem one encounters is the non-renormalizablity of gravity at the perturbative level. GTR is plagued with its notorious ultraviolet divergence[96]. Electromagnetism, weak and strong nuclear interactions are well described by renormalizable quantum theories, viz., quantum electrodynamics and quantum chromodynamics, respectively. GTR fails the usual tests of renormalizability while checked using the precise covariant rules for calculating Feynman diagrams in quantum theory of gravitation. The attempts of unification of all the four forces are waiting till we know how to tackle the UV divergence of gravity.

A heuristic picture of the problem can be visualized by a simple dimensional analysis. For a field theory, the integral for a Feynman diagram of order N will behave like, $\int p^{A-Nd}dp$, where A counts the processes under consideration and is independent of N and d is the dimension of the coupling constant $[mass]^d$. Now if $d < 0$, at sufficiently large orders, the integral diverges. For Newton's constant(G_N), the coupling constant of gravity, $d = -2$. This implies that the quantum field theory of gravity have ultraviolet divergence everywhere. For graviton, the propagator scales with the four-momentum, k_μ as,

$$G(\omega, k) = \frac{1}{k^2}, \tag{5.1}$$

where $k^2 = \omega^2 - k^2$. Each loop in the Feynman diagram contributes an integral, $\int d\omega d^3k \propto k^4$, resulting to a total contribution from the combination of one loop and one internal propagator,

$$k^4 k^{-2} = k^2 \to \infty, \quad as \quad k \to \infty \tag{5.2}$$

To bring the divergence of the higher loop orders under control, it is necessary to introduce infinitely many number of counter terms in curvature. One way to improve the UV behavior is to add relativistic higher-derivative curvature terms to the Lagrangian. For instance, an addition of a quadratic term, R^2 will change the graviton propagator as,

$$\frac{1}{k^2} + \frac{1}{k^2} G_N k^4 \frac{1}{k^2} + \frac{1}{k^2} G_N k^4 \frac{1}{k^2} G_N k^4 \frac{1}{k^2} + ... = \frac{1}{k^2 - G_N k^4} \tag{5.3}$$

Now the propagator at high energies is scaled as $\frac{1}{k^4}$ and the total contribution from one loop and one internal propagator now is

$$k^4 k^{-2} = k^0 \to finite, \quad as \quad k \to \infty \tag{5.4}$$

This cures the problem of the UV divergence but at the same time brings new issues. This can be immediately understood if we rewrite the propagator as,

$$\frac{1}{k^2 - G_N k^4} = \frac{1}{k^2} - \frac{1}{k^2 - 1/G_N} \tag{5.5}$$

The first term on the right had side represents the massless graviton while the second is a ghost term which also causes the unitary violation.

It is the higher order time derivatives that we introduced actually makes the problem rather than the space derivatives. This observation immediately points to a possible resolution. One can think of

introducing higher order spatial derivatives by omitting the higher order time derivatives. The former should improve the UV behavior of the propagator as we have already seen, whereas the latter guarantees the absence of ghosts, but at the cost of giving up the Lorentz invariance as a fundamental symmetry of the theory.

5.1.2 Hořava-Lifshitz theory of gravity

In 2009 Petr Hořava proposed a new theory[52–54] based on the idea that the time and space may have different dynamical scaling in the UV limit. This was inspired from the Lifshitz model of scalar field theory in condensed matter physics, introduced to explain quantum critical phenomena. Hence the theory is now dubbed as "Hořava-Lifshitz"theory. This arguments paved a new step in achieving a renormalizable theory for gravity. In the following we briefly review the main contents of the theory.

According to the theory, space and time follow anisotropic scaling,

$$x \to bx, \qquad t \to b^z t, \tag{5.6}$$

with the degree of anisotropy characterized by the "dynamical critical exponent", $z \geq 1$. In the IR limit, $z = 1$ and the Lorentz invariance is "accidentally restored". It is assumed that the Lorentz symmetry should appear as an emergent symmetry at IR scale, but can be fundamentally absent at high energies.

The action for Hořava-Lifshitz gravity (with $z = 3$) is given by,

$$
\begin{aligned}
S_{HL} &= \int dt d^3x \sqrt{g} N \Bigg\{ \frac{2}{\kappa^2}(K_{ij}K^{ij} - \lambda K^2) - \frac{\kappa^2}{2W^4} C_{ij}C^{ij} \\
&+ \frac{\kappa^2 \mu}{2W^2} \epsilon^{ijk} R^{(3)}_{i\ell} \bigtriangledown_j R^{(3)\ell}_{k} - \frac{\kappa^2 \mu^2}{8} R^{(3)}_{ij} R^{(3)ij} \\
&+ \frac{\kappa^2 \mu^2}{8(1-3\lambda)} \left(\frac{1-4\lambda}{4} (R^{(3)})^2 + \Lambda_W R^{(3)} - 3\Lambda_W^2 \right) \Bigg\}, \quad (5.7)
\end{aligned}
$$

where the extrinsic curvature, K_{ij} and the Cotton tensor, C^{ij} are given by,

$$K_{ij} = \frac{1}{2N} \left(\dot{g}_{ij} - \nabla_i N_j - \nabla_j N_i \right), \quad (5.8)$$

$$C^{ij} = \epsilon^{ikl} \nabla_k \left(R^{(3)j}_{l} - \frac{1}{4} R^{(3)} \delta^j_l \right), \quad (5.9)$$

and κ, λ, W are dimensionless coupling constants whereas μ, Λ_W have the mass dimensions $[\mu] = 1$, $[\Lambda_W] = 2$. Now the modified graviton propagator in the theory has the form,

$$\frac{1}{\omega^2 - c^2 k^2 - G(k^2)^z}. \quad (5.10)$$

At high energies, the propagator is dominated by the anisotropic term $1/\omega^2 - G(k^2)^z$ and for $z > 1$, this modification improves the short-distance behavior. The c^2k^2 term becomes important only at lower energies. Using these ideas he formulated a theory of gravity which would be powercounting renormalizable in $3 + 1$ dimensions. It assumes a Lifshitz-like anisotropic scaling between space and time at short distances, with z = 3 and thus breaking the Lorentz invariance. While in the IR limit it flows to $z = 1$, retrieving the Einstein's GTR. In this limit, the action in Eq.5.7 becomes,

$$S = \int dt d^3x \sqrt{g} N \left\{ \frac{2}{\kappa^2} \left(K_{ij} K^{ij} - \lambda K^2 \right) + \frac{\kappa^2 \mu^2}{8(1-3\lambda)} \left(\Lambda_W R - 3\Lambda_W^2 \right) \right\} \tag{5.11}$$

If we identify the speed of light c and Newtons constant G and Λ as,

$$c^2 = \frac{\kappa^2 \mu^4}{2}, \quad G_N = \frac{\kappa^2}{32\pi c}, \quad \Lambda = \frac{3}{2}\Lambda_W, \quad \lambda = 1, \tag{5.12}$$

the action reduced to the standard Einstein-Hilbert action,

$$\begin{aligned} S_{EH} &= \frac{1}{16\pi G_N} \int d^4x \sqrt{-g} N \left[\left(K_{ij} K^{ij} - K^2 \right) + R - 2\Lambda \right] \\ &= \frac{1}{16\pi G_N} \int d^4x \sqrt{-g^{(4)}} \left(R^{(4)} - 2\Lambda \right). \end{aligned} \tag{5.13}$$

The HL theory is regarded as a potential candidate of the UV completion of gravity and has received a growing interest. Even though the theory has the remarkable features, there are some open issues regarding Hořava-Lifshitz gravity. Firstly, the realization of renormalizability relay on power counting arguments. Even though this is a strong indication for UV completeness, a more rigorous conformation of renormalizability beyond power counting is still lacking. Secondly, the coupling of matter to gravity have not been fully clarified yet. The discussions on the consequences of theory in the fundamental and application level are still going on. A detailed review of the topic is given in [97–99]. As a new theory, it is interesting to investigate its various aspects in parallel.

5.2 Black holes in HL gravity

The HL theory has the same Newtonian and post Newtonian corrections as those of GTR. So systems of strong gravity, like black holes, are needed to get observable deviation from the standard GTR. Various black hole solutions are found in HL theory[100–119]. The IR vacuum of pure HL gravity is found to be anti-de Sitter[100, 101]. Even though HL gravity could recover GTR in IR at the action level for a particular value of the parameter $\lambda = 1$, there found a significant difference between these black hole solutions and the usual Schwarzschild AdS solution. The asymptotic fall-off of the metric for these black hole solutions is much slower than that of usual Schwarzschild AdS black holes in GTR.

Meanwhile Kehagias and Sfetsos[120](KS) could find a black hole solution in asymptotically flat Mankowski spacetimes by applying deformation in HL theory by adding a term proportional to the Ricci scalar of three-geometry, $\mu^4 R^{(3)}$ to the action in Eq.5.7 while the cosmological constant $\Lambda_W \to 0$. This will not alter the UV properties of the theory but it does the IR ones leading to Mankowski vacuum analogous to Schwarzschild spacetime in GTR.

Consider the metric ansatz for a static, spherically symmetric spacetime,

$$ds^2 = -N(r)^2 dt^2 + f(r)^{-1} dr^2 + r^2 d\Omega^2. \tag{5.14}$$

Substituting this ansatz into Eq.5.7, the Lagrangian after angular integration can be reduced to,

$$\begin{aligned} \mathcal{L} &= \frac{k^2\mu^2}{8(1-3\lambda)} \frac{N}{\sqrt{f}} \left((2\lambda - 1) \frac{(f-1)^2}{r^2} - 2\lambda \frac{f-1}{r} f' \right. \\ &+ \left. \frac{\lambda - 1}{2} f'^2 - 2\omega \left(1 - f - r f'\right) \right), \end{aligned} \tag{5.15}$$

where $\omega = 8\mu^2/(3\lambda-1)\kappa^2$. The equations of motion can be obtained by varying the functions f and N,

$$(2\lambda-1)\frac{(f-1)^2}{r^2}-2\lambda\frac{f-1}{r}f'+\frac{\lambda-1}{2}f'^2-2\omega(1-f-rf')=0, \quad (5.16)$$

$$\left(log\frac{N}{\sqrt{f}}\right)'\left((\lambda-1)f'-2\lambda\frac{f-1}{r}+2\omega r\right)+(\lambda-1)\left(f''-\frac{2(f-1)}{r^2}\right). \quad (5.17)$$

For $\lambda = 1$, one gets the KS solution with asymptotic flat spacetime,

$$N(r)^2 = f(r) = \frac{2(r^2-2Mr+\alpha)}{r^2+2\alpha+\sqrt{r^4+8\alpha Mr}}, \quad (5.18)$$

where $\alpha = 1/2\omega$ and M is the integration constant reduced to mass. The event horizons of the black hole are at,

$$r_\pm = M \pm \sqrt{M^2-\alpha}. \quad (5.19)$$

When $\alpha = 0$ the solution reduces to the Schwarzschild spacetime case.

Various aspects of KS black hole were explored in the past[121–133]. The dynamical evolution of scalar field in Hořava black hole spacetimes is studied using Horowitz-Hubeny approach[134]. The spectrum of entropy/area is discussed from the viewpoint of QNMs of scalar field in HL gravity[135, 136]. QNMs of various fields around KS black hole spacetime were calculated using WKB method[137–140]. It is interesting to see how various other field perturbations decay in KS black hole spacetime. In what follows, we present the study of the evolution of various massless field perturbations in the KS black hole spacetime and probe the signature of the new theory by comparing with the results in the standard GTR.

5.3 Massless fields around KS black hole

The evolution of massless neutral scalar field Φ, electromagnetic field A_μ and massless Dirac field ψ in the spacetime $g_{\mu\nu}$, specified by Eq.(5.14) are governed by the Klein-Gordon(Eq.(2.14) with $m = 0$ and $e = 0$), Maxwell's(Section 3.3.2) and the Dirac equations(Section 4.2) respectively,

$$\frac{1}{\sqrt{-g}}\partial_\mu(\sqrt{-g}g^{\mu\nu}\partial_\nu)\Phi = 0, \tag{5.20}$$

$$F^{\mu\nu}_{;\nu} = 0, \qquad with \qquad F_{\mu\nu} = A_{\nu,\mu} - A_{\mu,\nu}, \tag{5.21}$$

$$\left[\gamma^a e^\mu_a(\partial_\mu + \Gamma_\mu)\right]\psi = 0. \tag{5.22}$$

The radial part of the above perturbation equations can be decoupled from their angular parts and can be reduced to the form,

$$\left(-\frac{\partial^2}{\partial t^2} + \frac{\partial^2}{\partial r_*^2}\right)\psi_\ell(t,r) = -V(r)\psi_\ell(t,r) = 0, \tag{5.23}$$

where r_* is the tortoise coordinate and the effective potentials, $V(r)$ for different fields are given by,

$$V_S = f(r)\left(\frac{\ell(\ell+1)}{r^2} + \frac{1}{r}\frac{\partial f(r)}{\partial r}\right), \qquad \ell = 0,1,2,..., \tag{5.24}$$

$$V_{EM} = f(r)\left(\frac{\ell(\ell+1)}{r^2}\right), \qquad \ell = 1,2,3,..., \tag{5.25}$$

$$V_{D\pm} = \frac{\sqrt{f}|k|}{r^2}\left(|k|\sqrt{f} \pm \frac{r}{2}\frac{\partial f}{\partial r} \mp f(r)\right), \qquad |k| = 1,2,3,... \tag{5.26}$$

here k is positive or negative nonzero integer related to the total orbital angular momentum by $\ell = |k + \frac{1}{2}| - \frac{1}{2}$ and V_{D+} and V_{D-} are

the super symmetric partners and give same spectra. So we choose V_{D+} for our study and omit the subscript.

The effective potential experienced by scalar field in the spacetime of KS black hole is plotted in Figure 5.1. We can observe that the KS spacetime creates a higher potential barrier for the field than the Schwarzschild spacetime. Also the height of the potential barrier increases with the increase in the value of the parameter α. But at large distances, the potentials in the two cases coincide. The same is the case for the electromagnetic and Dirac fields.

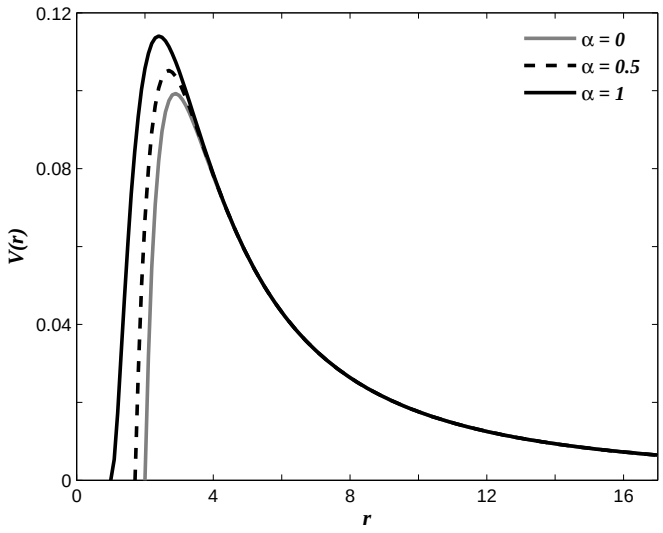

Figure 5.1: Effective potential faced by the $\ell = 1$ mode of scalar field around the KS spacetime for different values of α.

To get the time evolution picture of the field we write the perturbation equations, Eq.(5.23) in terms of the null coordinates $u = t - r^*$ and $v = t + r^*$ as,

$$-4\frac{\partial^2}{\partial u \partial v}\psi(u,v) = V(u,v)\psi(u,v), \tag{5.27}$$

and integrate this equation numerically using the finite difference scheme described in Section 3.4, We set initial conditions, $\psi(u, v = 0) = 0$ and a Gaussian profile $\psi(u = 0, v) = exp\left[-\frac{(v-v_c)^2}{2\sigma^2}\right]$, having width $\sigma = 3$, centered at $v_c = 10$.

The computationally expensive part in the numerical integration is to evaluate the potential at $r(r_*) = r((v - u)/2)$ on each grid points. The complexity of the function, $f(r)$ given in Eq.5.18 made it very difficult to find an expression for the tortoise coordinate, defined by $dr_* = \frac{1}{f}dr$. So we use the Runge-Kutta method to numerically integrate the equation for the tortoise coordinate and find the values of $r(r_*)$ at each step by cubic spline interpolation as suggested in [141]. Once the integration is completed the wave function Ψ is extracted on the surface of constant r, and plotted as a function of time.

5.3.1 Evolution of massless scalar field

The typical behavior of time evolution of a massless scalar field is shown in Figure 5.2. The *top* panel of the plot shows how the generic behavior of wave function, the initial outburst, quasinormal oscillations, and power-law decay, in HL theory is differed from that in pure Schwarzschild spacetime, taking the case of the $\ell = 1$ mode. We can see that the QNM phase extends for a longer time in HL theory. The late-time tail starts at a later time $t \approx 257$ for KS black hole with $\alpha = 0.8$ whereas it is at $t \approx 198$ for the Schwarzschild case. It is also clear from the figure that the oscillation frequency and the damping time have a higher values in HL theory.

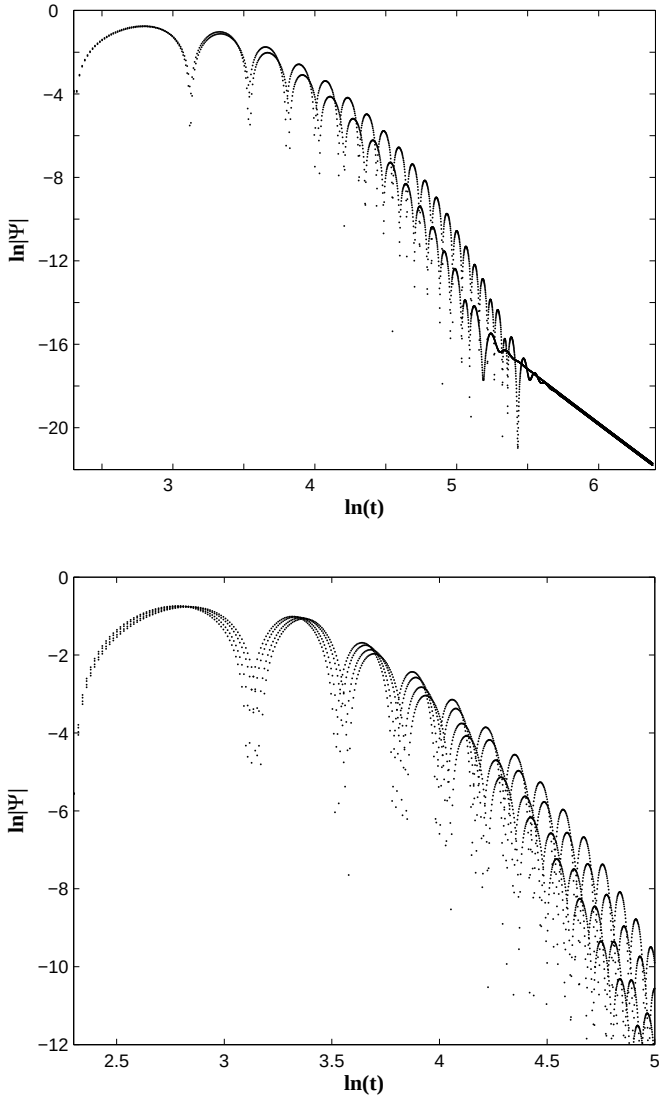

Figure 5.2: Evolution of scalar field with $\ell = 1$ mode. On the *top*, the field around KS black hole with $\alpha = 0.8$*(top curve)* and the Schwarzschild black hole*(bottom curve)* are shown. The plot on the *bottom* shows the QNM region of the field evolution for different values of α. Curves from *bottom* to *top* is for $\alpha = 0, 0.4, 0.8$ and 1, respectively.

The graph on the *bottom* panel of Figure 5.2 describes the dependence of QNM region on the value of the HL parameter, α. The oscillation frequency increases with the increase in the value of α, whereas the it shows a slower damping for higher values of α.

After the QNM stage the massless field dies off as an inverse power of time. Figure 5.3 illustrates this nature, where the plot on the *top* panel shows the late-time behavior of the wave function for different values of α, with multipole index $\ell = 1$. It is clear from the figure that the late-time behavior of massless field follows a power-law decay, and is independent of the value of the HL parameter α. The tail phase is identical to the Schwarzschild black hole spacetime case. To further confirm this we have studied the field evolution for different multipole indices for a fixed value of $\alpha = 0.5$. The plot on the *bottom* panel of the Figure 5.3 illustrates the results obtained. The field falls off as $\Psi \sim t^{-3.06}, t^{-5.08}, t^{-7.07}$ and $t^{-9.08}$ for $\ell = 0, 1, 2$ and 3 respectively, suggesting the power-law form $\Psi \sim t^{-(2\ell+3)}$. This is the same decay pattern that was found for the Schwarzschild spacetime[11].

Thus, it becomes evident that the QNM phase is the significant differing phase in the time evolution of scalar field around the KS black hole when one compares with the evolution in Schwarzschild black hole. So we further concentrate on the quantitative study of the QNM phase. The exact values of the QNM frequencies can be calculated from the numerically integrated data by nonlinear χ^2 fitting. We also use the WBK method described in Section 2.3.2 to evaluate the QNMs. The QNMs calculated from the numerically integrated data are given in Tables 5.1 and 5.2. It can be read from the table that the oscillation frequency of QNMs increase with the increase of the value of α, while the damping of the field decreases.

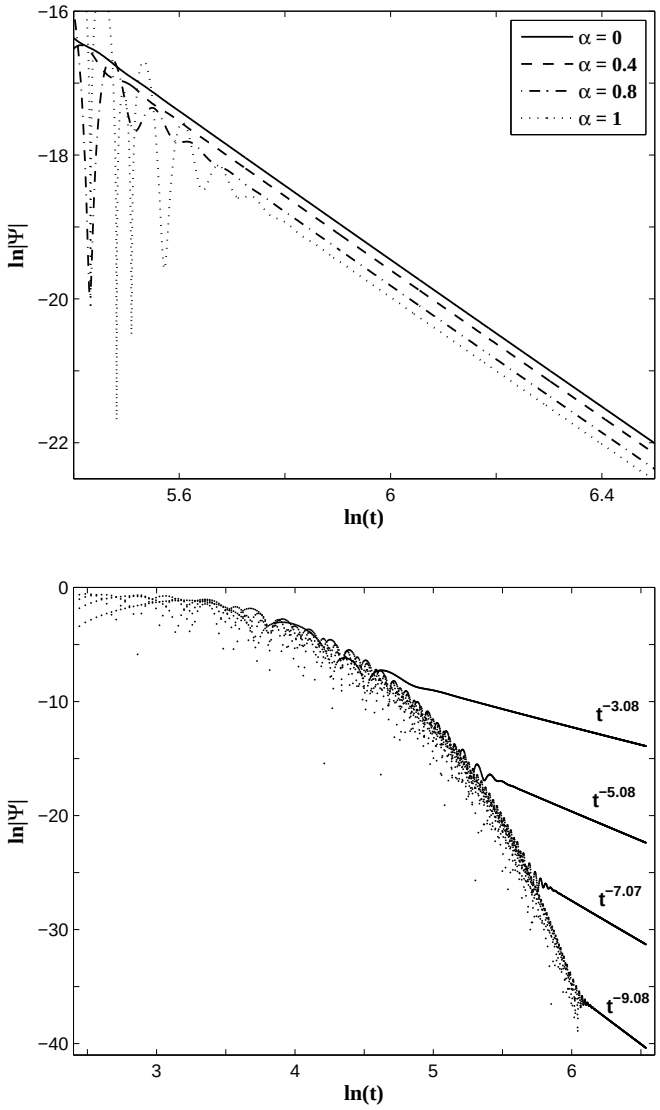

Figure 5.3: Late-time decay of scalar field around KS black hole for $\ell = 1$ mode. The plot on the *top* is the $\ell = 1$ mode of field, for different values of α. On the *bottom*, the field with $\alpha = 0.5$ for different angular momentum. Curves from *top* to *bottom* is for the $\ell = 0, 1, 2$ and 3, respectively.

	WKB		Time domain	
α	$Re(\omega)$	$Im(\omega)$	$Re(\omega)$	$Im(\omega)$
0	0.29111	-0.09800	0.29224	-0.09758
0.2	0.29564	-0.09424	0.29750	-0.09418
0.4	0.30071	-0.09008	0.30154	-0.09027
0.5	0.30345	-0.08777	0.30474	-0.08817
0.6	0.30636	-0.08526	0.30850	-0.08564
0.8	0.31260	-0.07937	0.31416	-0.07979
1	0.31918	-0.07162	0.32057	-0.07247

Table 5.1: QNM frequencies of massless scalar field for various values of α with $\ell = 1$, evaluated using WKB method and numerical integration data.

	WKB		Time domain	
α	$Re(\omega)$	$Im(\omega)$	$Re(\omega)$	$Im(\omega)$
0	0.48321	-0.09681	0.48332	-0.09676
0.2	0.49085	-0.09351	0.49087	-0.09356
0.4	0.49942	-0.08969	0.49911	-0.08981
0.5	0.50412	-0.08752	0.50266	-0.08767
0.6	0.50915	-0.08511	0.50831	-0.08527
0.8	0.52039	-0.07926	0.52029	-0.07947
1	0.53356	-0.07108	0.53272	-0.07138

Table 5.2: QNM frequencies of massless scalar field for various values of α with $\ell = 2$, evaluated using WKB method and numerical integration data.

5.3.2 Evolution of electromagnetic field

To study the evolution of electromagnetic field in HL black hole spacetime we numerically integrate the perturbation equation Eq.(5.23) with effective potential Eq.(5.25) using the time domain method. In Figure 5.4(*top*) the time evolution of the electromagnetic field, $\Psi(t, r)$, evaluated at the fixed radius $r_* = 10$ is plotted in comparison with the

corresponding Schwarzschild case. We can see that the time length of the QNM phase of electromagnetic field increases in HL theory.

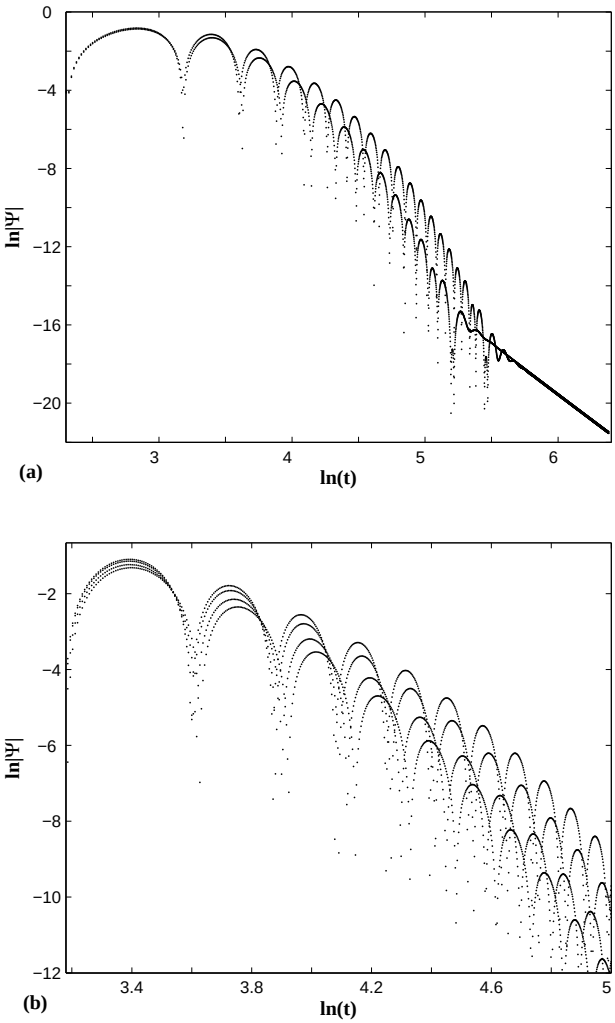

Figure 5.4: Evolution of $\ell = 1$ mode of electromagnetic field. (*top panel*)Field around KS black hole with $\alpha = 0.8$*(top curve)* and the Schwarzschild black hole*(bottom curve)*. (*bottom panel*)QNM region of the time evolution of field for different values of α. Curves from *bottom* to *top* is for $\alpha = 0, 0.4, 0.8$ and 1, respectively.

The late-time tail starts at $t \approx 300$ for KS black hole with $\alpha = 0.8$ whereas it is at $t \approx 230$ for the Schwarzschild case. The oscillation frequency of QNMs of electromagnetic field have higher values in HL theory and observed a lower than in the Schwarzschild case. The variation of oscillatory region of $\Psi(t, r)$ with the parameter α is shown in Figure 5.4(*bottom*). The oscillation frequency increases with α and shows a slower damping for higher values of α.

Figure 5.5(*top*) shows the late-time behavior of wave function for different values of α, with multipole index $\ell = 1$. We find that the late-time behavior of electromagnetic field is independent of α and follows the behavior of the Schwarzschild case with $\Psi \sim t^{-5.1}$. In Figure 5.5(*bottom*) field evolution for different multipole index is shown with $\alpha = 0.5$. The field falls off as $\Psi \sim t^{-5.08}$, $t^{-7.09}$ and $t^{-9.09}$ for $\ell = 1, 2$ and 3 respectively. The perturbation dies off at late-time as $t^{-(2\ell+3)}$ as in the case of Schwarzschild case.

We have seen that quasinormal ringing phase is dominated form of decay in the evolution of perturbations after the initial transient phase. The QNMs calculated from the numerically integrated data are given in Tables 5.3 and 5.4. We can find a good agreement with the earlier obtained results, using the WKB method[140]. The table shows that the QNM frequency electromagnetic field increase with the increase of the value of α, meantime the damping of the field reduces.

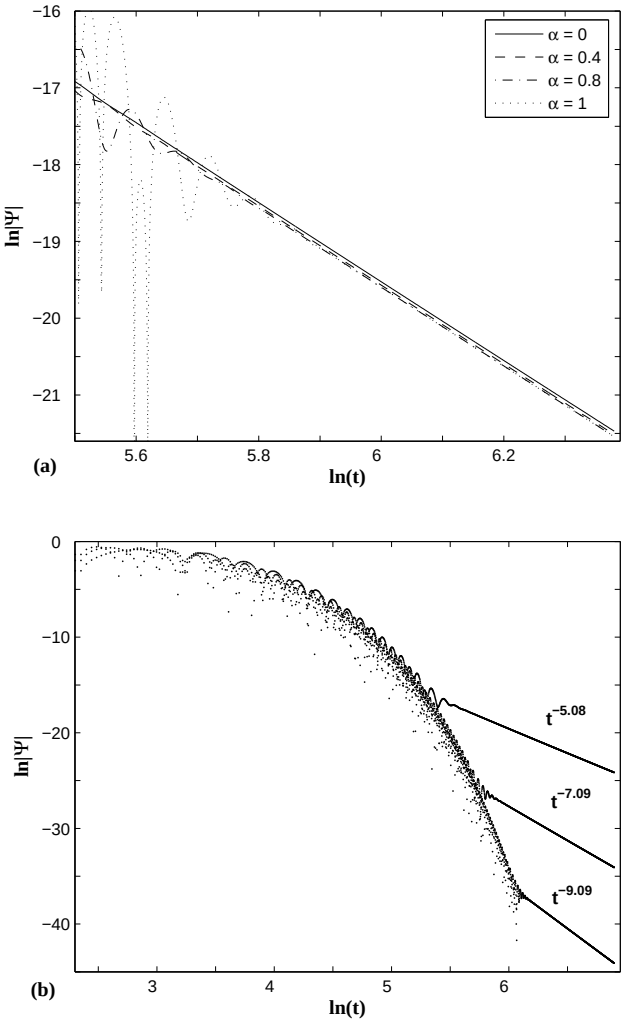

Figure 5.5: Late-time decay of electromagnetic field, (*top*) for different values of α with $\ell = 1$. The Field decay as an inverse power of time with $t^{-5.08}$, for all values of α. (*bottom*)Decay of field with different multipole order ℓ with $\alpha = 0.5$. The field decay as $t^{-5.08}, t^{-7.09}$ and $t^{-9.09}$ for $\ell = 1, 2$ and 3, respectively.

	WKB		Time domain	
α	$Re(\omega)$	$Im(\omega)$	$Re(\omega)$	$Im(\omega)$
0	0.24587	-0.09311	0.24401	-0.09051
0.2	0.25152	-0.08942	0.25225	-0.08706
0.4	0.25796	-0.08530	0.25733	-0.08447
0.5	0.26151	-0.08299	0.26383	-0.08135
0.6	0.26532	-0.08047	0.26575	-0.08009
0.8	0.27375	-0.07435	0.27771	-0.07454
1	0.28308	-0.06569	0.28478	-0.06581

Table 5.3: QNM frequencies of electromagnetic field for various values of α with $\ell = 1$, evaluated using WKB method and numerical integration data.

	WKB		Time domain	
α	$Re(\omega)$	$Im(\omega)$	$Re(\omega)$	$Im(\omega)$
0	0.45713	-0.09506	0.45088	-0.09471
0.2	0.46531	-0.09179	0.46239	-0.09117
0.4	0.47453	-0.08799	0.47153	-0.08711
0.5	0.47961	-0.08582	0.47835	-0.08502
0.6	0.48507	-0.08339	0.48332	-0.08183
0.8	0.49736	-0.07743	0.49756	-0.07439
1	0.51197	-0.06887	0.52823	-0.06897

Table 5.4: QNM frequencies of electromagnetic field for various values of α with $\ell = 2$, evaluated using WKB method and numerical integration data.

5.3.3 Evolution of massless Dirac field

Now we present the study of the evolution of Dirac field in HL black hole spacetime. The perturbation equation Eq.(5.27) with the effective potential Eq.(5.26), is numerically integrated using the time domain method. Figure 5.6(*top*) displays the time evolution of the Dirac wave function, $\Psi(t, r)$ at a fixed radius $r_* = 10$, for $k = 2$.

The deviation of generic time dependence of wave function in the HL theory from pure Schwarzschild spacetime is clear in the plot. QNM region lasts for a longer time in HL theory.

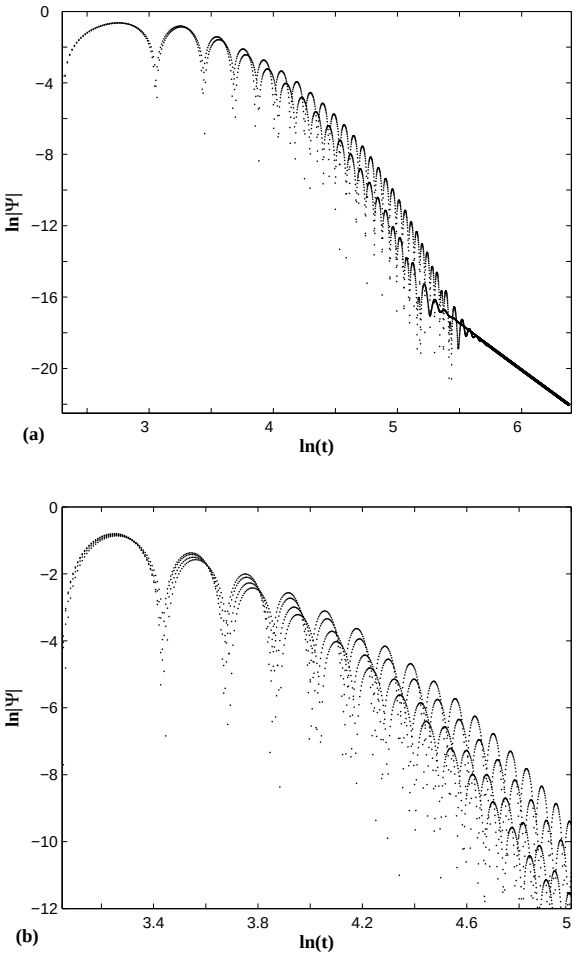

Figure 5.6: Time evolution of Dirac field with $k = 2$, $(left)$around KS black hole with $\alpha = 0.8$*(top curve)* and the Schwarzschild black case *(bottom curve)*. (*bottom*)QNM region of the time evolution of Dirac field for different values of $\alpha = 0.5$. Curves from *bottom* to *top* is for $\alpha = 0, 0.4, 0.8$ and 1, respectively.

The late-time tail starts at $t \approx 310$ for $\alpha = 0.8$ whereas it is at $t \approx 240$ for the Schwarzschild case. Also the oscillation frequency and the damping time have a higher values in HL theory. The variation of oscillatory region of $\Psi(t, r)$ with the parameter α is shown in Figure 5.6(*bottom*). The oscillation frequency increases with α and shows a slower damping for higher values of α.

Figure 5.7(*top*) shows the late-time behavior Dirac field for different values of α, with $k = 2$. The late-time behavior is independent of α and field decays in the inverse power of time as $t^{-5.08}$. In Figure 5.7(*bottom*), field evolution for different multipole indices are shown with $\alpha = 0.5$. The perturbation dies off at late-time as $\Psi \sim t^{-3.08}, t^{-5.08}$ and $t^{-7.09}$ for $k = 1, 2$ and 3 respectively.

The quasinormal ringing phase of the perturbation can be seen clearly in these figures. The calculated values of QNMs from the time domain data are given in Tables 5.5 and 5.6. We can find a good agreement of the values obtained previously [139] using the WKB scheme. Results show that the oscillation frequency and the damping time increase with α.

	WKB		Time domain	
α	$Re(\omega)$	$Im(\omega)$	$Re(\omega)$	$Im(\omega)$
0	0.17645	-0.10011	0.17830	-0.10744
0.2	0.18187	-0.09614	0.17952	-0.09481
0.4	0.18709	-0.09167	0.18756	-0.09312
0.5	0.18963	-0.08916	0.19040	-0.09249
0.6	0.19212	-0.08639	0.19333	-0.09172
0.8	0.19681	-0.07981	0.19635	-0.07572
1	0.20053	-0.07113	0.200101	-0.06939

Table 5.5: QNM frequencies of Dirac field for various values of α with $k = 1(\ell = 0)$, evaluated using WKB method and numerical integration data.

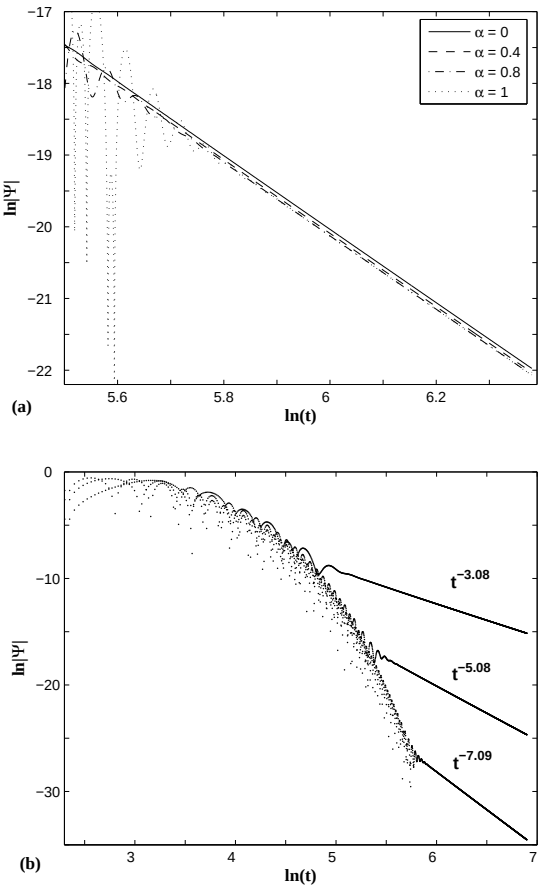

Figure 5.7: Late-time decay of Dirac field, (*top*)for different values of α with $k = 2$. The field decay as an inverse power law of time with $t^{-5.08}$ for all values of α. (*bottom*)Decay of Dirac field for different k with $\alpha = 0.5$. The field decay as $t^{-3.08}, t^{-5.08}$ and $t^{-7.09}$ for $k = 1, 2$ and 3 respectively.

Finally, we compare the time evolution of different fields in HL gravity. In Figure 5.8 massless scalar, Dirac and electromagnetic fields are plotted for $\alpha = 0.5$. The only difference between evolution of these three fields is in the QNM phase whereas the late-time tails follow the same decay pattern with same power law exponent. Figure

	WKB		Time domain	
α	$Re(\omega)$	$Im(\omega)$	$Re(\omega)$	$Im(\omega)$
0	0.37863	-0.09654	0.37348	-0.08850
0.2	0.38489	-0.09317	0.38126	-0.09488
0.4	0.39195	-0.08932	0.38935	-0.09014
0.5	0.39583	-0.08712	0.39126	-0.08816
0.6	0.39998	-0.08468	0.39153	-0.08388
0.8	0.40920	-0.07869	0.40337	-0.07758
1	0.41978	-0.07021	0.41415	-0.07239

Table 5.6: QNM frequencies of Dirac field for various values of α with $k = 2(\ell = 1)$, evaluated using WKB method and numerical integration data.

5.9 shows the variation of real and imaginary part of QNMs with α. All the three fields show the same dependence on the parameter α.

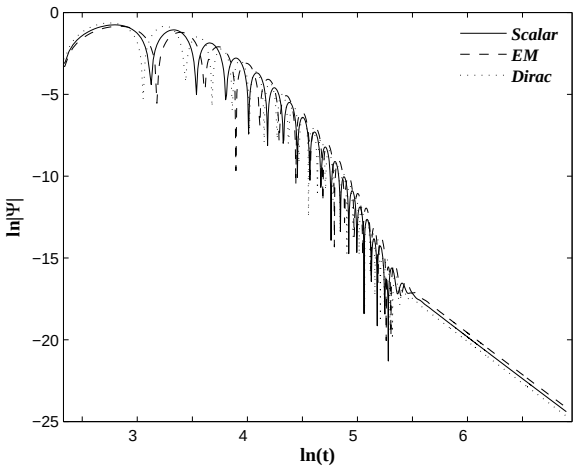

Figure 5.8: Evolution of $\ell = 1$ mode of massless scalar, Dirac and electromagnetic fields around KS black hole with $\alpha = 0.5$.

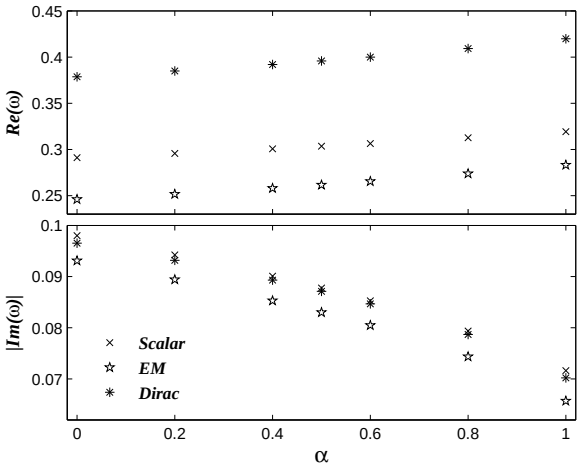

Figure 5.9: QNMs of massless scalar, Dirac and electromagnetic fields as a function of α, with $\ell = 1$.

5.4 Conclusion

This chapter describes the study which probes the signature of the Hořava-Lifshitz gravity, on the temporal evolution of different spin fields around the black hole spacetimes. The evolution of electromagnetic, massless scalar and Dirac perturbations around the asymptotically flat, spherically symmetric KS black hole solution are studied. We find a considerable deviation in the nature of field evolution in HL theory from that in the Schwarzschild spacetime. Comparing with the Schwarzschild case, the QNM phase of evolution prolongs to a longer time in HL theory before the power-law tail decay begins. In the QNM phase, the field is found to be oscillate with larger frequency in HL theory but it decays more slowly than the Schwarzschild case. The late-time decay of field, regardless of the spin, is found to be independent the HL parameter α, and follows the same power-law tail behavior as in the case of Schwarzschild black hole.

6

Evolution of massive fields around black hole in Hořava-Lifshitz gravity

6.1 Introduction

It is well understood in standard GR that massive field perturbations in the vicinity of black holes behave differently from the massless ones. A study on the propagation of massive scalar perturbations in Schwarzschild and Kerr spacetimes, using third order WKB approximation revealed that the QNMs of massive fields decay more slowly than massless ones[144]. Similar observation was made in the study of massive charged scalar field in a RN black hole spacetime exploiting WKB method[145]. These attempts are restricted to small values of the field mass due to the limitations arised from the validity of WKB approximation. A detailed investigation on the behavior of QNMs on the field mass is presented in[76]. They solved the QNMs using continued fraction method and showed that there may have modes with arbitrary long life, called the *quasi-resonant modes*, for specific values of the field mass. It has been proven in [146] that the quasi-resonant modes, which are arbitrary long living (purely real) modes, can exist only if the effective potential is not zero at least at one of the bound-

aries of the R-region. The QNMs of massive scalar and Dirac fields are further investigated in [75].

Late-time tail phase of massive fields also reported to have a different behavior in the black hole spacetimes of GR. In contrast with the massless fields, where the field at late-time dies off as $\Psi \sim t^{-(2\ell+3)}$, massive fields have an oscillatory inverse power-law behavior. At intermediate late times, $Mm \ll mt \ll 1/(mM)^2$, massive field with mass m, decay as $\Psi \sim t^{-(\ell+3/2)}sin(mt)$ [142]. But it was shown analytically that in the asymptotic late times ($mt \gg 1/(mM)^2$) another pattern of oscillatory tail of the form $\Psi \sim t^{-(5/6)}sin(mt)$ dominates[143] and it was numerically verified for various spacetimes and fields[87, 147–149].

All these studies argued that late-time relaxation does not have any relation to the spacetime parameters. Inspired from the hints that QNMs show dependence on spacetime parameter in three dimensional AdS[150] and de Sitter[151] spacetimes, a detailed numerical study of relaxation process in RN spacetime was done in [152]. They showed that for $Mm \ll 1$ relaxation depends only on the field parameters, but when $Mm \gg 1$ spacetime parameters affect the relaxation and found that for a Schwarzschild black hole bigger the black hole mass is, the faster the perturbation decays.

In the light of these fascinating results, it deserves a close analysis of massive field evolution in HL theory. Most of the previous studies on the field evolution around black holes in HL theory has so far been restricted to the massless fields. Eventhough the QNMs of massive scalar field is discussed in [136], they are mostly concerned on the thermodynamic aspects of the KS black hole and a clear picture of the evolution is not clear in their study. This chapter investigates the modifications of different stages of evolution of a massive scalar field

around black hole in HL theory. The rest of the chapter is organized as follows. In Section 6.2 we derive the master wave equation for massive scalar field around KS black hole and analyze the effective potential. The results of the numerical simulations for massive field perturbation is presented in Section 6.3 and Section 6.4 comprises the conclusion.

6.2 Massive scalar field around KS black hole

To study the properties of massive field we take the simplest case, massive scalar field with mass, m around the KS black hole spacetime. The scalar field evolves according to the Klein-Gordon equation,

$$\frac{1}{\sqrt{-g}}\partial_\mu(\sqrt{-g}g^{\mu\nu}\partial_\nu)\Phi - m^2\Phi = 0, \tag{6.1}$$

where $g_{\mu\nu}$ is the metric defined in Eq. (5.14). Resolving the field into scalar spherical harmonics, and employing the tortoise coordinate, the above equation can be reduced to the form(Section 2.3.1),

$$\left(-\frac{\partial^2}{\partial t^2} + \frac{\partial^2}{\partial r_*^2}\right)\Psi_\ell(t,r) = -V(r)\Psi_\ell(t,r) = 0, \tag{6.2}$$

with the effective potential $V(r)$ is given by,

$$V(r) = f(r)\left(\frac{\ell(\ell+1)}{r^2} + \frac{1}{r}\frac{\partial f(r)}{\partial r} + m^2\right). \tag{6.3}$$

The behavior of the effective potential $V(r)$, is plotted in Figure 6.1. The dependence of the potential with the parameter α is plotted in Figure 6.1(a), for massless and massive($m = 0.3$) fields. For a given mass, as the parameter α increases, the peak of the potential increases where as the asymptotic region of potential is largely unaffected by the

HL parameter. It is clear from Figure 6.1(b) that as the mass of the field increases the hight of the potential increases and its asymptotic value raises as m^2. The barrier nature of potential will be spoiled for high masses of the field.

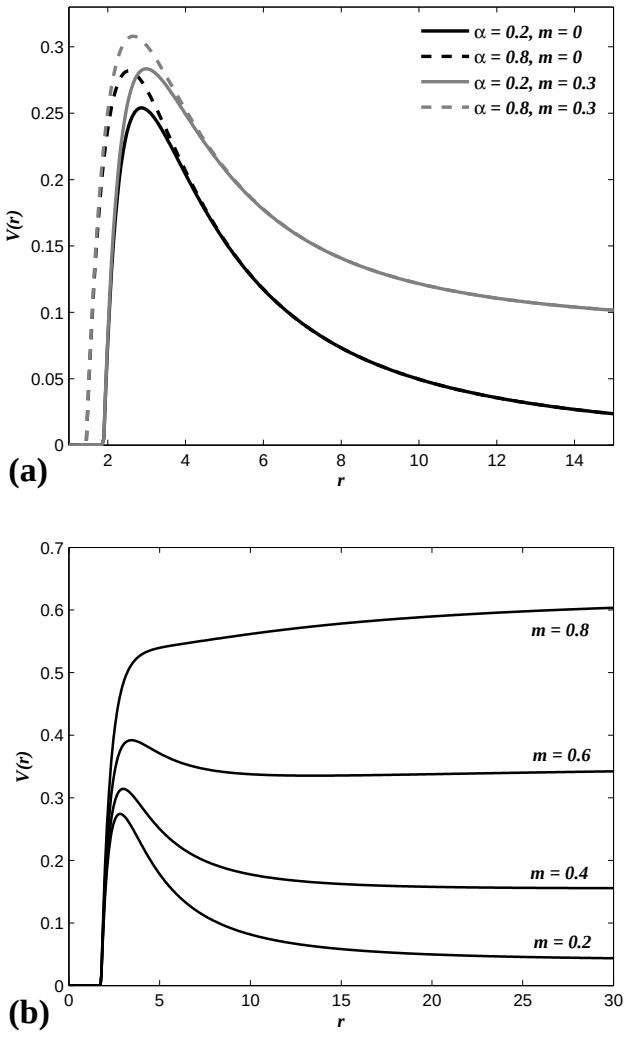

Figure 6.1: Profiles of effective potential, $V(r)$ for $\ell = 2$ mode. **(a)** $V(r)$ for $\alpha = 0.2(solid)$ and $\alpha = 0.8(dotted)$. **(b)** $V(r)$ with different field masses for $\alpha = 0.4$.

To study the evolution of the field we perform the numerical integration on an uniformly spaced grid by setting the initial conditions $\psi(u, v = 0) = 0$ and a Gaussian profile on $\Psi(u = 0, v)$ as the initial values. To evaluate the potential at $r(r_*) = r((v-u)/2)$ on each step, we numerically integrate the equation for the tortoise coordinate using the Runge-Kutta method[141] and by cubic spline interpolation, obtained $r(r_*)$ at each step.

6.3 Evolution of massive field

Now we describe the findings on the massive field evolution in the spacetime of KS black hole and compare the results with the existing results in standard GR. Here in the first series of simulations we set the mass of the black hole, $M = 1$ and choose the the field mass, m such that $Mm \leq 1$.

6.3.1 Quasinormal modes

For the study the QNMs of the massive field, we set the initial Gaussian profile with width, $\sigma = 3$ centered at $v_0 = 10$. In Figure 6.2 the wave function for massive scalar field($m = 0.1$) is plotted in comparison with the corresponding Schwarzschild case for $\ell = 2$. After the prompt response in the beginning, the quasinormal ringing starts. From the plot one can note two significant difference between the two cases. Firstly the QNM phase has a lower damping rate in HL theory, than in the standard GR. Secondly, in HL theory the ringdown phase last for a longer time. Figure 6.3 shows the variation of QNMs with the field mass, m for $\alpha = 0.4$. As the mass of the field increases the QNM phase shrinks in time.

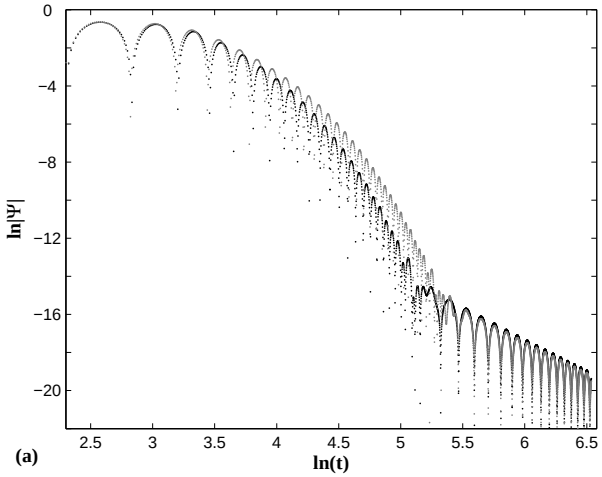

Figure 6.2: Time evolution of the $\ell = 2$ mode of the massive scalar field($m = 0.1$) in KS spacetime with $\alpha = 0.8$(*top curve*) in comparison with the corresponding case in Schwarzschild spacetime(*bottom curve*)

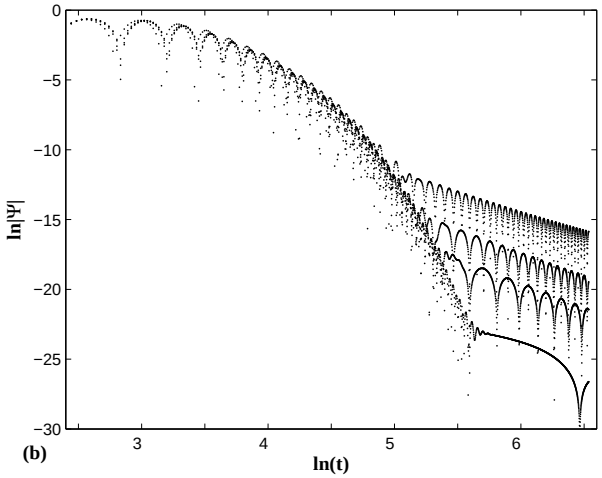

Figure 6.3: Time evolution of the $\ell = 2$ mode of the massive scalar field with different masses for $\alpha = 0.4$. Curves from *bottom* to *top* is for $m = 0.01, 0.05, 0.1$ and 0.2.

To see the effects of the HL parameter, α and field mass, m in QNM phase, we calculate the exact values of QNMs from the numerically integrated data in the time domain, by a nonlinear χ^2 fitting. We also use the third order WKB method to obtain the results. The WKB method is found to be accurate for low lying modes and can be used to explore the QNM behavior of black holes for field with low masses. The calculated values are given in Table 6.1 and Table 6.2.

The following points can easily be observed from the tables. QNMs of massive field in HL theory have a higher oscillation frequency $Re(\omega)$ and a lower damping rate, $|Im(\omega)|$ than the Schwarzschild case. Also the $Re(\omega)$ and $|Im(\omega)|$ found to be decreasing with the increase of the HL parameter, α. WKB method gives verse results for higher field masses since the barrier nature of potential gets spoiled at these mass ranges. This justifies the discrepancies in the QNMs evaluated by time domain and WKB methods at high field mass given in Table 6.2.

	WKB		Time domain	
α	$Re(\omega)$	$Im(\omega)$	$Re(\omega)$	$Im(\omega)$
0	0.48637	-0.09572	0.48552	-0.09573
0.2	0.49388	-0.09253	0.49377	-0.09256
0.4	0.50231	-0.08884	0.50159	-0.08888
0.6	0.51188	-0.08438	0.51142	-0.08437
0.8	0.52293	-0.07868	0.52143	-0.07893
1	0.53587	-0.07069	0.53569	-0.07106

Table 6.1: Fundamental($n = 0$) QNM frequencies of massive($m = 0.1$) scalar field for $\ell = 2$, calculated using WKB method and numerical integration data.

	WKB		Time domain	
m	$Re(\omega)$	$Im(\omega)$	$Re(\omega)$	$Im(\omega)$
0	0.49942	-0.08969	0.49886	-0.08951
0.02	0.49953	-0.08966	0.49979	-0.08969
0.05	0.50014	-0.08948	0.49839	-0.08948
0.07	0.50083	-0.08928	0.50156	-0.08922
0.1	0.50231	-0.08883	0.50159	-0.08875
0.2	0.51101	-0.08622	0.51083	-0.08701
0.3	0.52571	-0.08169	0.52737	-0.08029
0.4	0.54665	-0.07501	0.53933	-0.06758
0.5	0.57423	-0.06568	0.54165	-0.05451

Table 6.2: QNM frequencies afor different mass of the scalar field m. QNMs calculated using WKB method and numerical integration data ($\ell = 2$ and $\alpha = 0.4$).

6.3.2 Late-time decay of massive field

The QNM phase is followed by a phase of late-time tail behavior of the field decay. In the light of the previous results obtained for the massive field decay in the standard GR, we monitor the decay of field for a longer period of time. We observe following behavior for the field decay in different regimes, in HL theory.

A. Intermediate late-time decay

First we look at the late-time tails in intermediate range, $Mm \ll mt \ll (mM)^2$. The decay of field along black hole outer horizon H_+(approximated by the null surface $u_{max} = 0.5 \times 10^4$) and future time like infinity i_+ (approximated on fixed radius $r_* = 50M$) are evaluated with the initial field profile parameters $v_0 = 50$ and $\sigma^2 = 2$. The result for $\alpha = 0.4$ with $m = 0.01$ and $\ell = 0$ is shown in Figure 6.4.

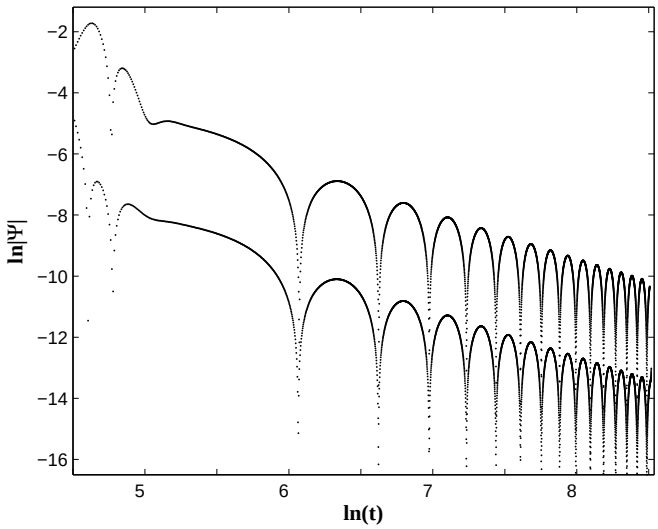

Figure 6.4: Decay of massive field with $m = 0.01$, along outer horizon $H_+(top\ curve)$ and future time like infinity i_+ $(bottom\ curve)$. The amplitude of field decay as power law with exponent -1.49 and period of oscillation $T = 314.8$.

After the QNM phase the amplitude of the oscillatory field decays as a power law with exponent -1.49 along I_+ and H_+ with a period of oscillation $T = 314.8$. We have analyzed for different values of HL parameter α and found that the tail behavior is almost independent of α and the decay is identical to the Schwarzschild case according to the form,

$$\Psi \sim t^{-(\ell+3/2)} sin(mt). \tag{6.4}$$

This can be expected since the late-time tail is originated by the backscattering by the effective potential in the asymptotic region and as it is clear from Figure 6.1, that the parameter α has no effect on this asymptotic region of the potential but can only change its shape near the peek.

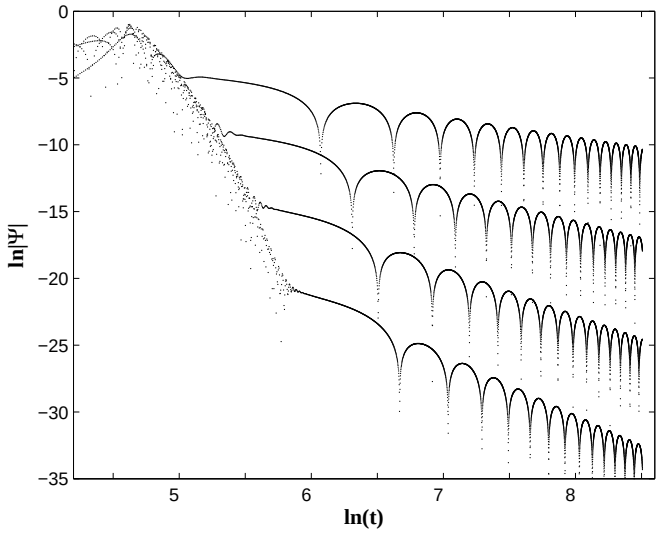

Figure 6.5: Decay of massive field with $m = 0.01$ along i_+ for different ℓ. The field dies off as power-law with exponents $-1.49, -2.5, -3.51$ and -4.51 for $\ell = 0, 1, 2$, and 3 respectively. The period of oscillation $T = 314.7 \pm 0.03$.

The field decay for different multipole indices is plotted in Figure 6.5 with $m = 0.01$. The decaying tail is found to have a period of oscillations $T = 314.7 \pm 0.03$ and the power-law exponents $-1.49, -2.5, -3.51$ and -4.51 for $\ell = 0, 1, 2$, and 3 respectively. An excellent agreement with the decay rate of the form $t^{-(\ell+3/2)}$ can be seen. We find that the frequency and damping rate of the oscillatory tails are independent of the parameter α and follow the Schwarzschild case. Thus we confirmed that Eq. (6.4) will be the form of the intermediate late-time behavior of massive field decay in HL theory also.

B. Asymptotic late-time decay

In the asymptotic late-time, $mt \gg 1/(Mm)^2$, the decay of field does not follow pattern given by Eq. (6.4). Another pattern of oscillatory tail dominates in the asymptotic late times. This can be seen from Figure 6.6, where the maxima of oscillations are shown for $\alpha = 0.4, \ell = 0$ and $m = 0.02, 0.05, 0.07$. The deviation from straight line with slop -1.5 is visible in the asymptotic late-time. When $mt \gg 1/(Mm)^2$ smaller the Mm the later the asymptotic tail starts. In Figure 6.7 asymptotic region is shown for $m = 1$ and $\ell = 0$ and 2. We find that the asymptotic tail is independent of the multipole order and follows the $\Psi \sim t^{-5/6} sin(mt)$ form as in the standard GR. We have analyzed the asymptotic tail for different values of α and find that this regime is also independent of the HL parameter α.

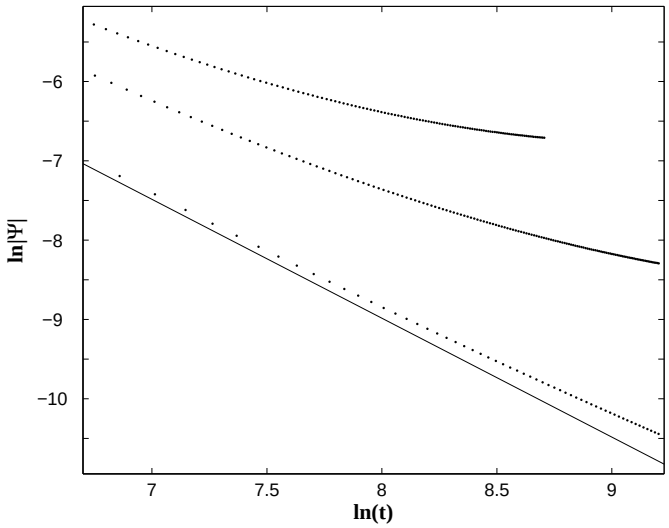

Figure 6.6: Late-time behavior of field for $\alpha = 0.4$. The maxima of oscillation of the wavefunction are plotted for $\ell = 0$. Graphs from *bottom* to *top* is for $m = 0.02, 0.05$ and 0.07, respectively. The *solid* line has a slop -1.5.

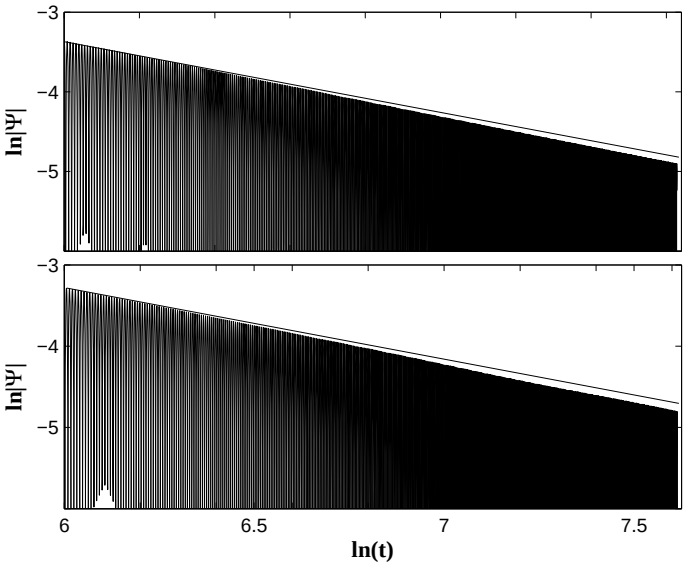

Figure 6.7: Asymptotic regime of field decay is shown for $\ell = 0(top)$ and $\ell = 2(bottom)$, with $m = 1$ and $\alpha = 0.4$. The straight lines have a slop $-5/6$.

Now we study the role of the black hole parameter on the decay of field for $Mm \ll 1$. The numerical results for different black hole mass with field mass $m = 0.01$ are shown in Figure 6.8. The field falls off with power law exponents $-1.458, -1.459$ and and -1.462 for $M = 0.5, 1$ and 1.5, respectively and we can conclude that, apart from the possible numerical error, the decay rate is independent of black hole mass for $Mm \ll 1$. We are not going for the $Mm \gg 1$ case of computationally expensive part of study. For $Mm \gg 1$ range we have good reasons to believe that the relaxation will show similar results of the Schwarzschild case as shown in[152], since we have already shown that the parameter α has no effect on the asymptotic region of the potential and the late-time relaxation is independent of the HL parameter.

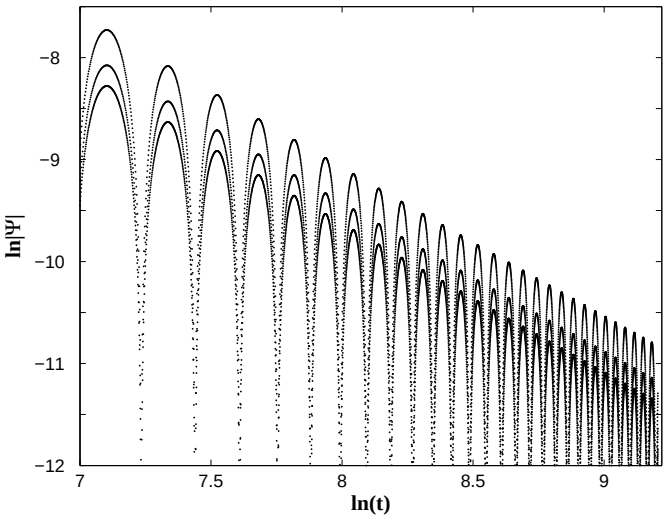

Figure 6.8: Decay of field with different black hole mass for $m = 0.01$, $\alpha = 0.4$ and $\ell = 0$. For $M = 0.5, 1$ and 1.5(curves from *top* to *bottom*) the decay rates of field are $-1.458, -1.459$ and -1.462 respectively.

6.4 Conclusion

In view of the intriguing behavior of massive fields in the standard GR, the evolution of massive scalar field is studied in the KS black hole spacetime in HL theory. Significant differences between the behavior of massive field in KS spacetime and the Schwarzschild spacetime are observed only for the ringdown phase. The evolution profile and the exact estimation of QNMs from the numerical integration establishes that the QNMs involved in the evolution of massive field in HL theory have a higher oscillation frequency but damps more slowly than in the Schwarzschild spacetime case. As the field mass increases the QNM phase squeezes to a smaller time interval. However the late-time evolution of massive field fails to show any distinction from the Schwarzschild case. Since the HL parameter, α has no effect on the

asymptotic region of the potential the late-time relaxation is found to be independent of the HL parameter. A th0rough investigation of the latetime behavior in different time regimes confirmed that in the intermediate range the field decays as $t^{-(\ell+3/2)}sin(mt)$, but in the asymptotic late-time the decay is dominated by $t^{-5/6}sin(mt)$ tail as in the case of Schwarzschild spacetime case.

7
Summary and Conclusion

The response of black holes to external perturbations are studied in two physically pertinent, modified theories of gravity,

- a model for accelerating Universe, the quintessence model and
- a model for quantum gravity, the Hořava-Lifshitz gravity.

The aim is to know whether one can find some distinguishable features of the new theories from the evolution of various field perturbations in their black hole spacetimes. The time evolution is studied using WKB approximation and numerical integration. The major results are summarized below.

Field evolution in quintessence model

Comparing with the results in pure Schwarzschild spacetime we observe the following deviations in the behavior of QNMs in the quintessence case.

Field	Oscillation(ω_R)	Damping($\|\omega_I\|$)
Scalar, EM, GR & Dirac	decreases	decreases

The late-time behavior also shows the signature of quintessence. A dependence, for late-time tails, on the spin of the perturbing field

also emerges in the presence of quintessence. The late-time behavior obtained for various spin field perturbations are summarized below.

Field	Mode	Schw	$\epsilon = -1/3$	$-2/3$	-1
Scalar	$\ell = 0$	power-law	power-law	no decay	no decay
	$\ell > 0$	"	"	exponential	exponential
EM	$\ell \geq 1$	"	"	exponential	exponential
GP	$\ell \geq 2$	"	"	exponential	exponential
Dirac	$\ell \geq 0$	"	"	no decay	no decay

Eventhough the scalar monopole does not decay at late times for lower values of quintessence EOS, it can be considered as a constant mode with the *same* constant value between the black hole EH and CH. The nature of Dirac field for lower ϵ is intriguing. It relaxes to a constant value at late-times, but it varies on different surfaces. It has the lowest value on the EH, increases as the radial distance increases and maximizes on the CH. This behavior may indicate the presence of a fermionic hair of the black hole in de Sitter like spacetimes.

Field evolution in HL gravity

We noticed the following deviations in the behavior of QNMs of the KS black hole spacetime in HL gravity in comparison with the Schwarzschild spacetime case.

Field	Oscillation(ω_R)	Damping($\lvert\omega_I\rvert$)
Massive scalar, EM & Dirac	increases	decreases

The late-time behavior fails to show any distinction from the Schwarzschild case and can be summarized as given below.

Field	Intermediate	Asymptotic
Massless(Scalar, EM & Dirac)	power-law $\sim t^{-(2\ell+3)}$	power-law $\sim t^{-(2\ell+3)}$
Massive(Scalar)	oscillatory power-law $\sim t^{-(\ell+3/2)} sin(mt)$	oscillatory power-law $\sim t^{-5/6} sin(mt)$

Both models cast their own signature QNMs of their black hole spacetimes. But the late-time tails show deviation only in the quintessence model. One can in principle, distinguish these theories once they are captured by the future gravitational wave detectors.

Towards future

In view of above results, we can point some interesting problems that can be addressed in the future.

- The studies of late-time tails of charged or rotating black holes will be of special interest. The knowledge of late-time behavior in a black hole with de Sitter like asymptotes is helpful for the better understanding of their interiors. The non decaying nature of Dirac field and the possible connection with the negative well in the potential deserve a close analysis.

- The perturbative study of the gravitational field itself, in HL gravity is still not addressed. This will be a tedious task since one has to find the linearized gravitational equation in HL theory, but it will be an important problem in understanding the theory.

References

[1] K. S. Thorne, *"Black Holes and Time Warps: Einstein's Outrageous Legacy"*, W W Norton & Company, New York (1994).

[2] J. R. Oppenheimer and H. Snyder, *Phys. Rev.* **56** 455 (1939).

[3] A. M. Ghez et al., *The Astrophys. J.*, **689** 1044 (2008).

[4] S. Chandrasekhar, *"The Mathematical Theory of Black Holes"*, Oxford Univ. Press, Oxford UK (1992).

[5] C. W. Misner, K. S. Thorn, and J. A. Wheeler, *"Gravitation"* (Freeman, San Francisco) p.876 (1973).

[6] T. Regge and J. A. Wheeler, *Phys. Rev.* **108** 1063 (1957).

[7] L. A Edelstein and C. V. Vishveshwara, *Phys. Rev. D*, **1** 3514 (1970).

[8] F. J. Zerilli, *Phys. Rev. D* **2** 2141, *Phys. Rev. Lett.* **24** 737 (1970).

[9] C. V. Vishveshwara, *Phys. Rev. D*, **1** 2870 (1970).

[10] B. S. Kay and R. M. Wald, *Class. Quantum Grav.* **4** 893 (1987).

[11] R. H. Price, *Phys. Rev. D* **5**, 2419, **5** 2439 (1972).

[12] H. T. Cho, *Phys. Rev.* D **68** 024003 (2003).

[13] C. V. Vishveshwara, *Nature* **229** 936 (1970).

[14] C. V. Vishveshwara, *Currennt Science* **71** 824 (1996). (Text of 'Fourt Vaidya-Raichaudhuri Endowment Lecture.')

[15] S. Chandrasekhar and S. Detweiler *Proc. R. Soc. Lond. A.* 344, 441 (1975).

[16] H. W. Leaver, *Phys. Rev. D* **34** 384(1986).

[17] L. S. Finn, *Phys. Rev. D* **46** 5236 (1992).

[18] J. D. Bekenstein, *Lett. Nuovo Cimento* **11** 467 (1974).

[19] S. Hod, *Phys. Rev. Lett.* **81** 4293 (1998).

[20] H. P. Nollert, *Phys. Rev. D* **47** 5253 (1993).

[21] O. Aharony et. al, *Phys. Rep.* **323** 183 (2000).

[22] K. D. Kokkotas and B. G. Schmidt, *Living Rev. Relativ.* **2** 2 (1999).

[23] H. P. Nollert, *Class. Quantum Grav.* **16** R159 (1999).

[24] V. Ferrari and L. Gualtieri *Gen. Rel. Grav.* **40** 945 (2008).

[25] E. Berti1, V. Cardoso and A. O. Starinets, *Class. Quant. Grav.* **26** 163001 (2009).

[26] R. A Konoplya and A. Zhidenko, *Rev. Mod. Phys.* **83** 793 (2011).

[27] C. Gundlach, R. H. Price and J. Pullin, *Phys. Rev. D* **49** 883 (1994).

[28] W. Krivan, P. Laguna, and P. Papadopoulos, *Phys. Rev. D* **54** 4728 (1996).

[29] S. Hod, *Phys. Rev. D* **58**, 104022 (1998), **61** 064018 (2000).

[30] L. Barack and A. Ori, *Phys. Rev. Lett.* **82** 4388 (1999).

[31] C. Gundlach, R. H. Price and J. Pullin, *Phys. Rev. D* **49** 890 (1994).

[32] L. M. Burko and A. Ori, *Phys. Rev. D* **56** 7820 (1997).

[33] E.S.C. Ching, P. T. Leung, W. M. Suen and K. Young, Phys. Rev. Lett. **74** 2414, *Phys. Rev. D.* **52** 2118 (1995).

[34] S. Hod, *Class. Quant. Grav.* **18** 1311 (2001).

[35] C. M. Chambers and I. G. Moss, *Phys. Rev. Lett.* **73** 617 (1994).

[36] P. R. Brady, C. M. Chambers, W. Krivan and P. Laguna, *Phys. Rev. D* **55** 7538 (1997).

[37] S. W. Hawking and G. F. R. Ellis, *"The Large Scale Structure of Space Time"*, Cambridge University Press, Cambridge, England, (1973).

[38] A. Ori, *Phys. Rev. Lett.* **67** 789 (1991), **68** 2117 (1992).

[39] B. Wang, *Braz. J. Phys.*, **35** 1029 (2005).

[40] E. Berti, V. Cardoso and C. M. Will, *Phys. Rev. D* **73** 064030 (2006).

[41] J. M. Maldacena, *Adv. Theor. Math. Phys.* **2** 231 (1998).

[42] J. M. Maldacena, *Int. J. Theor. Phys.* **38** 1113 (1999).

[43] G. T. Horowitz and V. E. Hubeny, *Phys. Rev. D* **62** 024027 (2000).

[44] B. Wang, C. Y. Lin, and E. Abdalla, *Phys. Lett. B* **79**, 481 (2000).

[45] V. Cardoso, R Konoplya and P. S. Lemos *Phys. Rev. D* **68**, 044024 (2003).

[46] B. Wang, C. Molina, and E. Abdalla, *Phys. Rev. D* **63** 084001 (2000).

[47] V. Cardoso and P. S. Lemos *Phys. Rev. D* **64**, 084017 (2001).

[48] E. Berti, V. Cardoso and A. O. Starinets, *Class. Quantum Grav.* **26** 163001 (2009).

[49] P. J. E. Peebles, B. Ratra, *ApJ. Lett.* **325** L17 (1988).

[50] B. Ratra and P.J.E. Peebles, *Phys. Rev. D* **37** 3406 (1988).

[51] R. R. Caldwell, R. Dave and P. J. Steinhardt, *Phys. Rev. Lett.* **80** 1582 (1998).

[52] P. Hořava, *Phys. Rev. D* **79** 084008 (2009).

[53] P. Hořava, *JHEP* **03** 020 (2009).

[54] P. Hořava, *Phys. Rev. Lett.* **102** 161301 (2009).

[55] B. F. Schutz and C. M. Will, *Astropphys. J.* **291** L33-6 (1985).

[56] S. Iyer and C. M. Will, *Phys. Rev. D* **35** 3621 (1987).

[57] R. A. Konoplya, *Phys. Rev. D* **68** 024018 (2003).

[58] S. Iyer, *Phys. Rev. D* **35** 3632 (1987).

[59] A. G. Riess et al., *Astronom. J.* **116** 1009 (1998).

[60] S. Perlmutter et al., *Astropphys. J.* **517** 565 (1999).

[61] S. Weinberg, *Rev. Mod. Phys.* **61** 1 (1989).

[62] T. Padmanabhan *Phys. Rep.* **380** 235 (2003).

[63] V. V. Kiselev, *Class. Quant. Grav.* **20** 1187 (2003).

[64] S. Chen and J. Jing, *Class. Quantum Grav.* **22** 4651 (2005).

[65] C. Ma, Y. Guy, W. Wnag and F. Wang, *Cent. Eur. J. Phys.* **6(2)** 194 (2008).

[66] Y. Zhang and Y. X. Gui, *Class. Quant. Grav.* **23** 6141 (2006).

[67] Y. Zhang, Gui, F. Yu and F. Li, *Gen. Relativ. Gravit.* **39** 1003 (2007).

[68] Y. Zhang et al., Chin. *Phys. Lett.* **26** 030401 (2009).

[69] M. Saleh et al., *Chin. Phys. Lett.* **26**, 109802 (2009).

[70] C. Y. Wang, Z. Yu, G. Y. Xing and L. Jian-Bo, Commun. *Theor. Phys.(Beijing, China)* **53** 882 (2010).

[71] P. Xi, *Astrophys. Space. Sci.* **321** 47 (2009).

[72] S. Hod and T. Piran, *Phys. Rev.* D **58** 024017 (1998).

[73] R. A. Konoplya, *Phys. Rev.* D **66** 084007 (2002).

[74] K. D. Kokkotas and B. F. Schutz, *Phys. Rev. D* **37** 3378 (1988), E. W. Leaver, *Phys. Rev. D* **41** 2986 (1990).

[75] J. F. Chang and Y. G. Shen, *Int. J. Theor. Phys.* **46** 1570 (2007).

[76] A. Ohashi and M. Sakagami *Class. Quantum Grav.* **21** 3973 (2004).

[77] C. M. Chambers, *arXiv:gr-qc/9709025* (1997).

[78] P. R. Brady, C. M. Chambers, W. G. Laarakkers and E. Poisson, *Phys. Rev. D* **60** 064003 (1999).

[79] R. Ruffini, in *Black Holes: les Astres Occlus* (Gordon and Breach, New York, 1973).

[80] L. P. Eisenhart, *Reimannian Geometry*, Princeton University Press, Princeton(1949).

[81] C. Molina, D. Giugno, E. Abdalla and A. Saa, *Phys. Rev. D* **69** 104013 (2004).

[82] R. A Konoplya, A. Zhidenko and C. Molina, *Phys. Rev. D.* **75** 084004 (2007).

[83] V. Cardoso, S. Yoshida, O. J. C. Dias and J. P. S. Lemos, *Phys. Rev. D.* **68** 061503(R) (2003).

[84] J. L. Jing, *Phys. Rev. D* **70** 065004 (2004).

[85] J. L. Jing, *Phys. Rev. D* **72** 027501 (2005).

[86] X. He and J. L. Jing, *Nucl. Phys. B* **755** 313 (2006).

[87] R. Moderski and M. Rogatko, *Phys. Rev. D* **77** 124007(2008)

[88] G. W. Gibbson and M. Rogatko, *Phys. Rev. D* **77** 044034 (2008).

[89] S. Bhattacharya and A. Lahiri, *Phys. Rev. Lett.* **99** 201101 (2007).

[90] P. Bizoń, *Phys. Rev. Lett.* **64**, 2844 (1990).

[91] G. Lavrelashvili and D. Maison, *Nucl. Phys. B* **410** 407 (1993).

[92] J. D. Bekenstein, *arXiv:gr-qc/9605059.*

[93] A. Zhidenko, *Class. Quantum Grav.* **21** 273 (2004).

[94] N. D. Birrell and P. C. Davies, *Quantum Fields In Curved Space*, 2nd edn. (Cambridge, Uk: Univ. Pr. 1982).

[95] A. Anderson and R. H. Price, *Phys. Rev. D* **43**, 3147 (1991).

[96] S. Weinberg, *"Ultraviolet Divergences in Quantum Theories of Gravitation"*, in: *General Relativity. An Einstein Centenary Survey* (Cambridge U.P.) eds: S.W. Hawking and W. Israel (1980).

[97] A Padilla, *J. Phys. Conf. Ser.* **259** 012033 (2010).

[98] T. P. Sotiriou, *J. Phys. Conf. Ser.* **283** 012034 (2011).

[99] D. Blas, O. Pujolas and S Sibiryakov, *JHEP* **1104** 018 (2011).

[100] H. Lu, J Mei and C. N. Pope, *Phys. Rev. Lett.* **103** 091301 (2009).

[101] Mu-In Park, *JHEP* **09** 123 (2009).

[102] H. Nastase, arXiv:0904.3604 [hep-th].

[103] R. G. Cai, Y. Liu and Y. Sun , *JHEP* **06** 010 (2009).

[104] R. G. Cai, L. Cao and N. Ohta, *Phys. Rev. D* **80** 024003 (2009).

[105] A. Ghodsi and E. Hatefi, *Phys. Rev. D* **81** 044016 (2010).

[106] H. W. Lee Y. Kim and Y. S. Myung, arXiv:0907.3568 [hep-th].

[107] J. Z. Tang and B. Chen, *Phys. Rev. D* **81** 043515 (2010).

[108] E. Kiritsis and G. Kofinas, arXiv:0910.5487 [hep-th].

[109] T. Harada, U. Miyamoto and N. Tsukamoto, *Int. J. Mod. Phys. D* **20** 111 (2011).

[110] E. Kiritsis, *Phys. Rev. D* **81** 044009 (2010).

[111] D. Capasso and A. Polychronakos, arXiv:0911.1535v3 [hep-th].

[112] J. Tang, arXiv:0911.3849[hp-th].

[113] H. W. Lee, Y. Kim, Y. S. Myung, *Eur. Phys. J. C* **70** 367 (2010).

[114] G. Koutsoumbas and P. Pasipoularides, arXiv:1006.3199v3 [hep-th].

[115] J. Greenwald, A. Papazoglou and A. Wang, *Phys. Rev. D* **81** 084046 (2010).

[116] R. G. Cai and A. Wang, *Phys. Lett. B* **686** 166 (2010).

[117] G. Koutsoumbas, E. Papantonopoulos, P. Pasipoularides and M. Tsoukalas, arXiv:1004.2289v2 [hep-th].

[118] A. N. Aliev and C. Senturk, *Phys. Rev. D.* **82** 104016 (2010).

[119] E. Gruss, arXiv:1005.1353v1 [hep-th].

[120] A. Kehagias and K. Sfetsos, *Phys. Lett. B* **678**(1) (2009) 123.

[121] R. G. Cai, ,L. M. Cao and N. Ohta, *Phys. Lett. B* **679** 504 (2009).

[122] Y. S. Myung, arXiv:0905.0957v2 [hep-th].

[123] S. Chen, J. Jing, *Phys. Rev. D* **80** 024036(2009).

[124] Y. S. Myuang, *Phys. Rev. D* **81** 064006 (2010).

[125] J. J. Peng and S. Q. Wu, *Eur. Phys. J. C* **66** 325 (2010).

[126] L. Iorio and M. L. Ruggiero, *Int. J. Mod. Phys. A* **25** 5399 (2010).

[127] L. Iorio and M. L. Ruggiero, *Open Astron. J.* **3**167 (2010).

[128] T. Harko, Z. Kovacs and F. S. N. Lobo, *Proc. R. Soc.* **A467** 1390 (2011).

[129] T. Harko, Z. Kovacs and F. S. N. Lobo, *Phys. Rev. D* **80** 044021 (2009).

[130] M. R. Setare and M. Jamil, *Int. J. Theor. Phys.* **50** 511(2011).

[131] W. Janke, D. A. Johnston and R. Kenna, arXiv:1005.3392v2 [hep-th].

[132] B. Gwak and B. H. Lee, *JCAP* **09** 031 (2010).

[133] M. R. Setare and D. Momeni, *Int. J. Theor. Phys.* **49** 106 (2011).

[134] C. Ding. S. Chen and J. Jing,*Phys. Rev. D* **81** 024028 (2009).

[135] B. R. Majhi, *Phys. Lett. B* **686** 49(2010).

[136] M. R. Setare and D. Momeni, *Mod. Phys. Lett. A* **26** 151 (2011).

[137] S. Chen and J. Jing, *Phys. Lett. B* **687** 124 (2010).

[138] R. A. Konoplya *A. Phys. Lett. B* **679** 499 (2009).

[139] C. Wang and Y. Gui, *Astrophys and Space Sci* **325**, 85 (2010).

[140] K. Lin, N. Yang and J. Li, *Int. J. Theor. Phys* **50** 48 (2011).

[141] R. A. Konoplya and A. Zhidenko, *Phys. Rev. D* **77** 104004 (2008).

[142] S. Hod and T. Piran, *Phys. Rev. D.* **58** 044018 (1998).

[143] H. Koyama and A. Tomimatsu, *Phys. Rev. D.* **63** 064032 (2001).

[144] L. E. Simone and C. M. Will, *Class. Quantum Qrav.* **9** 963 (1992).

[145] R. A. Konoplya, *Phys. Lett. B* **550** 117 (2002).

[146] R. A. Konoplya and A. V. Zhidenko, *Phys. Lett. B* **609** 377 (2005).

[147] R. A. Konoplya and A. Zhidenko *Phys. Rev. D.* **75** 084004 (2007).

[148] L. M. Burko and G. Khanna, *Phys. Rev. D.* **70** 044018 (2004).

[149] J. L. Jing, *Phys. Rev. D.* **70** 065004 (2004).

[150] D. Birmingham, I. Sachs and S. N. Solodukhin *Phys. Rev. Lett.* **88** 151301 (2002).

[151] E. Abdalla, B. Wang, A. L. Santos, W. G. Qiu, *Phys. Lett. B* **538** 435 (2002).

[152] L. Xue and B. Wang, *Phys. Rev. D.* **66** 024032 (2002).

[153] T. R. Govindarajan and V. Suneetha, *Class. Quantum Qrav.* **18** 265 (2001).